

# Effects of the Satellite Power System on Low Earth Orbit and Geosynchronous Satellites

W.B. Grant

E.L. Morrison

J.R. Juroshek



**U.S. DEPARTMENT OF COMMERCE**  
**Malcolm Baldrige, Secretary**

Dale N. Hatfield, Acting Assistant Secretary  
for Communications and Information

June 1981



## PREFACE

This report summarizes work performed for the Department of Energy, Satellite Power System Project Office under the direction of Dr. Frederick A. Koomanoff. The work performed under Contract Numbers DE-A106-79RL10077 and DE-A101-80ER10160.00, is written for a wide audience, including the non-technical as well as the technical. Hence, rigorous mathematical calculations are kept to a minimum.



## TABLE OF CONTENTS

	PAGE
PREFACE	iii
LIST OF FIGURES	vi
LIST OF TABLES	vii
ABSTRACT	1
1. INTRODUCTION	1
2. GEO SATELLITES	20
2.1 Uplink Antenna Patterns	20
2.2 Signal Processing Satellites	27
2.3 GEO Satellite Receivers	27
2.4 GEO Satellite Effects	31
2.5 Interference to Geostationary Satellites	38
2.6 Station Keeping Problems	50
2.7 Mitigation Techniques	50
3. LEO SATELLITES	52
3.1 LANDSAT Satellite	53
3.2 GPS Satellite	62
3.3 Space Telescope	66
4. SUMMARY OF POTENTIAL INTERFERENCE TO SATELLITE COMMUNICATION SYSTEMS	75
5. CONCLUSIONS AND RECOMMENDATIONS	76
6. REFERENCES	77

## LIST OF FIGURES

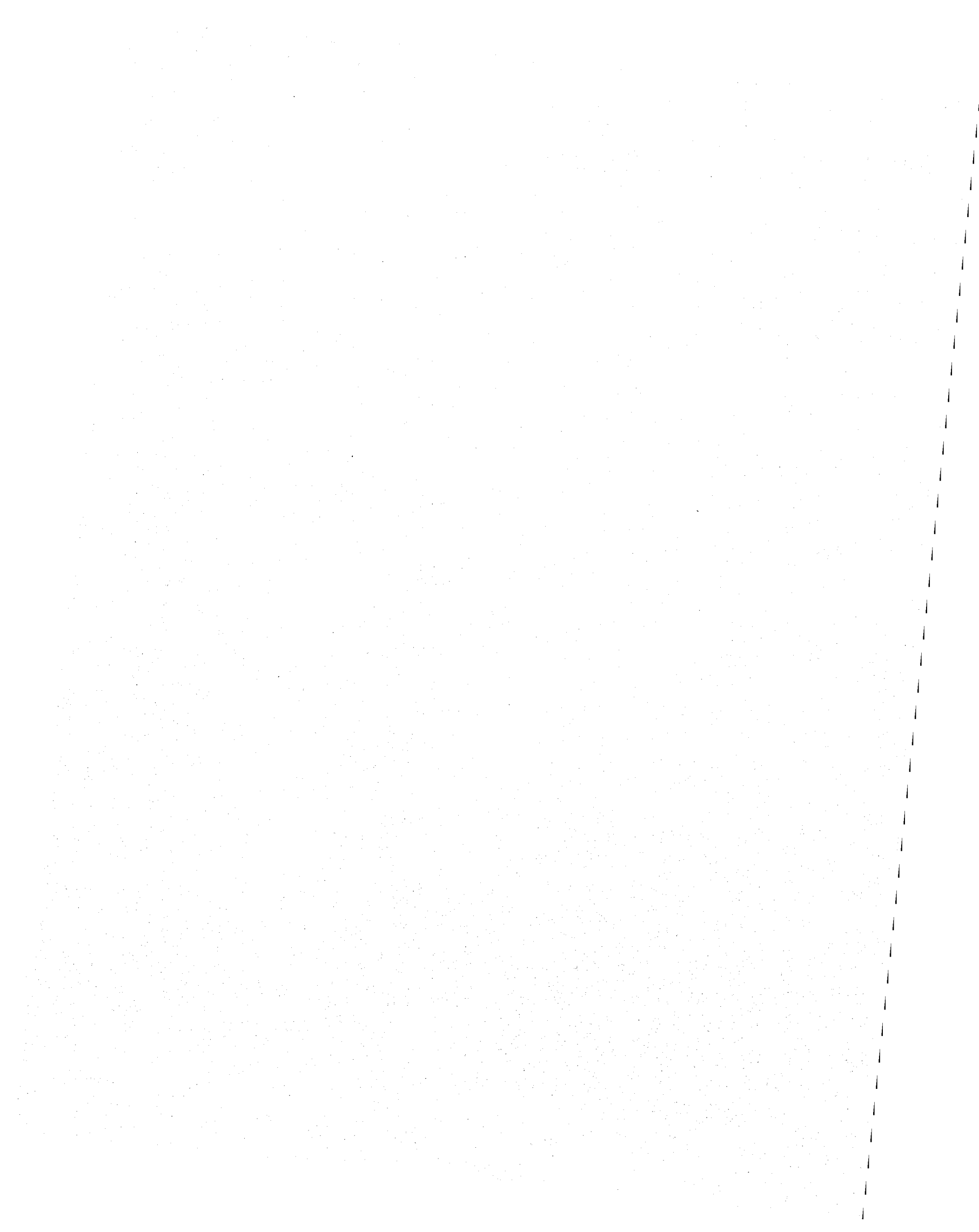
	PAGE
Figure 1. SPS radiation pattern on the earth.	2
Figure 2. High power klystron emission at harmonics of the fundamental frequency.	4
Figure 3. Spacetenna - $F_2$ pattern estimate.	6
Figure 4. Spacetenna - $f_3$ pattern estimate.	7
Figure 5. Spacetenna effective radiated power $90^\circ$ off boresight.	8
Figure 6. H-Field shielding effectiveness.	10
Figure 7. Magnetic shielding effectiveness of graphite/epoxy panel and panels joined by Hi-Loks.	11
Figure 8. E-Field shielding effectiveness of graphite/epoxy panel and panels joined with Hi-Loks.	12
Figure 9. Plane-wave shielding effectiveness of graphite/epoxy plain panel and panels joined with Hi-Loks (QR V).	13
Figure 10. Attachment interface cross-section of panel and access door.	14
Figure 11. H-Field shielding effectiveness of graphite/epoxy access door specimens.	15
Figure 12. E-Field shielding effectiveness of graphite/epoxy access door specimens.	16
Figure 13. Plane wave shielding effectiveness of graphite/epoxy access door specimens.	17
Figure 14. Satellite geometry showing possible signal multipath situation.	18
Figure 15. SPS on-board translator/repeater in support of satellite-to-satellite communication mode.	19
Figure 16. Functional diagram of a solar cell and conditioning system.	21
Figure 17. SCR intermodulation modes.	22
Figure 18. Block diagram of possible SPS control loop configuration.	23
Figure 19. A typical satellite hemisphere coverage pattern.	25
Figure 20. A typical satellite spot beam antenna pattern.	26
Figure 21. SPATS error response - single cw interferer.	28
Figure 22. General signal processing satellite block diagram.	29
Figure 23. Multipath modulation spectra.	30
Figure 24. Functional organization of two types of satellite receivers.	32
Figure 25. SS-TDMA repeater performance characteristic.	33
Figure 26. Matrix switched transponder response.	34

LIST OF FIGURES (CONT.)

	PAGE
Figure 27. SS-TDMA repeater error characteristic - two cw interferor cases.	35
Figure 28. Single conversion transponder response.	36
Figure 29. TDMA/PCM error characteristic - two signal interferor.	37
Figure 30. Communication satellite uplink/downlink frequency trends.	39
Figure 31. Power density from SPS as a function of distance along the geostationary orbit.	40
Figure 32. Global beam footprint from INTELSAT IV.	43
Figure 33. Geometry for calculating angle from SPS boresight to line joining INTELSAT IV.	43
Figure 34. SPS rectenna gain versus range of angles where possible interference with INTELSAT IV may occur.	44
Figure 35. CONUS beam for the advanced WESTAR.	47
Figure 36. Satellite station keeping problem potential interference.	51
Figure 37. LANDSAT wideband communications subsystems mechanical configuration.	54
Figure 38. LANDSAT communication links.	55
Figure 39. SPS microwave beam geometry at LANDSAT orbit altitude.	56
Figure 40. LANDSAT functional impact modes.	57
Figure 41. Image dissector star tracker error characteristics.	59
Figure 42. Thematic mapper test plan configuration.	60
Figure 43. SPS microwave beam geometry at NAVSTAR orbit altitude.	64
Figure 44. GPS functional impact modes.	65
Figure 45. Star tracker - stabilized platform altitude responses.	67
Figure 46. Cross-sectional view of the satellite observatory.	69
Figure 47. SPS power beam geometry for space telescope EMC analysis.	70
Figure 48. CCD video noise spectra.	72
Figure 49. CCD video noise spectra - SPS illumination.	73
Figure 50. CCD array imaging characteristic.	74

LIST OF TABLES

Table 1. Estimates of the Power Coupled into a 1640 MHz Satellite Transponder Separated 0.1 Degrees from a SPS.	42
Table 2. TDRSS Interference Estimates.	49



# EFFECTS OF THE SATELLITE POWER SYSTEM ON LOW EARTH ORBIT AND GEOSYNCHRONOUS SATELLITES

W. B. Grant, E. L. Morrison and J. R. Juroshek\*

The large amount of power contained in the main beam and principal sidelobes of the proposed Solar Power System (SPS), now under study by DOE and NASA, potentially presents an EMC problem for other satellite systems. This report examines selected geosynchronous orbit (GEO) satellites in adjacent slots to an SPS, GEO satellites on a chord passing an earth horizon, and low-earth-orbit (LEO) satellites which may pass through the SPS power beam. Potential functional and operational impacts to on-board systems are analyzed. Mitigation techniques for SPS effects are examined, and recommendations summarized to allow satellites to operate satisfactorily in an SPS environment.

## 1. INTRODUCTION

The SPS concept proposes a large geostationary satellite which converts the sun's energy to direct current (dc) and converts the dc to microwave energy via high-power klystrons. The microwave energy is formed into a beam using a large phased-array antenna 1 km in diameter. The energy is transmitted to earth and collected at a receiving antenna (rectenna) where some billion dipoles convert the microwave energy back to dc where it is summed on summing busses. Each satellite is capable of radiating approximately 6.85 GW of microwave power, with the design intended to provide 5 GW of electrical power for distribution. The current design (DOE/ER-0023, Oct. 1978) emphasizes the 2.45 GHz ISM band for satellite-earth power transmission.

One principal element in the Environmental Assessment Program supporting the SPS concept definition phase addresses the electromagnetic compatibility (EMC) of the proposed system. The scope of the EMC evaluation is in part dictated by the high microwave power of the SPS and the wide range of susceptibility of radio frequency receivers and other electronic equipment. On the earth, an exclusion area surrounding the rectenna keeps systems from operating in the high-energy portion of the power beam. However, a satellite in low earth orbit (LEO) may pass through the center of an SPS beam, subjecting it to extremely high field intensities. Also of concern with such a large satellite in geosynchronous orbit (GEO) and the high microwave powers involved is the potential interference problems that may exist between SPS and other satellites colocated in GEO.

The spacetenna radiation pattern for the 10 dB taper at the ground is shown in Figure 1. This pattern assumes no phase or amplitude distribution error, with 2%

---

\*The authors are with the U.S. Department of Commerce, National Telecommunications and Information Administration, Institute for Telecommunication Sciences, Boulder, Colorado 80303

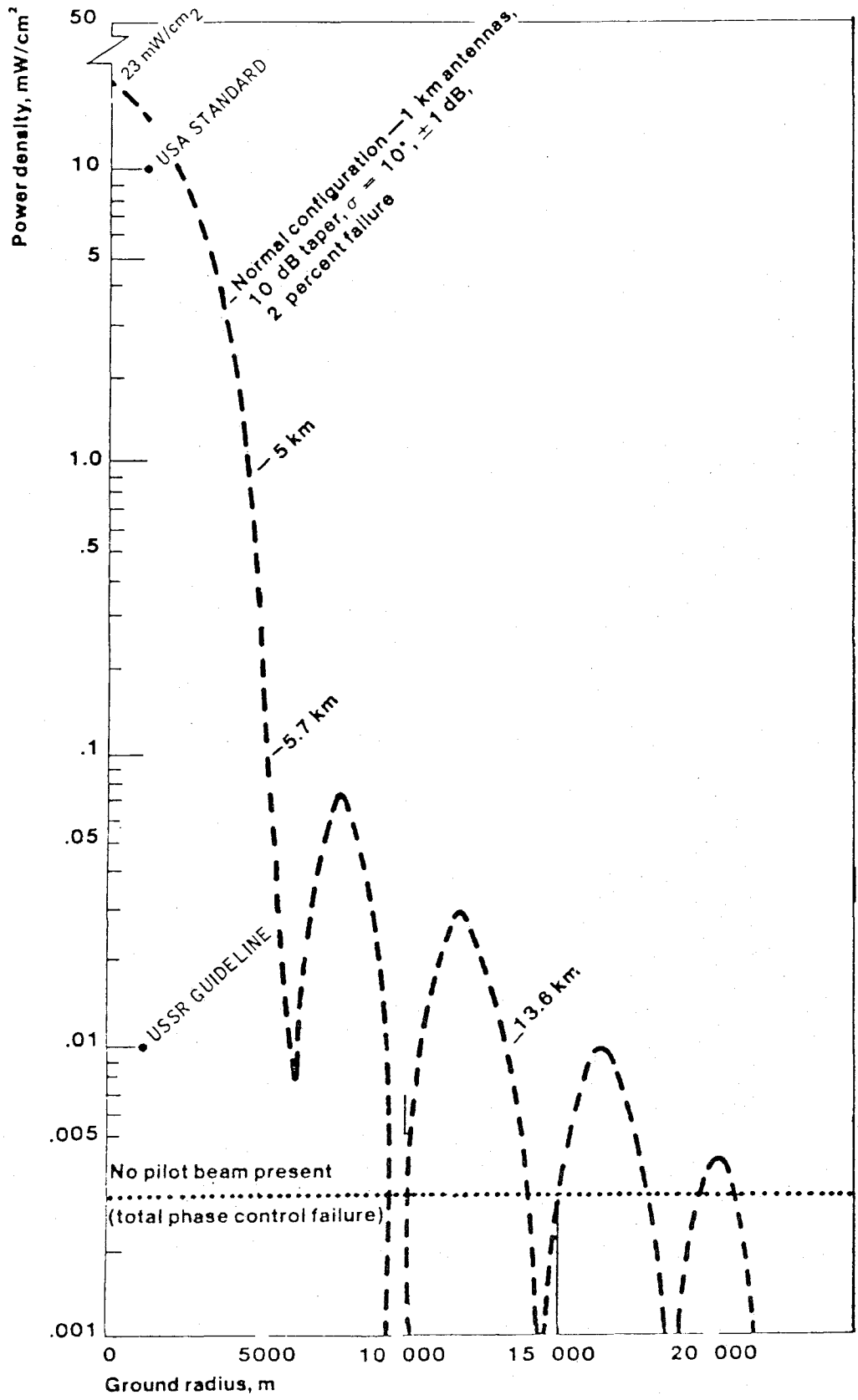


Figure 1. SPS radiation pattern on the earth.

klystron failure rate. The effect of antenna errors would be to decrease power in the main beam while increasing power in the sidelobes. At the surface, the peak power at the center of the rectenna, under ideal conditions, would be  $23 \text{ mw/cm}^2$ , dropping to  $1 \text{ mw/cm}^2$  at the edge of the rectenna, and  $0.08 \text{ mw/cm}^2$  for the first sidelobe. The spacetenna plane will develop  $22 \text{ kw/m}^2$  at the center, and about  $2.4 \text{ kw/m}^2$  at the edge.

At present there are no measured data available for the SPS antenna patterns and emissions at harmonics of the proposed 2.45 GHz frequency. To get estimates that would be useful for the EMC studies, data was derived from measurements of emissions from various high-power klystrons used in military radar applications. No wide-band systems were included so as to maximize the amplifier-output filter configuration relevance to the SPS. Harmonic components relative to the fundamental for high-power klystrons are given in Figure 2, based upon measurement extrapolations and the basic characteristics of beam bunching and acceleration effects in tube cavities (J. R. Rowe, 1965; Scherba et al., 1971).

Estimates of second ( $f_2$ ) and third ( $f_3$ ) harmonic spatial distributions for the SPS were derived from weighing pattern spatial components and correlation functions for  $f_0$ ,  $f_2$ , and  $f_3$  for the COBRA DANE and SPY-1 military radar systems, deriving aperture correlation functions for the harmonics. The SPY-1 and COBRA DANE systems use large phased-array antennas. Spectrum signature data for the SPY-1 and COBRA DANE systems has a measurement error of less than  $\pm 1$  dB in absolute gain. These functions were combined into a linear relationship to allow extrapolation to the aperture-wavelength ratio for the SPS. These SPS radar ratios were used with related correlation functions to develop spatial spectra estimates, referenced to boresight.

The procedure was tested initially in prediction of the third harmonic pattern for the SPY-1 radar system when steered to  $12^\circ$  off boresight with a pattern error distribution over the aperture extending from 0.08 on boresight to 0.17 at  $22^\circ$  off boresight. These values were sufficiently accurate for the SPS pattern estimates (Zaghloul et al., 1978).

Prediction procedures involved mapping the spatial frequencies for the  $f_2$  and  $f_3$  patterns relative to phased-array antenna element spacing and phase patterns (normalizing aperture-wavelength and element-wavelength ratios), and pattern smoothing with a first order spatial filter. Using 10 dB antenna element pattern

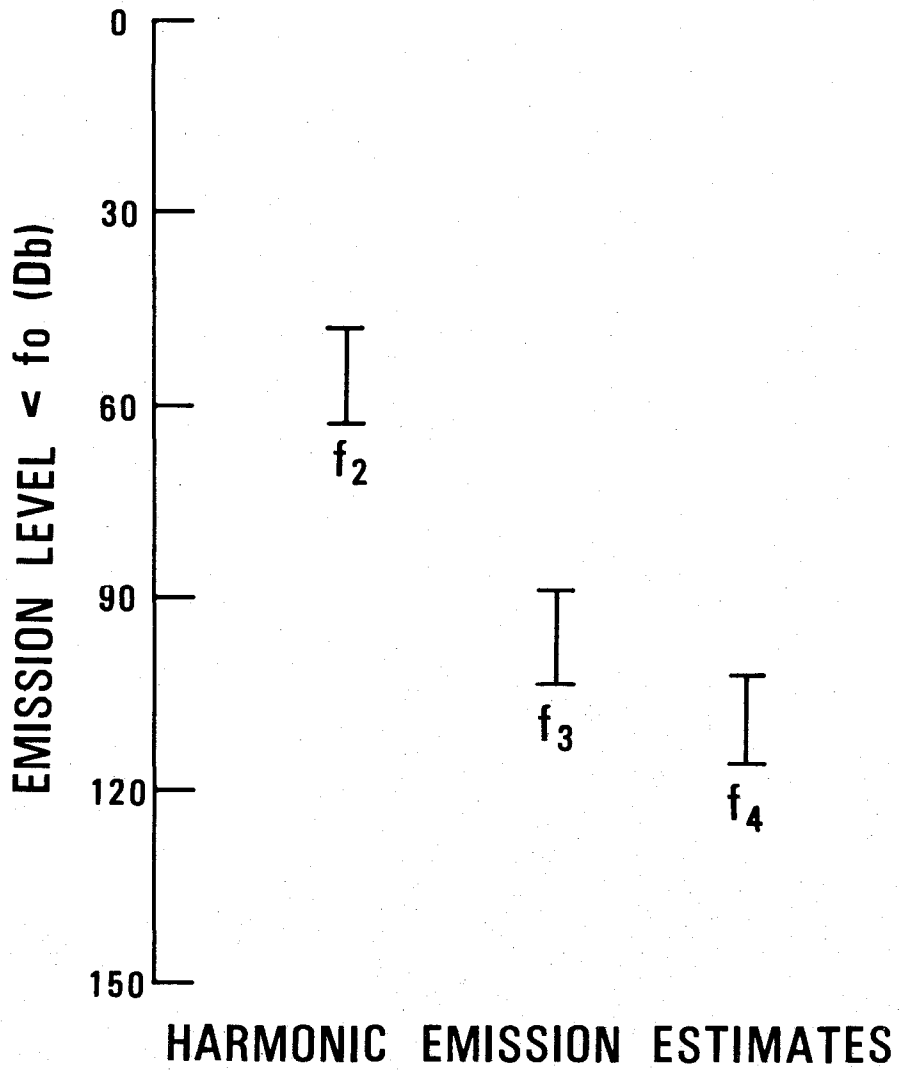


Figure 2. High-power klystron emission at harmonics of the fundamental frequency.

point ratios, and direct aperture-wavelength ratios for the SPS spaceteenna and comparison array spectra, the  $f_2$  and  $f_3$  pattern estimates were derived. These are plotted in Figures 3 and 4. These patterns are used with the fundamental frequency pattern ( $f_0$ ) to develop the total environments for other GEO and LEO satellite locations. With these antenna and tube characteristics, the effective radiated powers from a single SPS satellite at  $90^\circ$  off boresight were derived (Arndt, 1980) and are given in Figure 5.

The SPS space system intermodulation product emissions are an electromagnetic environmental factor primarily for GEO satellites positioned in adjacent orbit slots, and for wideband communications channels used by high altitude LEO satellites (altitudes ranging from 10,000 to 15,000 miles). There are three sources of intermodulation emissions from the SPS satellite:

- a. spaceteenna and space vehicle structures illuminated by the SPS fundamental and harmonic frequencies along with other terrestrial and space sources (e.g. communication terminals, communication satellites, space radar systems, etc);
- b. signal mixing in nonlinear circuit elements in the power generation chain; signal generators, power amplifiers, and phase and frequency control circuitry;
- c. signal mixing in the solar cells and power conditioning circuitry on the SPS space system.

The SPS reference design indicates use of graphite epoxy composite materials for the space vehicle structure, the solar blanket and supporting members, and the spaceteenna. These materials have significant advantages in strength and weight characteristics over any metal structure for a system having the area of an SPS satellite. Bonded joints of trusses and struts represent intermodulation sources where large variations in electrical characteristics over the bond area occur. Priority parameters include resistivity, permitivity, and reluctances (bond-composite boundaries and variations through the composite-bond-composite interfaces). Compared to metals, composites are apparently more sensitive to electrical parameter variations induced by torsional stress across bonded areas.

Intermodulation outputs from any junction are produced by multiple signal illumination of an area having nonlinear resistance and reluctance characteristics with the general relationships as defined as follows:

$$f_{1m} = af_1 \pm bf_2 \quad (1)$$

where a and b are even or odd integers. Frequencies and amplitudes depend on the

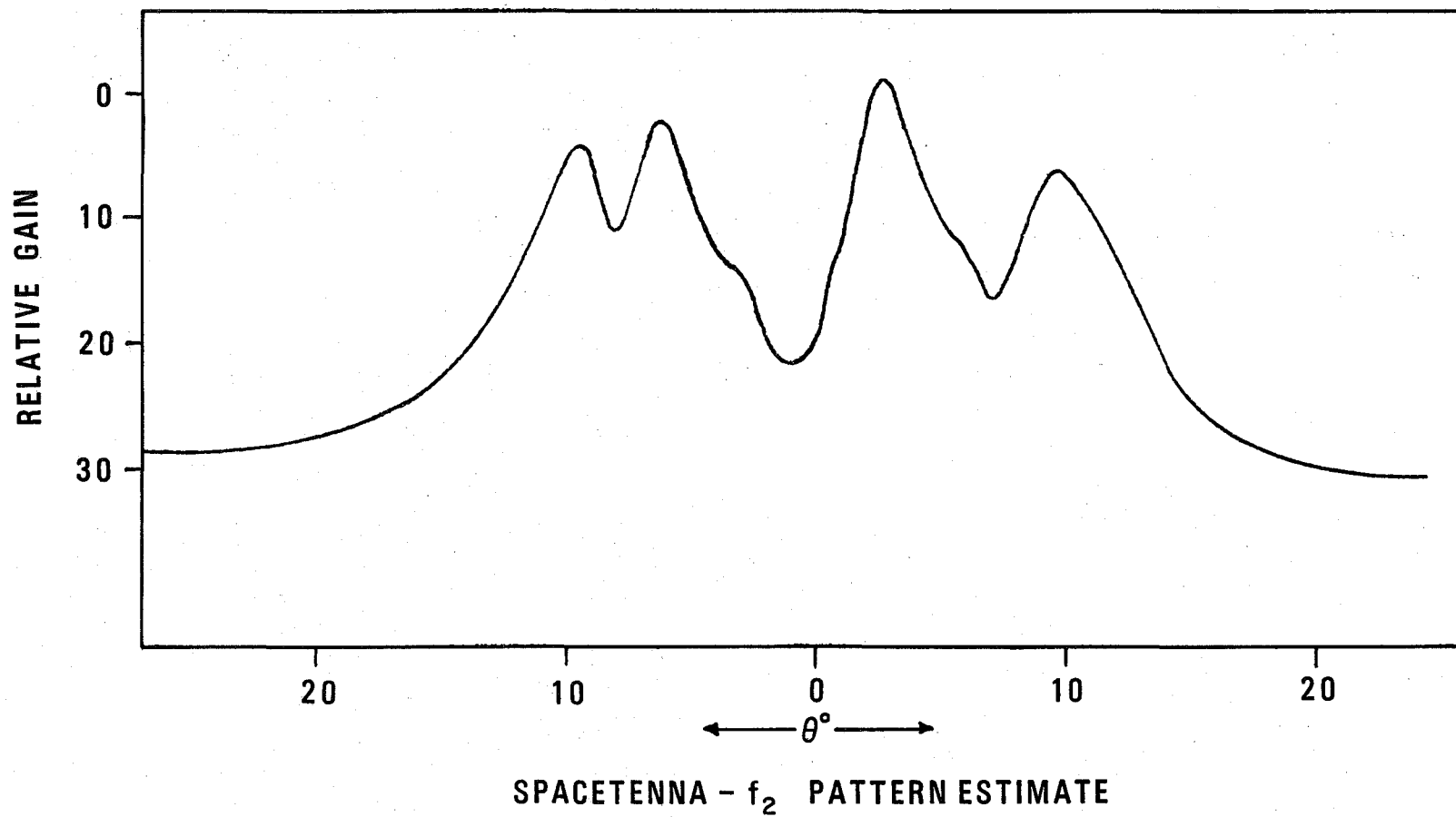


Figure 3. Spacetenna -  $f_2$  pattern estimate.

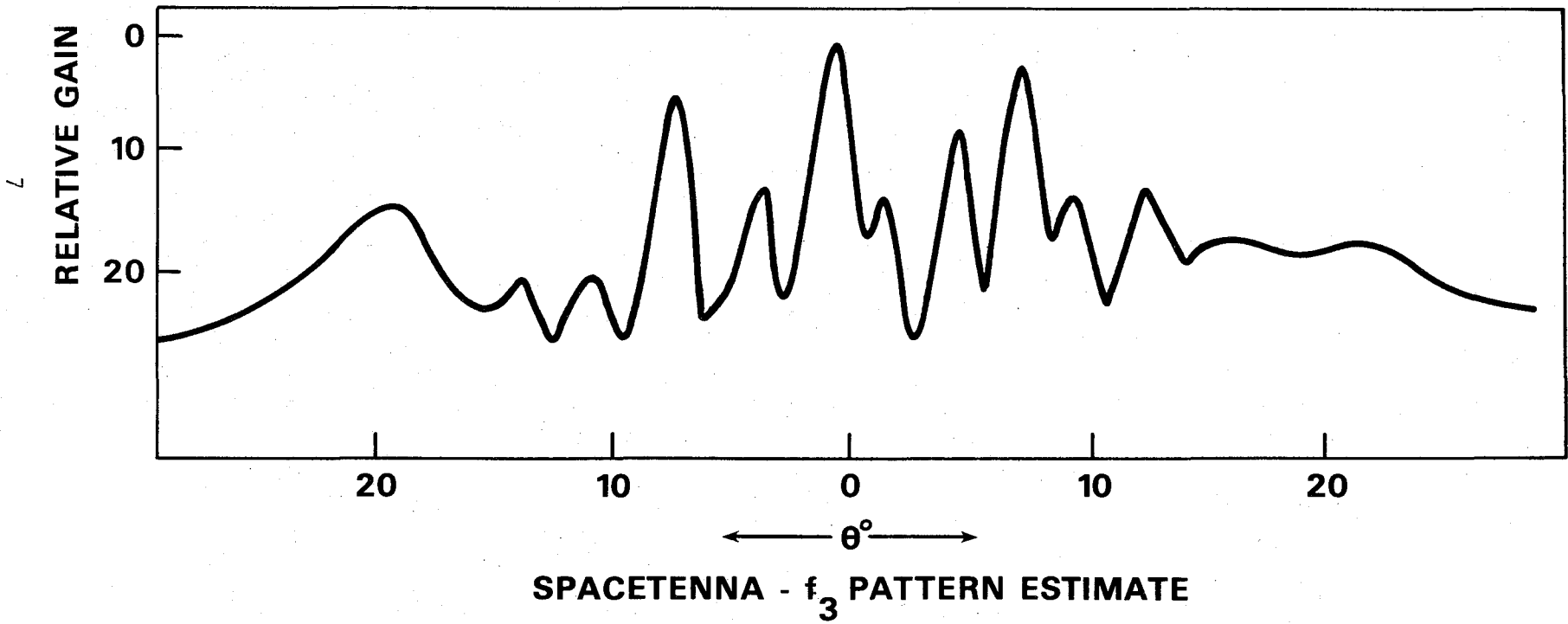


Figure 4. Spacenna -  $f_3$  pattern estimate.

parameters of the nonlinear junction, and the effective aperture and current return path impedances. Wide variations particularly in the junction characteristics, occur because of material impurities, time variant surface conditions, and the torsion stress factors.

	Fundamental (2.45 GHz)	2nd Harmonic (4.96 GHz)	3rd Harmonic (7.35 GHz)	4th Harmonic (9.80 GHz)
Transmit Power = 6.5 x 10 <sup>9</sup> watts at 2.45 GHz				
Transmit Power in dBm	128 dBm	75 dBm	34 dBm	15 dBm
Antenna Gain at 90¼ with respect to boresight	-20 dB	+18 dB	+18 dB	+18 dB
Effective Radiated Power	108 dBm	93 dBm	52 dBm	33 dBm

Figure 5. Spacetenna effective radiated power 90¼ off boresight.

The military services have initiated parameter measurements for various composites to quantify shielding characteristics and junction properties relative to intermodulation generation. Existing data is limited in scope, but indicates a trend toward amplitudes in the range 0.3 to 0.5 relative to aluminum or copper in identical configurations (Hiebert, 1977, 1978).

For composites, the emission frequencies tend toward higher order frequency components. This is correlatable with the higher distributed reluctances and conductivity indicated in the preliminary measurements. No generalizations are justified on the basis of these data.

The interests of the SPS program will be served by continuing military R & D in this area. Measurements during development of bond and surface studies, and depth variations of electrical parameters, will continue to provide data translatable to SPS needs. This information will support a task being initiated by ITS to relate material and bond characteristics, illumination frequencies and amplitudes, and dominant emissions. The military measurements will also include torsional stress variations to indicate bond parameter dependencies, which are uniquely important for the SPS because of the large moments caused by station-keeping orbit adjustments over a system operational lifetime.

Because of the high radiation power of the SPS, careful circuit coupling and configuration design are particularly important to minimize inadvertent intercoupling of signals. Shielding and filtering for power amplifiers, and modulator elements associated with phase or frequency control, must provide 40 to 60 dB isolation to assure suppression of intermodulation components into the final power module by at least 80 to 100 dB. This requires increased emphasis in the shielding area because of reduced isolation due to composite structure shielding characteristics. A representative comparison of shielding effectiveness for aluminum "thick wall" and foil versus various composites is shown in Figure 6. These data imply the possibility of dual shields for the high power modules and control of ground bus currents through large area-low resistance contact areas and single point topology.

Various shielding characteristic data for the 1 MHz to 1 GHz frequency range are presented in Figures 7 through 13 (Hiebert, 1977, 1978) for graphite epoxy forms. These data include sheets, and sheets with access areas having different bonding methods. These plots illustrate the shielding sensitivity for reduction of orbital intermodulation sources. Generally, in the frequency range of 100 MHz to 1 GHz, there is an indicated reduction in shielding effectiveness of composites relative to aluminum of 10 to 30 dB (Heibert, 1978; Wallenberg, 1980).

Another area of intermodulation generation, along with use of composites, would be the solar panel and conditioning circuitry directly coupled to groups of solar cells as these are exposed to SPS power along with exposure by other satellite illumination sources. Space radars to be employed for military, earth resource, and atmospheric monitor applications and transmissions from GEO satellites in orbital positions adjacent to SPS represent the primary EM environment as it would exist today. Future space communication operations that would be impacted by SPS concern satellite to satellite modes, where SPS will be stationed between communication satellites (see Figure 14). As the figure indicates, the large cross section of the SPS satellite ( $\sim 40 \text{ km}^2$ ) represents a generally unacceptable signal multipath situation as depicted by the single satellite geometry. The SPS will require an on-board frequency translator repeater to support this satellite to satellite communication mode, as shown in Figure 15. These additional signals will illuminate portions of the SPS satellite solar panels, thus mixing with ambient SPS power-beam fundamental and harmonic components. The large active solar panel area represents a major source of sum and difference frequency products for combinations of SPS, radar, and communication signals and increases spurious emissions and on-board EMI problems.

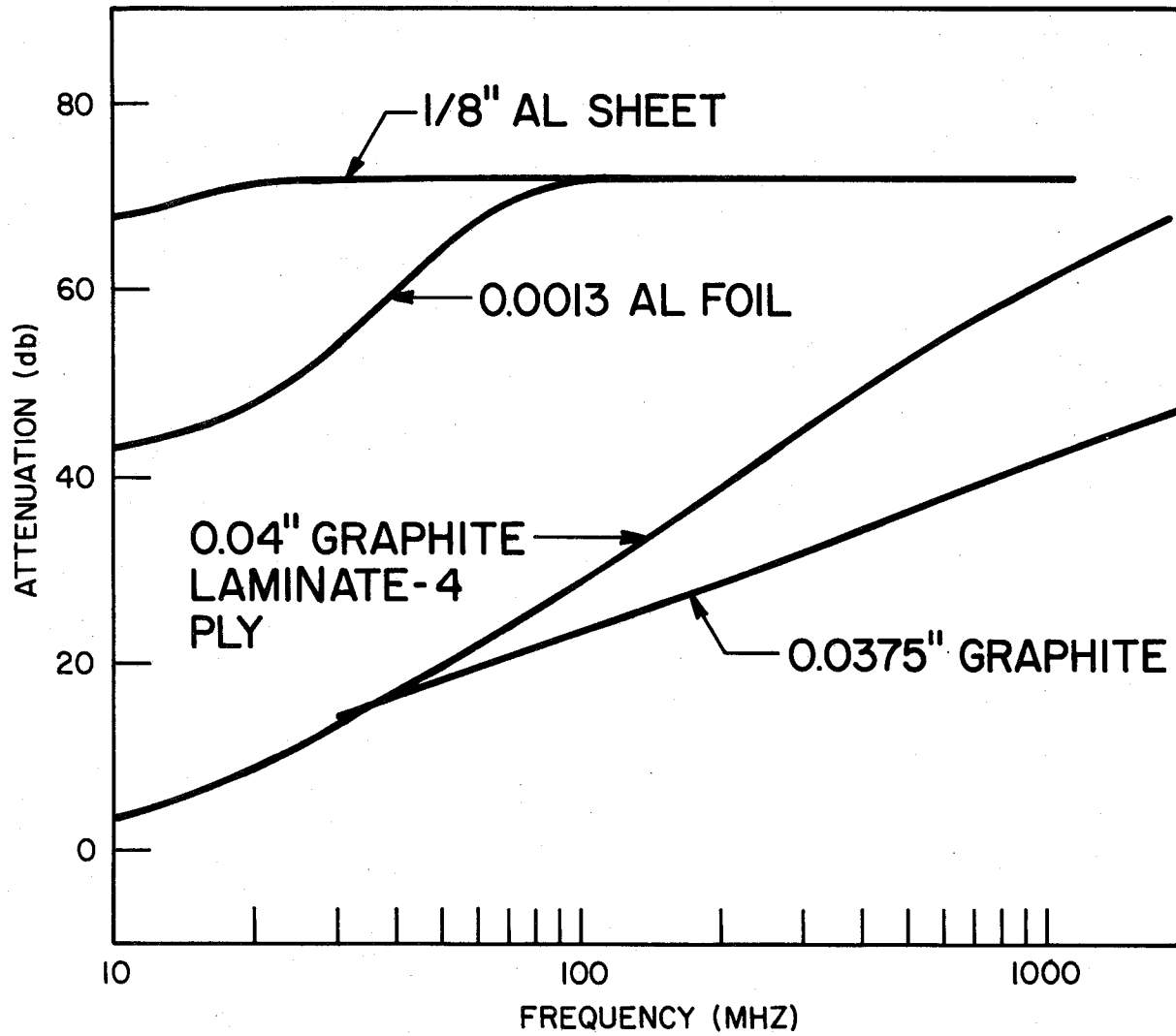


Figure 6. H-Field shielding effectiveness.

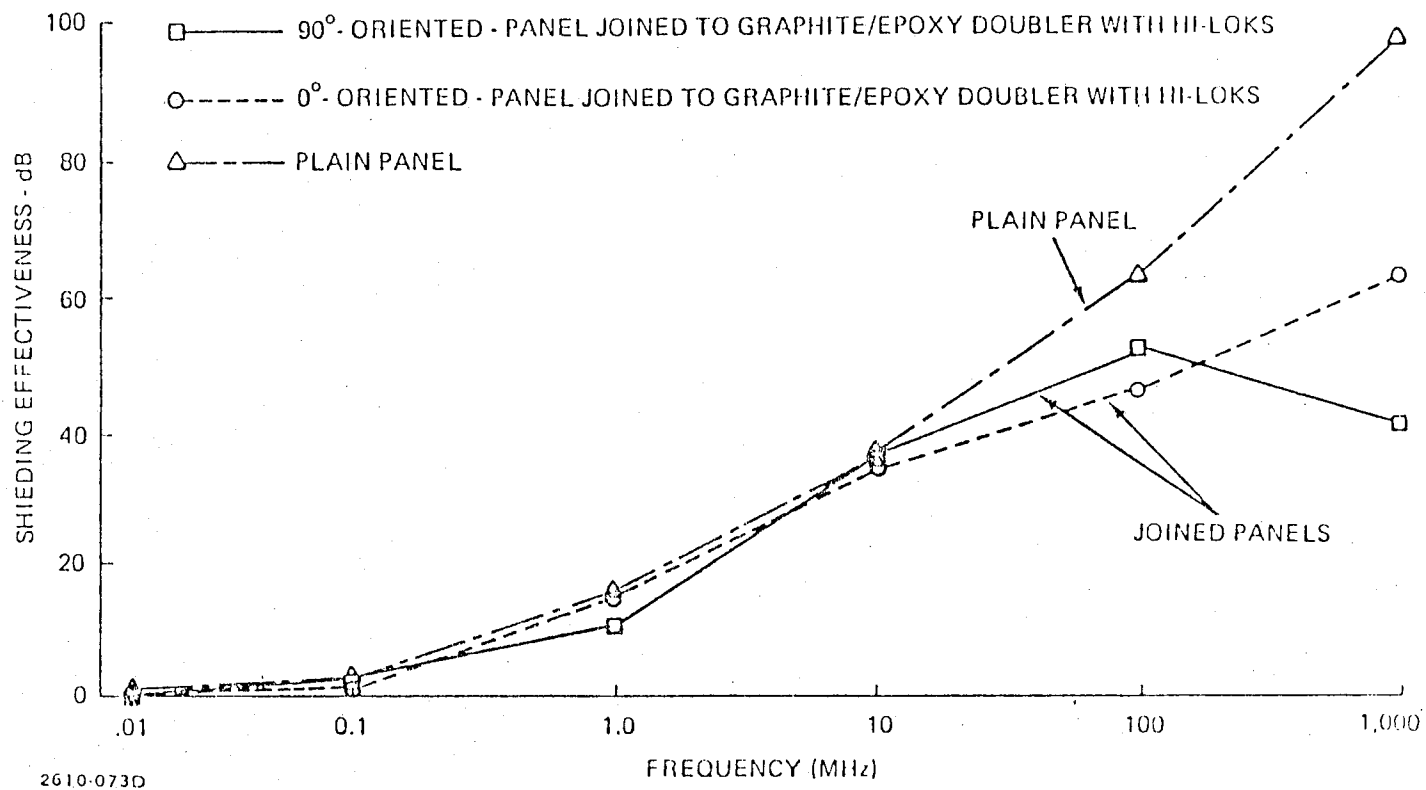


Figure 7. Magnetic shielding effectiveness of graphite/epoxy panel and panels joined by Hi-Loks.

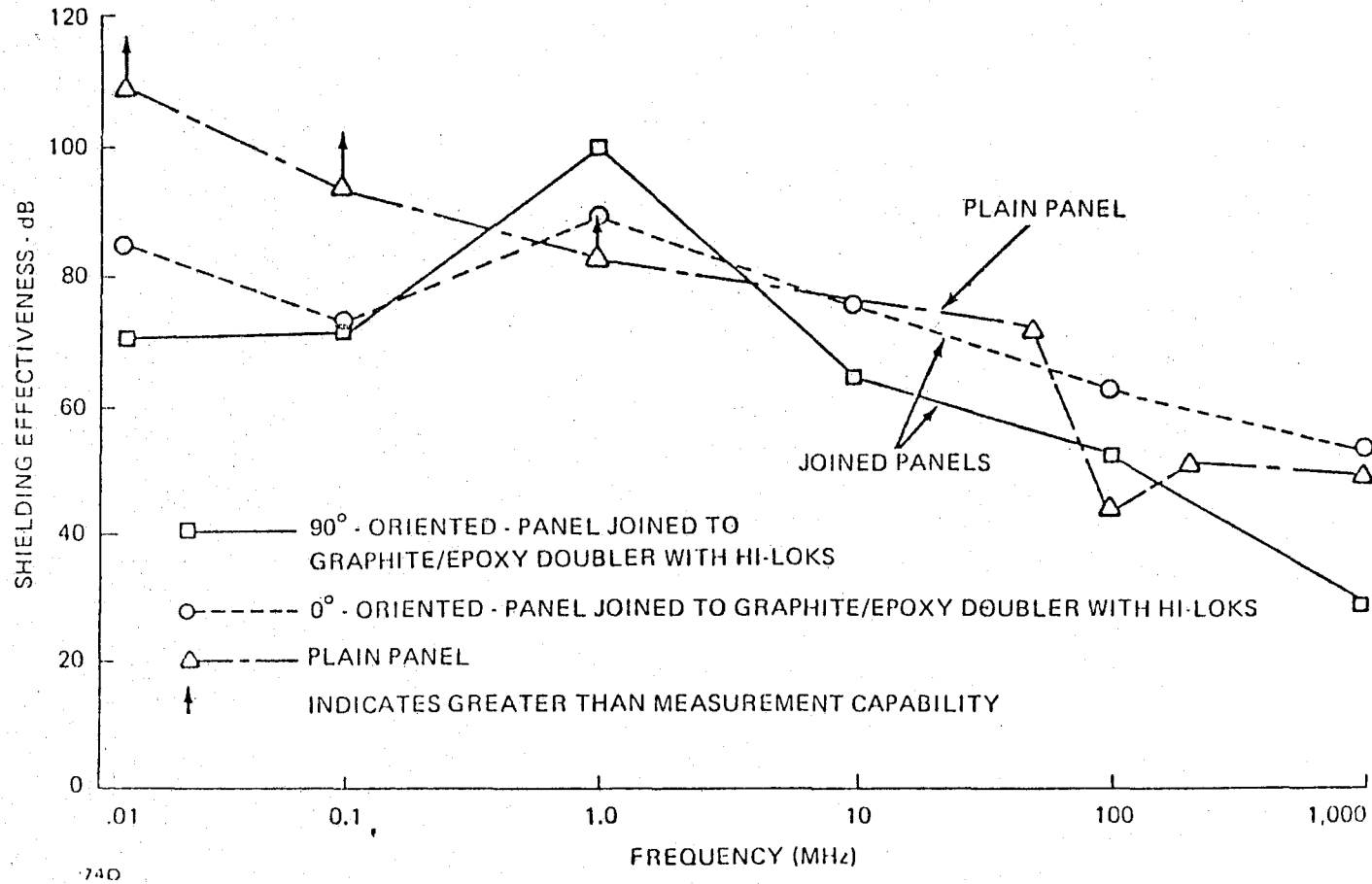


Figure 8. E-Field shielding effectiveness of graphite/epoxy panel and panels joined with Hi-Loks.

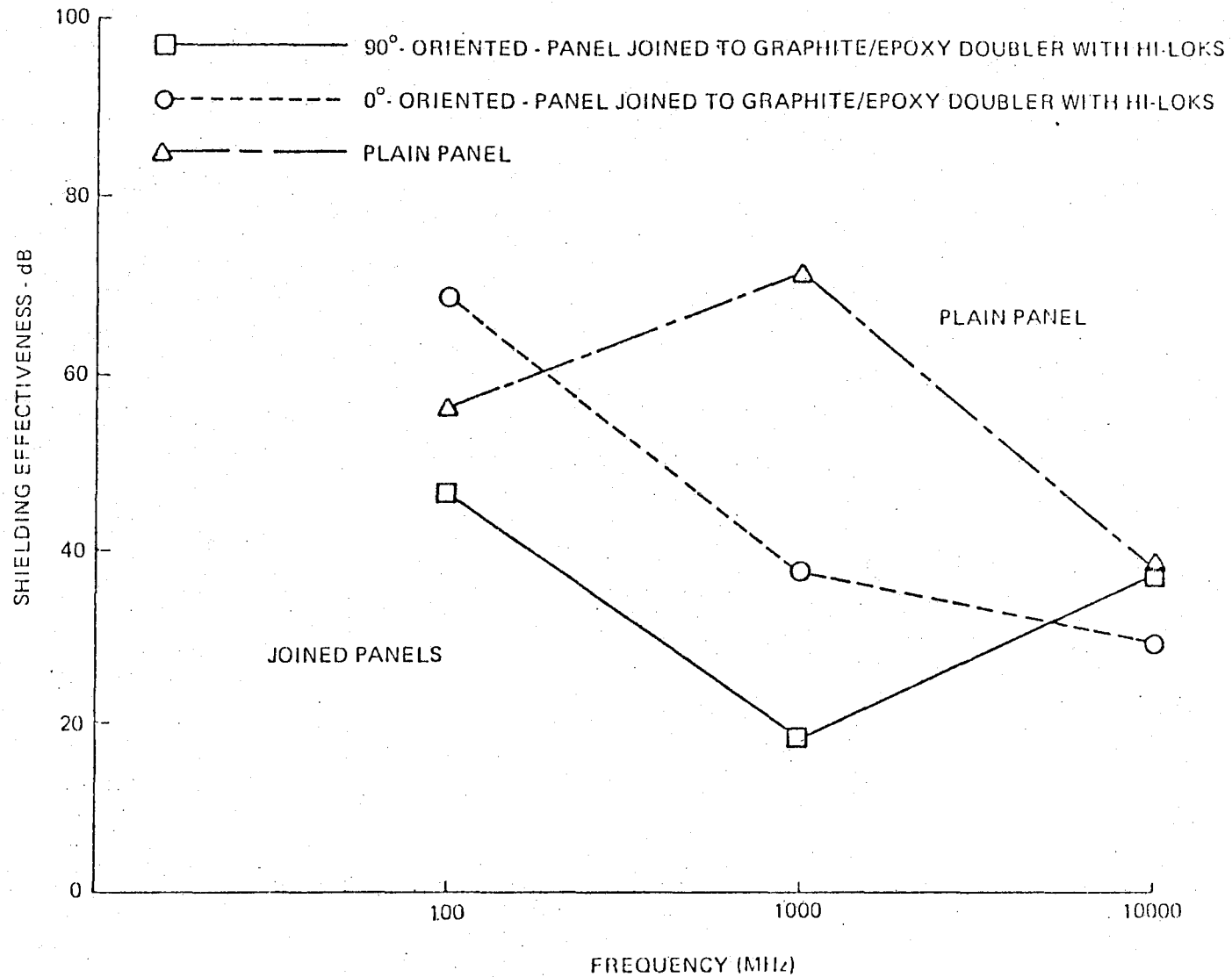


Figure 9. Plane-wave shielding effectiveness of graphite/epoxy plain panel and panels joined with Hi-Loks (QR V).

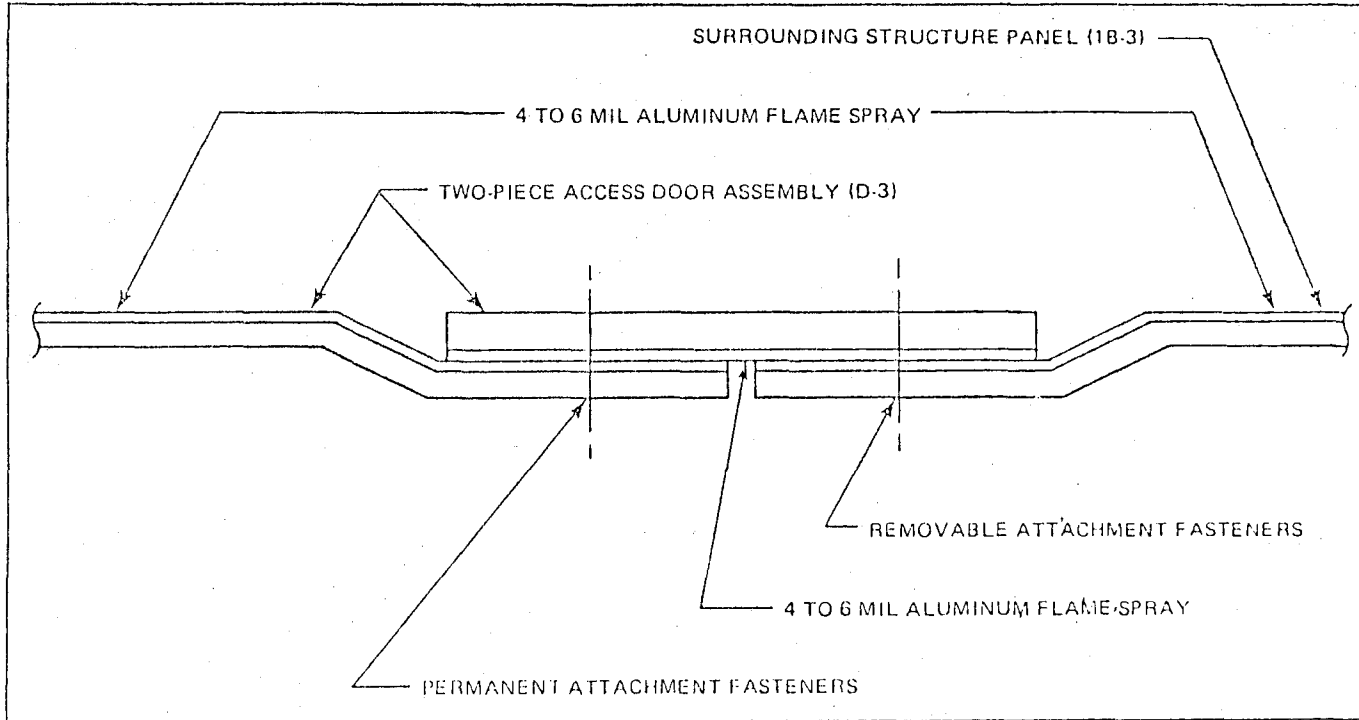


Figure 10. Attachment interface cross-section of panel and access door.

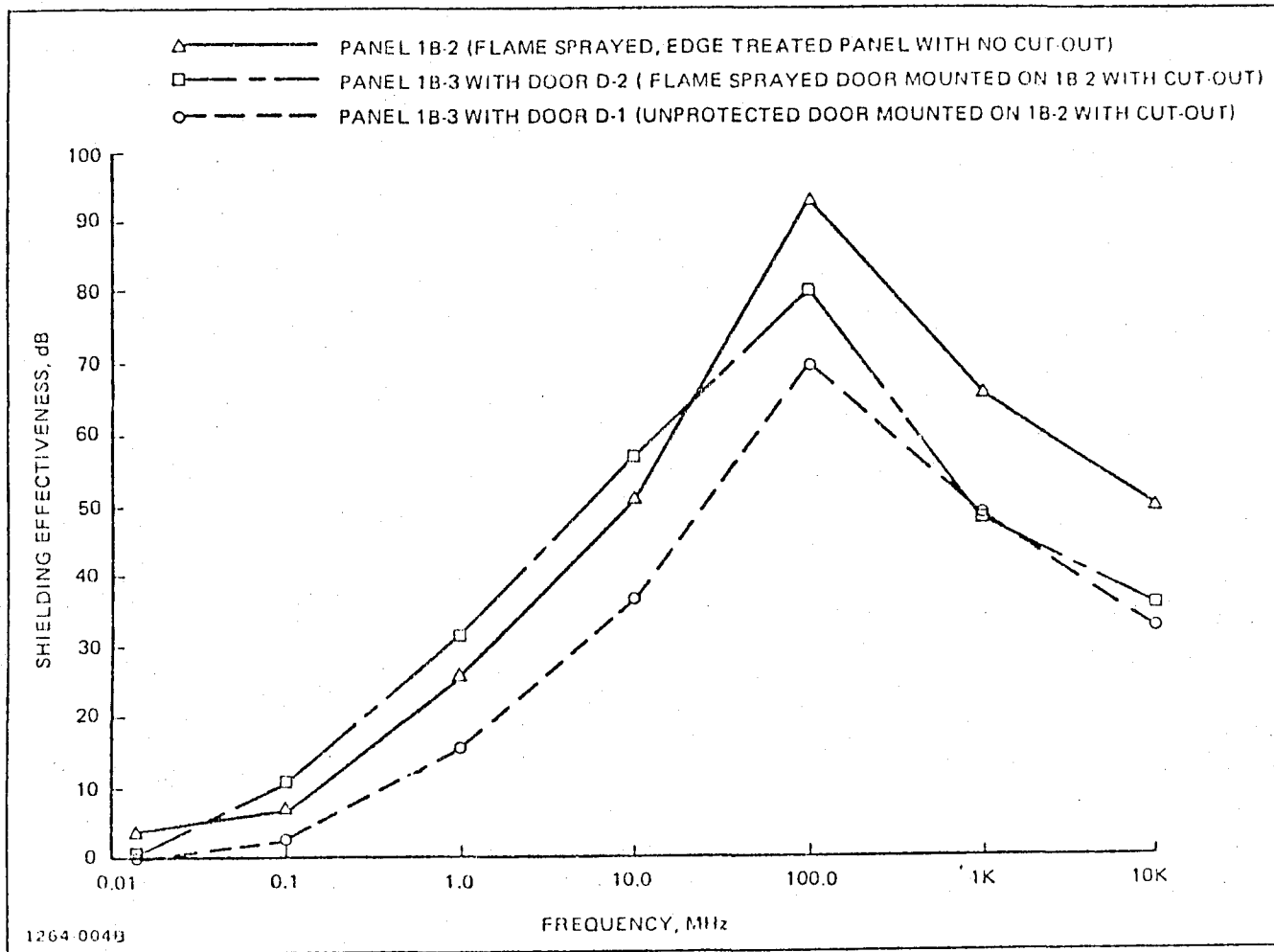


Figure 11. H-Field shielding effectiveness of graphite/epoxy access door specimens.

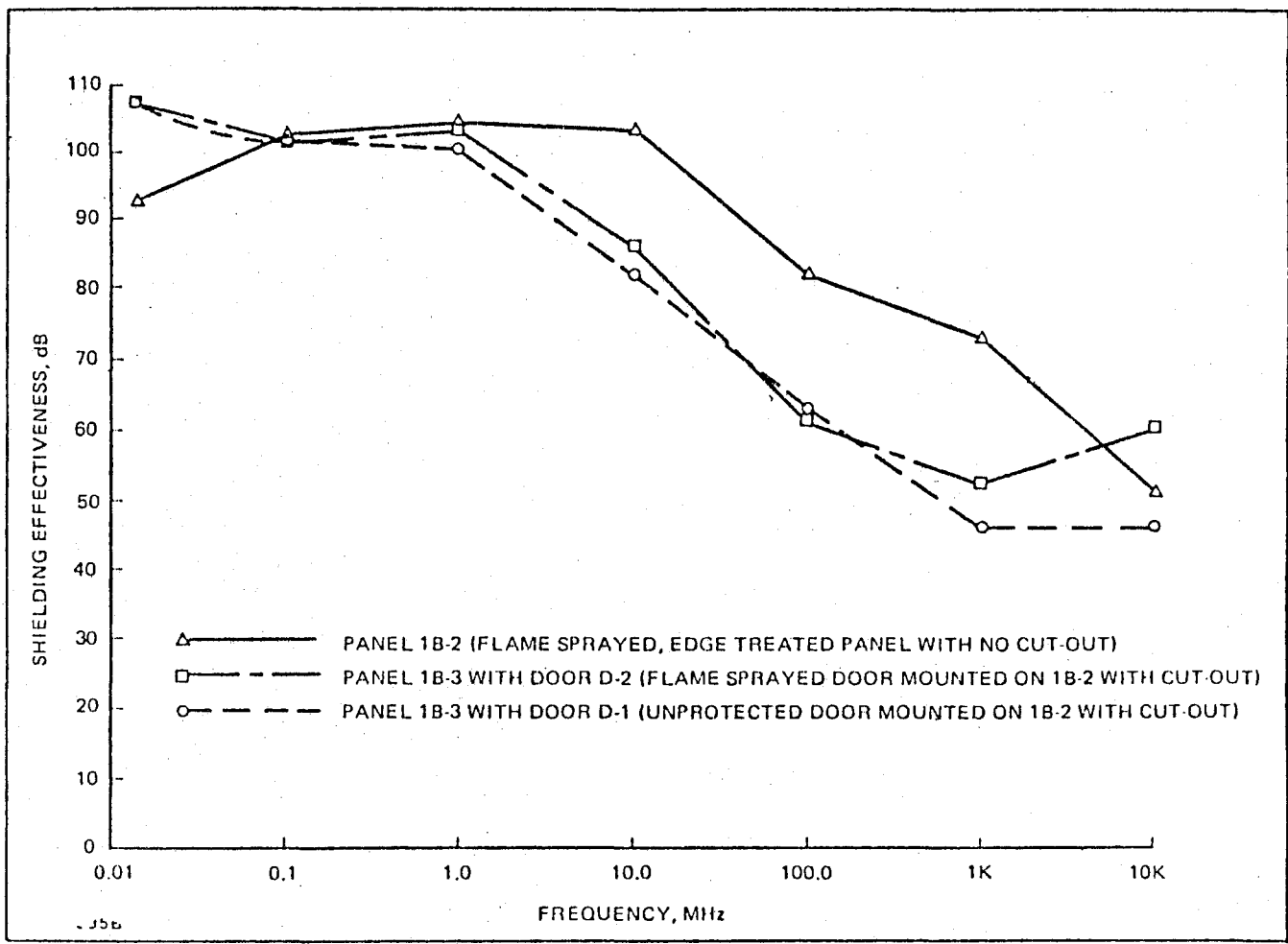


Figure 12. E-Field shielding effectiveness of graphite/epoxy access door specimens.

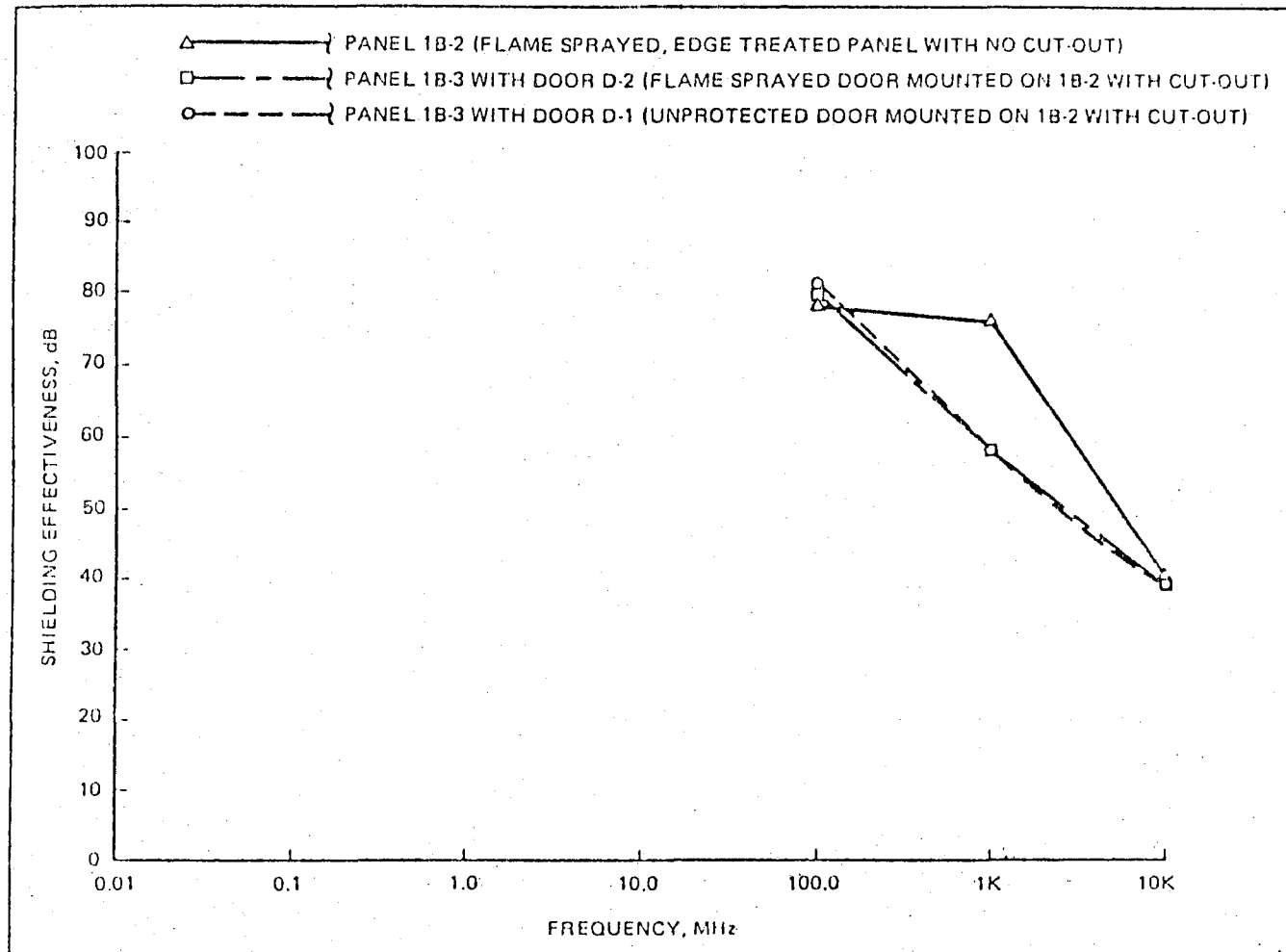


Figure 13. Plane-wave shielding effectiveness of graphite/epoxy access door specimen.

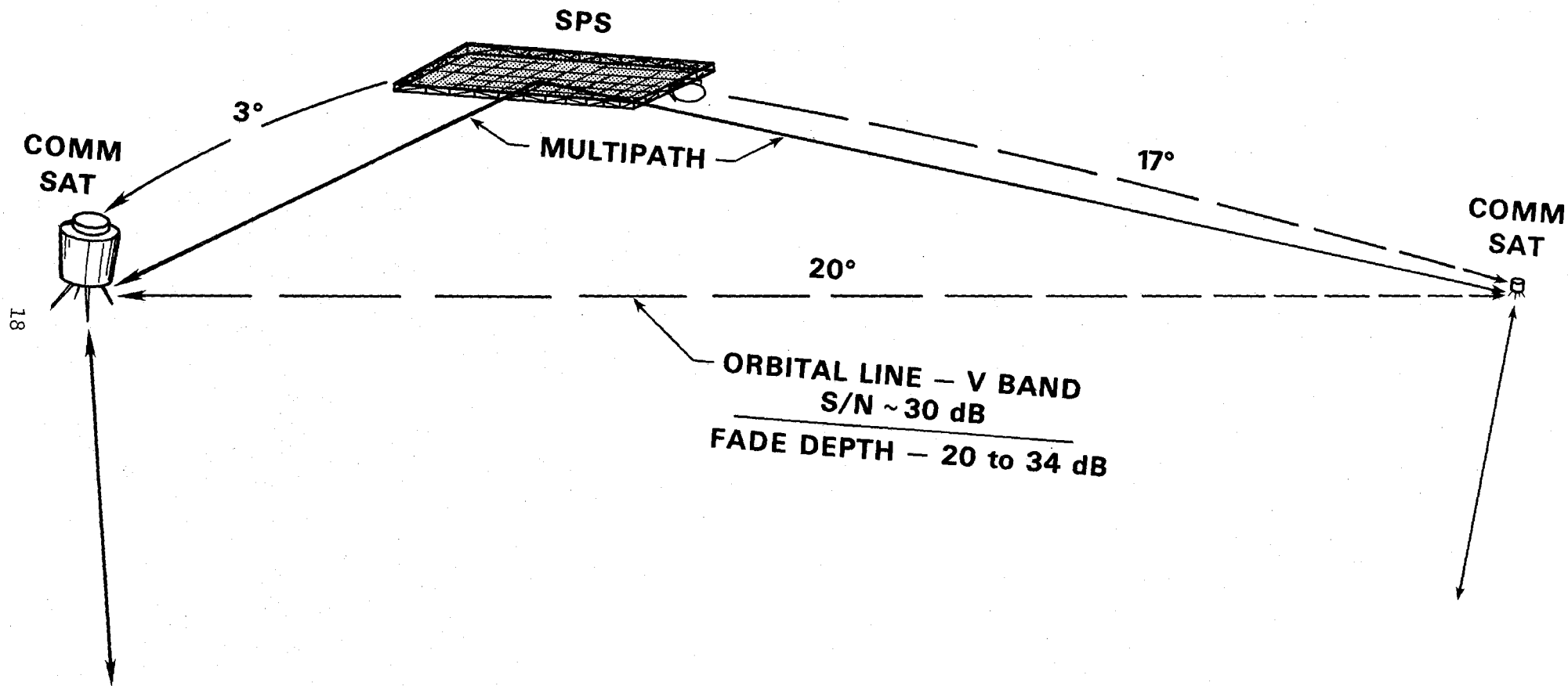


Figure 14. Satellite geometry showing possible signal multipath situation.

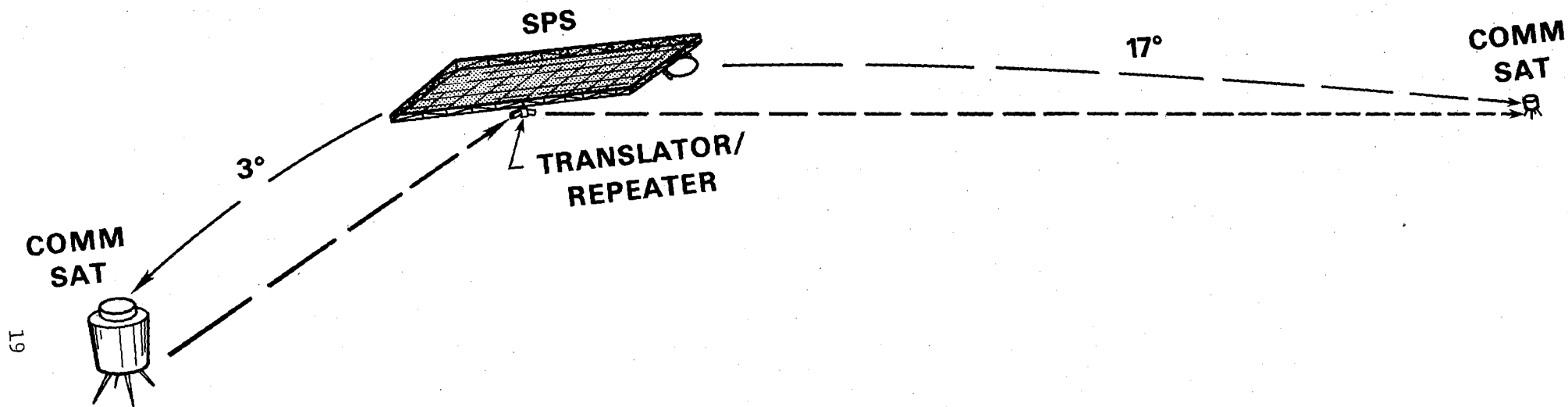


Figure 15. SPS on-board translator/repeater in support of satellite-to-satellite communication mode.

A functional diagram of the solar cell and conditioning system is diagrammed in Figure 16. The cell is electrically a diode usually biased to maximize current flow for a range of solar illumination. Cells are connected in combinations of series and parallel through voltage and current controllers. The voltage and current controllers would consist of summing amplifiers and silicon controlled rectifiers (SCR). The SCR units represent a nonlinear impedance at the input terminal, coupling switching frequency components into the cell circuits. The intermodulation modes are described in Figure 17.

Mitigation methods include band-stop filters in the cell current lines or a wire mesh around the cell blanket. The latter should be a square grid mesh with a mesh dimension of less than one half the wavelength of the highest illuminating frequency and a wire size in the AWG 26 to 32 range. This wire size prevents blockage of solar cell illumination from the sun. To minimize circulating current effects in the small diameter mesh, connections to a vehicle ground bus should be provided at 10-30 ft. intervals (Skolnik, 1962).

There may be some effect on the EM environment for GEO and high altitude LEO satellites from control loop instabilities for the SPS. Figure 18 shows a block diagram of a possible control loop configuration. Because of the time constants involved on such a long two-way path and the large spacetenna gain, aim point control instabilities caused by propagation anomalies and control characteristics represent a serious design problem. If there were such instabilities, as the control loop worked towards stabilization, the sidelobe amplitude and phase would vary accordingly, depending on perturbation magnitudes, time-spectrum properties, and control logic configuration. This would present a changing field for close-in satellites.

Principal driving forces affecting stability margins are transient meteorological events, periods of turbulent troposphere conditions, and mechanical oscillation of the solar cell panel-spacetenna structures. Control-loop modulation spectra in the 1 to 40 Hz range results from these longer term effects, with components extending to 100 Hz for transient events.

## 2. GEO SATELLITES

### 2.1 Uplink Antenna Patterns

Antenna patterns for terrestrial terminals and satellite receivers are of nearly equal importance in establishing orbit separation constraints between SPS

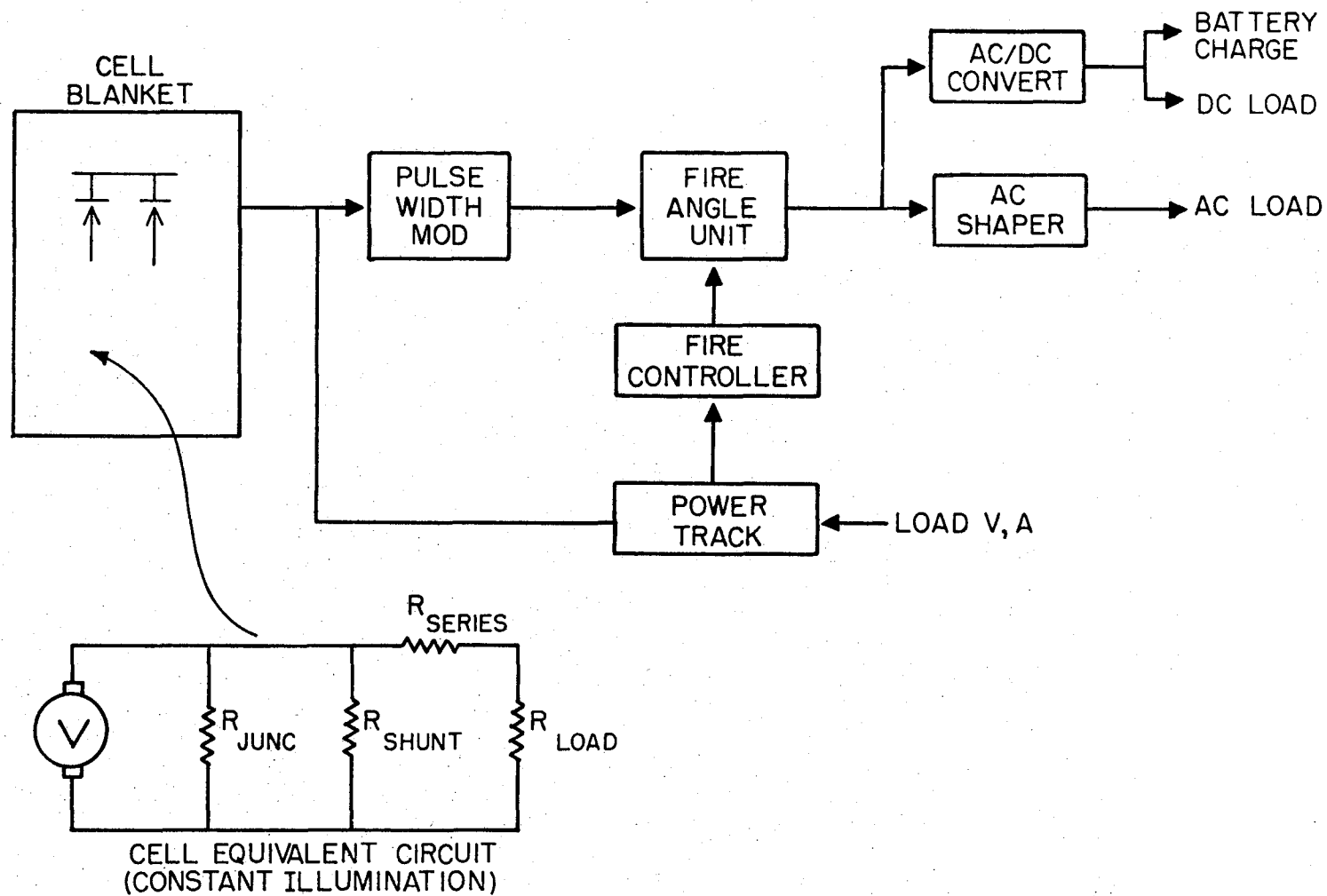


Figure 16. Functional diagram of a solar cell and conditioning system.

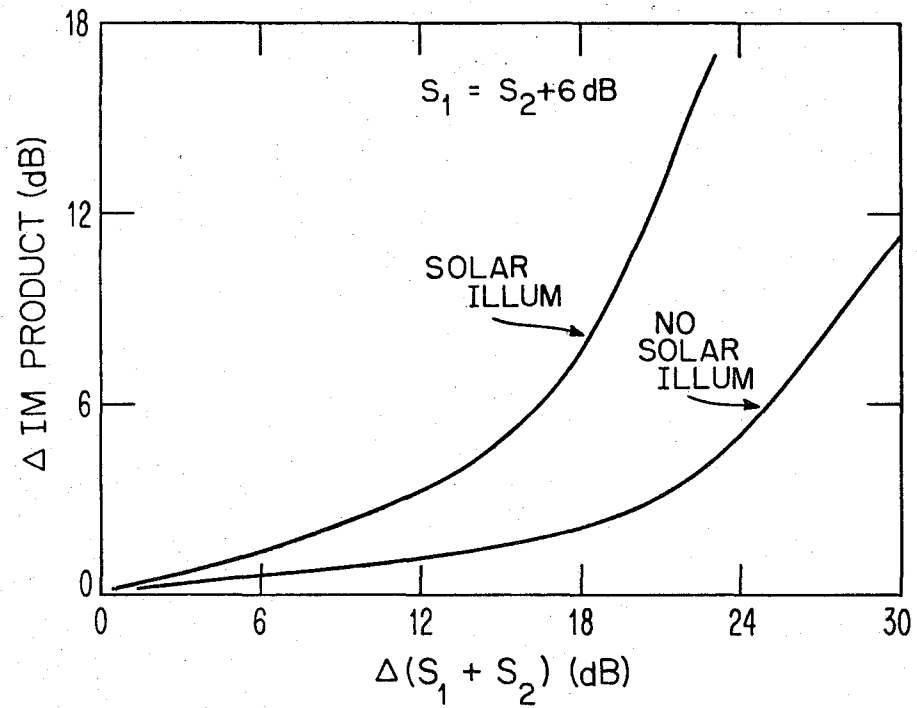


Figure 17. SCR intermodulation modes.

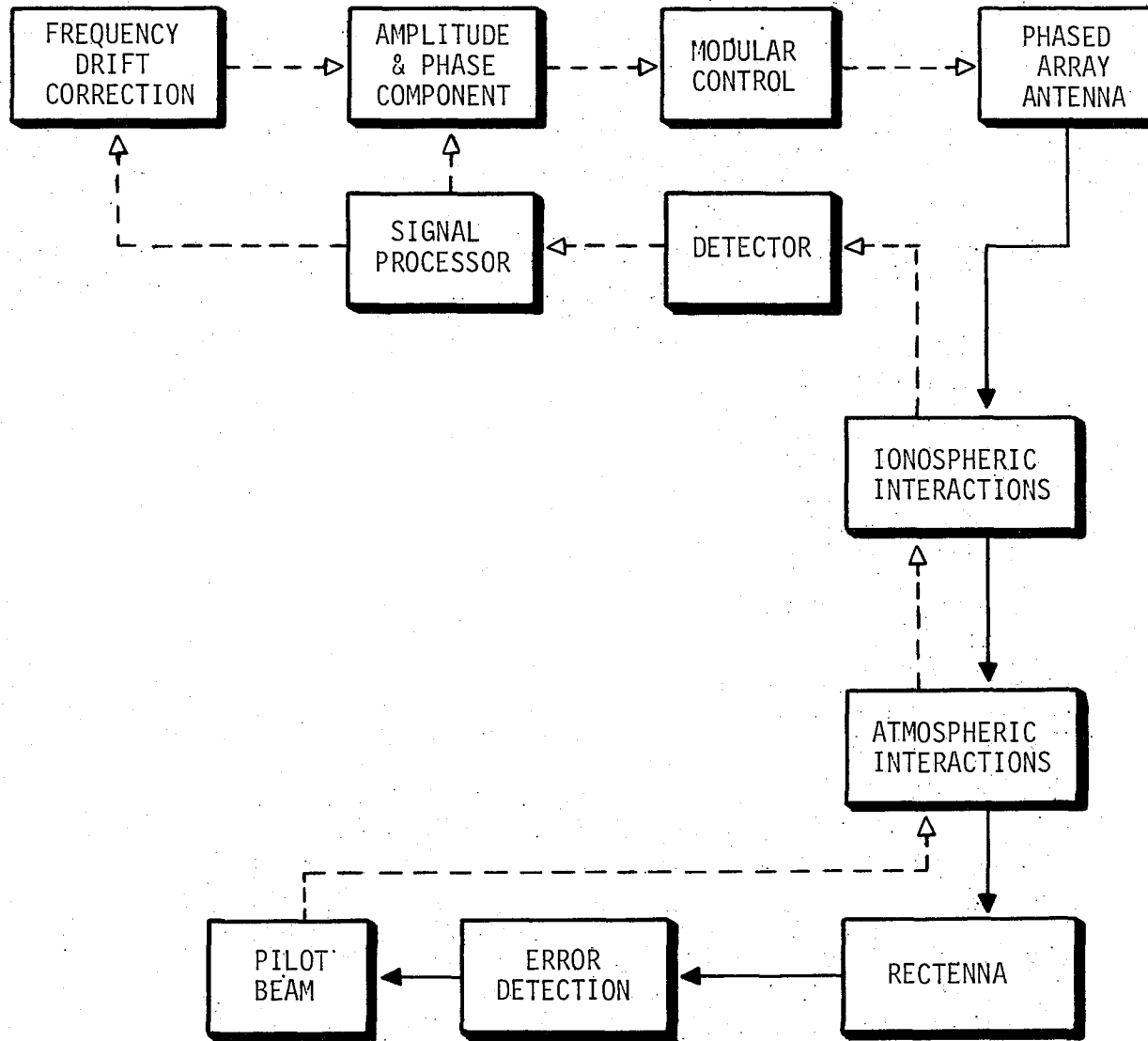


Figure 18. Block diagram of possible SPS control loop configuration.

and communications satellites. The satellite receiver antenna pattern is the primary mode of coupling of SPS fundamental and harmonic frequencies into a transponder signal channel. Terrestrial terminal patterns concern satellite signal tracking stability with interference from SPS emissions.

Satellite receiver antennas employ two patterns: earth or hemisphere coverage, and spot beams for small area coverage. The latter contributes to increased frequency usage efficiency as well as reducing interference potential from other terrestrial transmissions. A typical hemisphere coverage pattern is indicated in Figure 19, the pattern being approximately 6 to 12° in angle width. An earth coverage pattern requires a beamwidth of 25 to 30° depending on service requirements near the horizon. Spot beam modes use a beamwidth in the 0.25 to 1° range to transmit or receive between a satellite and a terminal serving a metropolitan area, county, or multi-county area. Spot beam operations will be concentrated in the 12 to 14 GHz and 20 to 30 GHz bands because of satellite aperture considerations. Earth and hemisphere beams presently use horn antennas. Spot beams employ single and multiple paraboloid antennas, with single and multiple feed elements for each reflector. Beam switching involves selection of feed unit and reflector. Since the beams are at least three times the aim point area, small variations in satellite attitude caused by drift and station-keeping control will not affect communication link performance, (Getsinger, 1977).

Future satellite antennas will use a single phased array for large area and spot coverage requirements. Beam coverage selection and spot beam selection based on channel usage and message address would be controlled through a computer/processor. Array patterns as controlled by phaser and gain components are selected by message addresses from NDRO storage. Total beam excursion would be about  $\pm 30^\circ$ , which is within current array technology. For frequencies in the 20 to 50 GHz range, spot beamwidth may be increased by 20 to 50% to reduce the probability of deep fades ( $\sim 20$  to 30 dB) because of atmosphere anomalies, (Edelson et al., 1978; Gould et al., 1975; Morgan, 1978; Welty, 1978).

A typical 0.5° spot pattern is plotted in Figure 20. Effects of SPS coorbital interference with the array operation are listed below. Coupling of SPS components is dependent on array patterns for the available phaser-gain functions at the SPS frequencies.

1. Interference entry through side lobes causing transient address errors and stepped beam jitter.
2. Incorrect beam selection because of interference induced message component error. This effect is magnified with spot beam operation because of the limited spatial coverage.

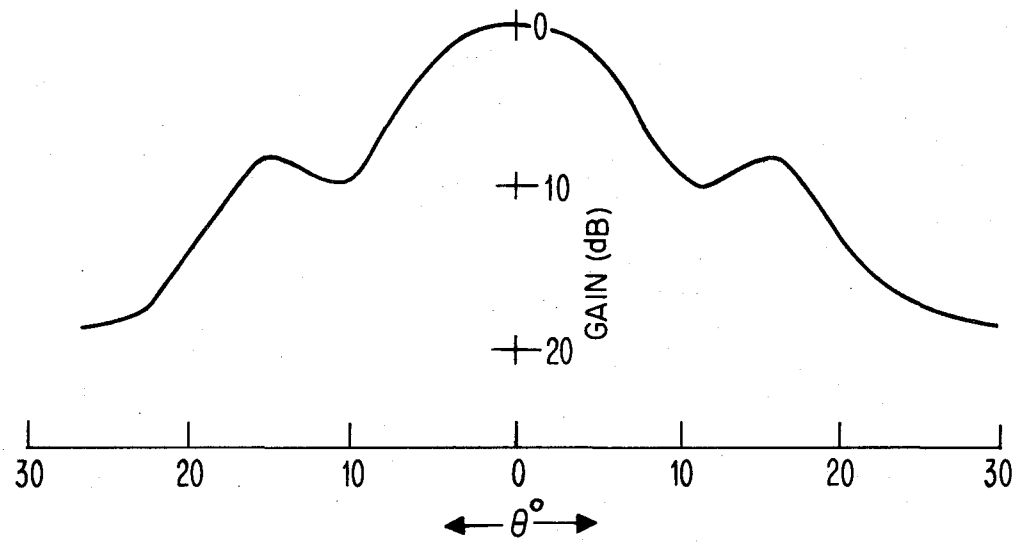


Figure 19. A typical satellite hemisphere coverage pattern.

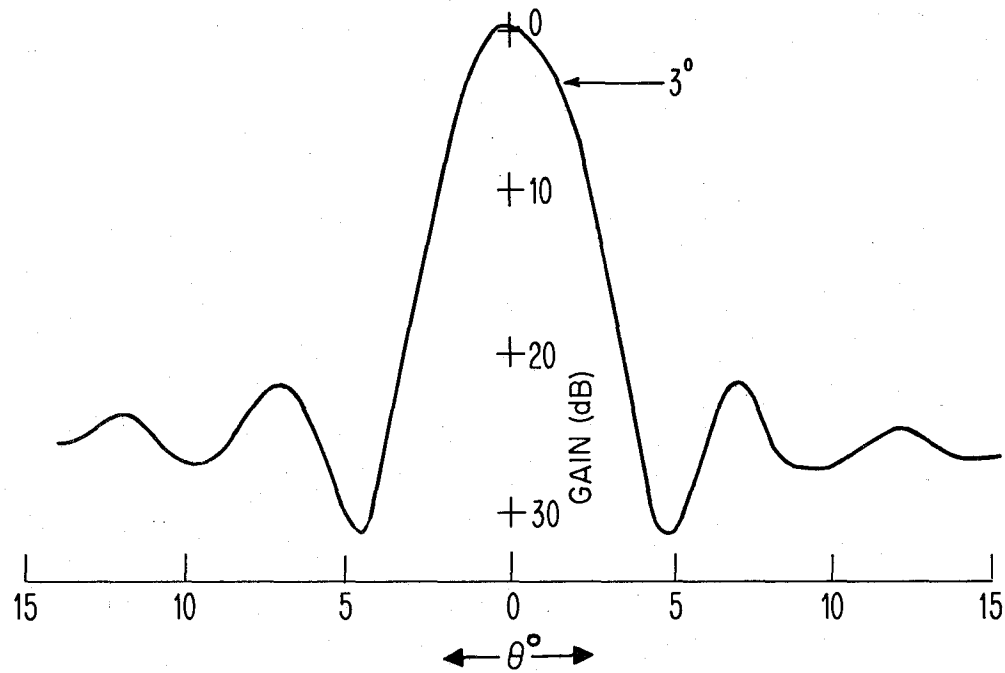


Figure 20. A typical satellite spot beam antenna pattern.

3. With the minimal beamwidth spot using pilot carrier tracking, sidelobe out-of-channel cw interference will cause angular jitter with attendant escalation in BER. Typical error responses as previously measured with out-of-band cw interference into Space Data and Tracking System (SPATS) receivers are presented in Figure 21.

## 2.2 Signal Processing Satellites

A general signal processing satellite configuration is diagrammed in Figure 22. This system provides an advanced message and channel processing capability relative to current transponders, a limited switching facility, and a message buffer. Area and spot-beam array antennas and the buffer capabilities provide time and space multiplexing operations for terrestrial point-to-point and point-to-area communications modes. These modes would primarily operate in the 12 to 14 GHz and 20 to 30 GHz bands for spot modes, and the 12 to 14 GHz and 6 to 4 GHz bands (Getsinger, 1977).

Interference sensitivities are listed.

1. Coupling of SPS emissions into array side lobes causing array step jitter and message BER increase.
2. Increase of message BER; synchronization uncertainties, address errors with incorrect spot beam assignments, and data errors.
3. Reduced system and channel through-put because of address and beam control errors.

To maximize space system efficiency, satellite-satellite message transfer will be employed to reduce uplink and downlink transfers for transcontinental traffic. The large reflection cross section ( $\sim 5 \cdot 10^4 \text{ m}^2$  at 6 GHz,  $\sim 10^9 \text{ m}^2$  at V band) of the SPS imposes an unacceptable multipath for the satellite-satellite mode. A typical multipath spectra for East-West satellite communications with an SPS reflection component is indicated in Figure 23. This spectra is based on an SPS orbital motion of  $\pm 0.1^\circ$  over a 24-hr period, and a communications satellite orbital movement of  $\pm 0.1^\circ$  over a 12-hr period. The SPS is represented as a flat reflector of 10 x 5 km with one-half the reflectance of an identical metal configuration at the 2.45 GHz frequency. This situation can readily be remedied with a frequency translator transponder on the SPS; having a transmitted power of 100 to 200 W for this V band example will provide a S/N at the receiving satellite of about 30 dB. No processing capabilities are required for the transponder.

## 2.3 GEO Satellite Receivers

Receivers employed for GEO communications satellites extend from frequency translators to systems that include switching between area and spot-beam antennas. Modulation and message modes include analog FM multiplier, digital FM multiplier, and spread-spectrum TDMA operations.

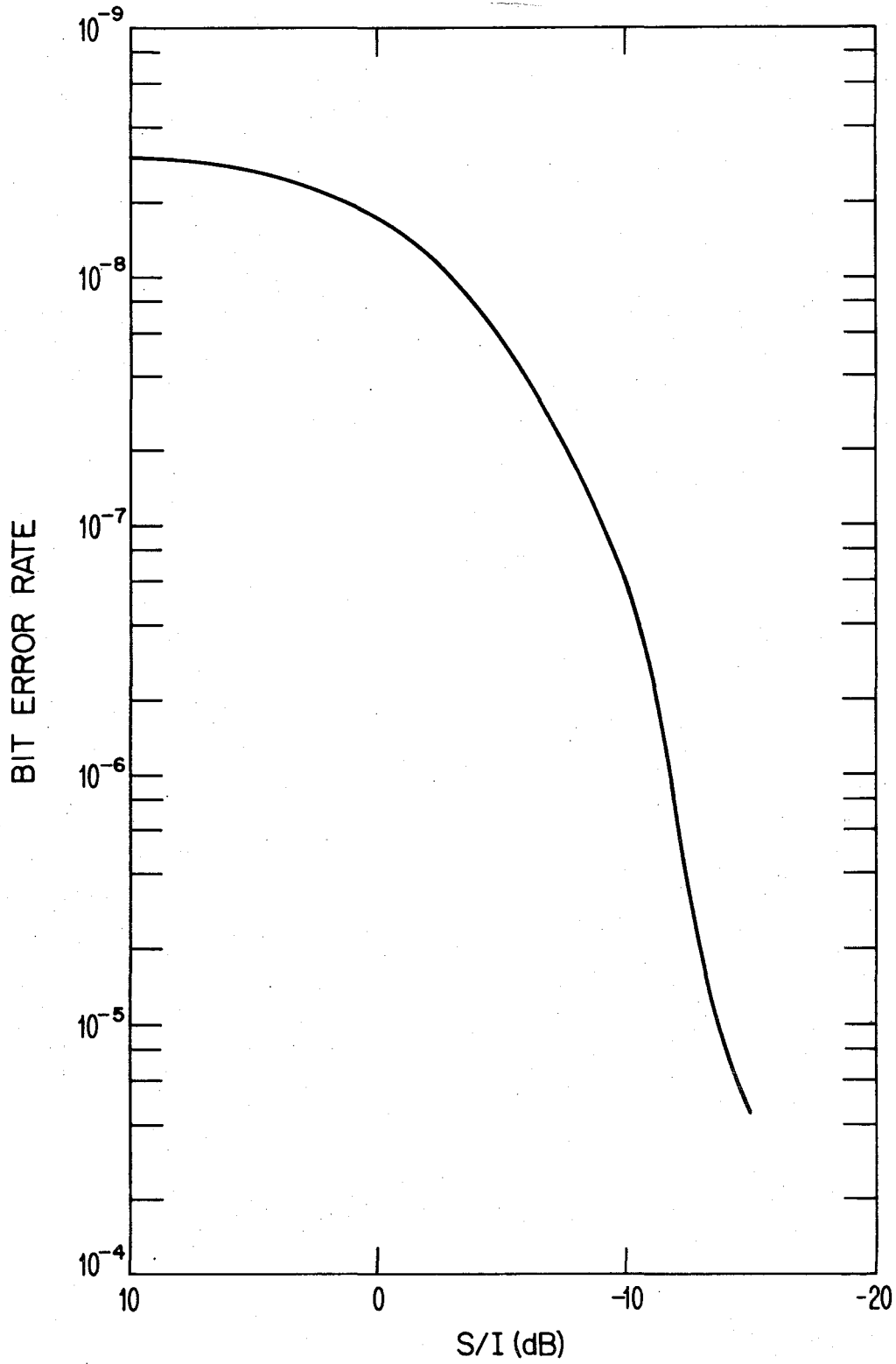


Figure 21. SPATS error response - single cw interferer.

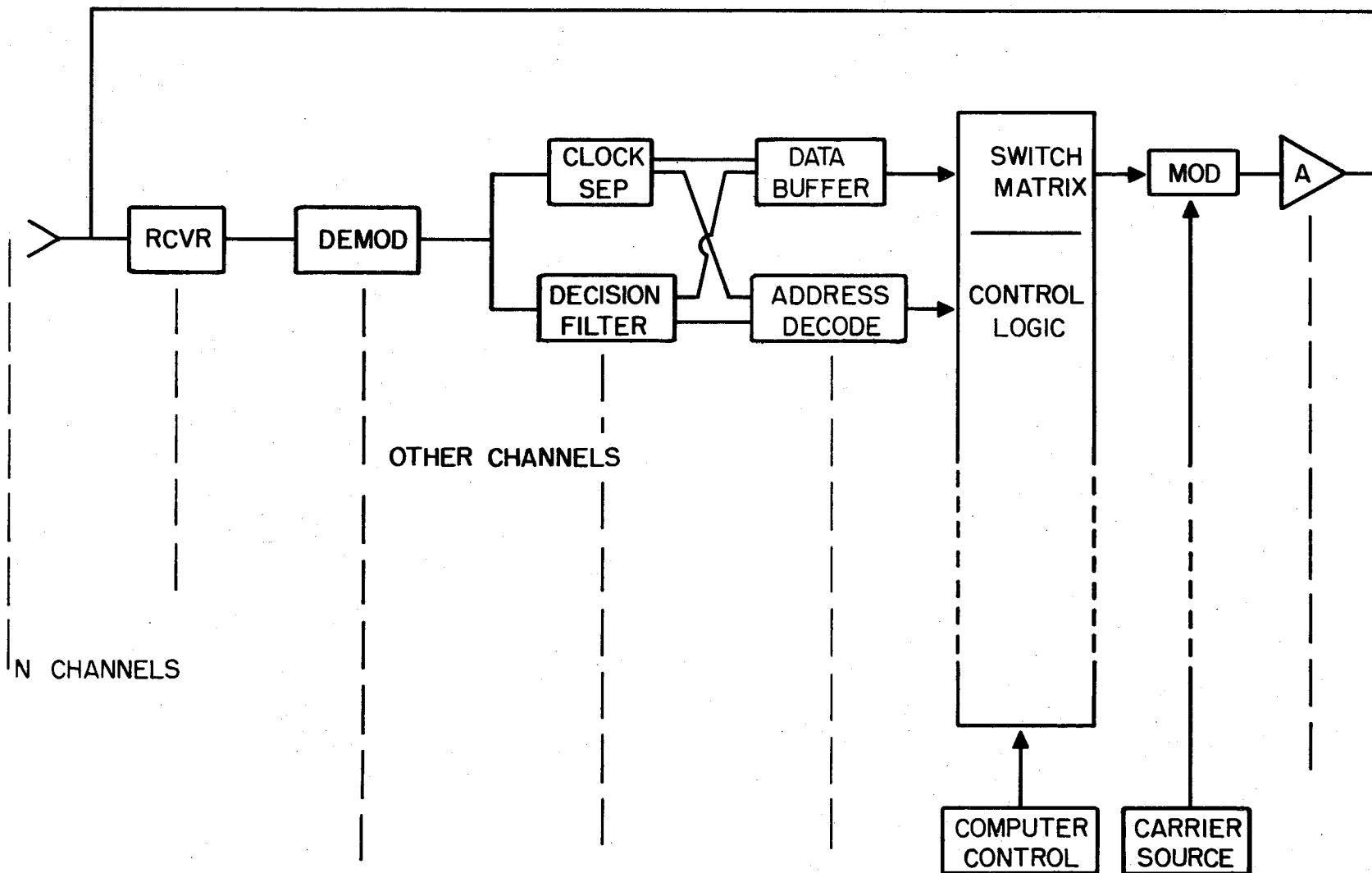


Figure 22. General signal processing satellite block diagram.

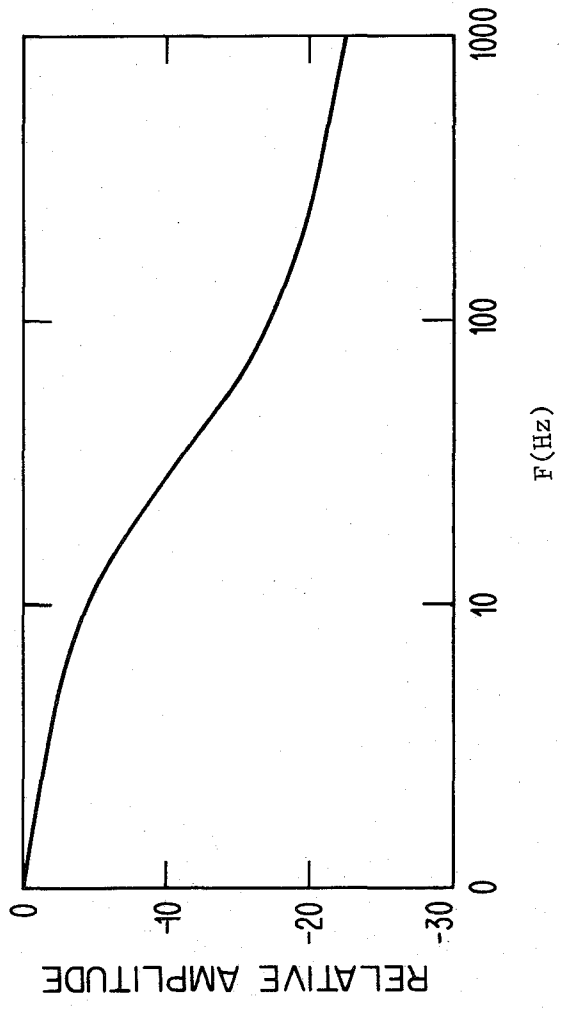


Figure 23. Multipath modulation spectra.

Functional organizations for these satellite receivers and message processing and conversion modes are presented in Figure 24. The principal functions include rf amplification, conversion, noise limiting, switching, and channel separation and combining, (Bargellini, 1972); Dicks and Brown, 1978; Morgan, 1978).

Receiver susceptibility to SPS emissions principally involves nonlinear responses in the tunnel diode and low noise FET input amplifiers for out of channel interferor components, and resultant intermodulation product effects in AGC limiter and conversion functions (Fuenzalida et al., 1973; Paulluel et al., 1973). For the repeater transponder systems (Figure 24), the primary result is a decreased S/N in the output channels. For reductions in S/N in the 10-25 dB range, increased cross-talk for frequency-multiplexed analog modes exaggerates channel noise. Typical repeater-transponder responses for out-of-band interferors at 2.45 GHz and 56 Hz are displayed in Figures 25 and 26. Approximate thresholds for cross-talk are indicated.

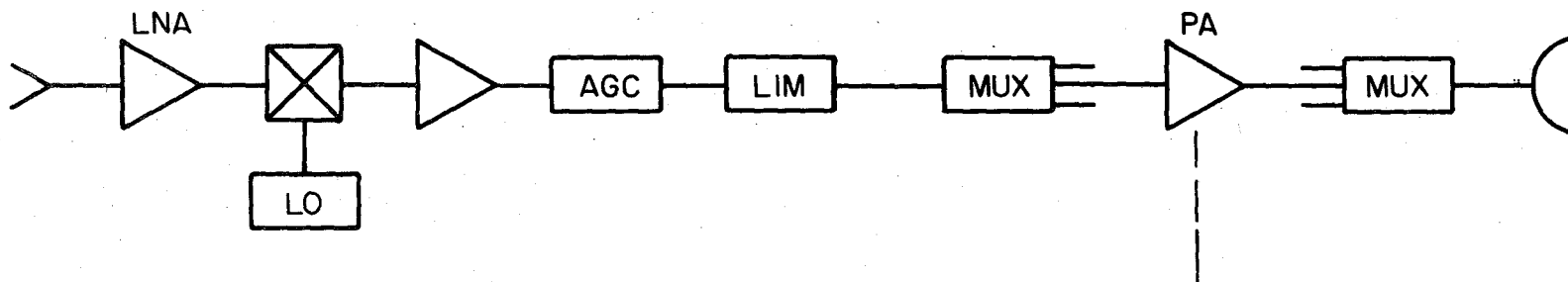
The basic degradation character for SS-TDMA repeaters is indicated in Figure 27, assuming the same two signal interferences. Noise and intermodulation components generated in the low noise input amplifiers and mixers increase the switching matrix errors, and reduce the S/N in the subsequent conversion and multiplexing operations. A more gradual slope for the channel error characteristic is noted relative to the regenerative and baseline repeaters. With a 10 to 15 dB increase in channel noise (input to the switch matrix), the graceful degradation characteristic decays to a catastrophic mode, as indicated in Figure 28.

The S/N characteristic of the DSCS repeater is affected by nonlinear responses in the tunnel diode amplifiers and limiters. Performance effects of noise and intermodulation components relate reduced channel S/N and cross-talk at the output of the diplexers and channel combiners. A representative channel S/N characteristic for two signal interference is indicated in Figure 29.

#### 2.4 GEO Satellite Effects

Satellite systems deployed include civilian and military communications relays supporting intercontinental services. Data, voice, and entertainment services are provided through these satellite operations. Satellites having potential interference degradation because of SPS operation include:

MARISAT	15° W
ATS 6	118° W (Variable)
SATCOM	119° W
COMSTAR	95° W & 128° W



SINGLE CONVERSION TRANSPONDER

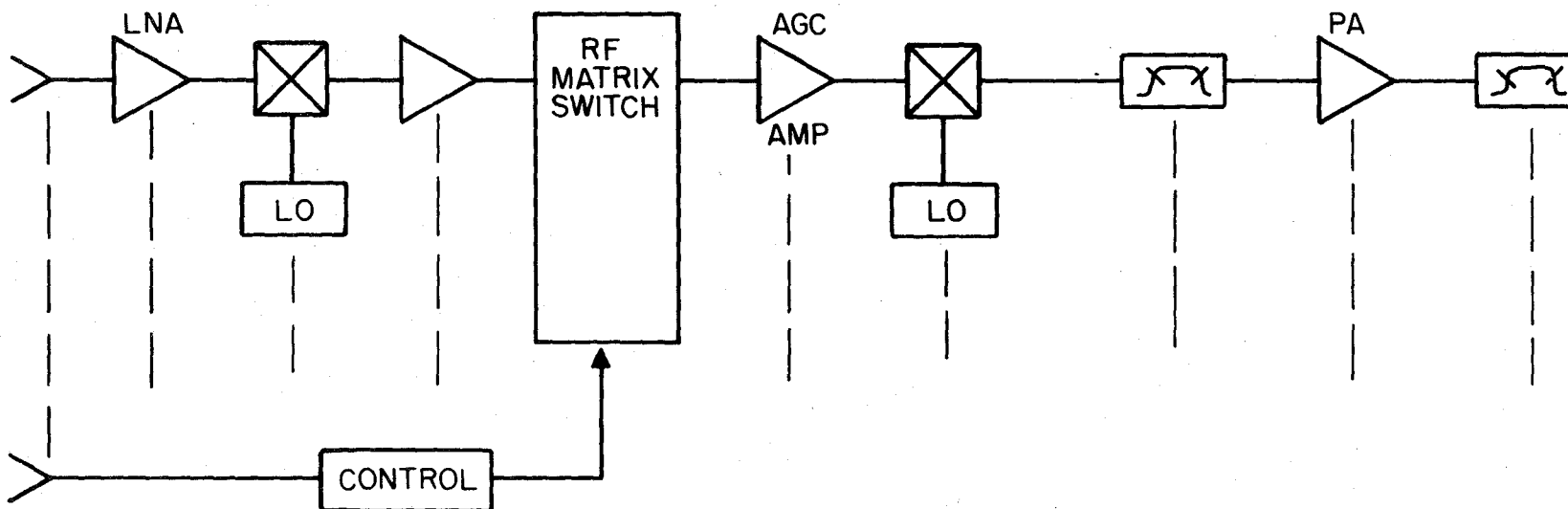


Figure 24. Functional organization of two types of satellite receivers.

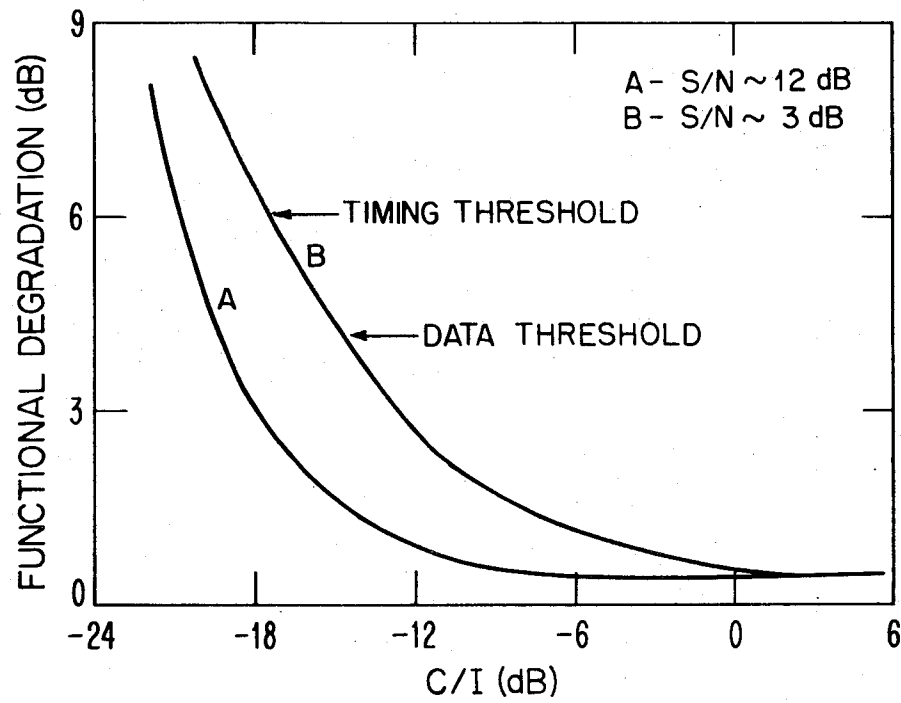


Figure 25. SS-TDMA repeater performance characteristic.

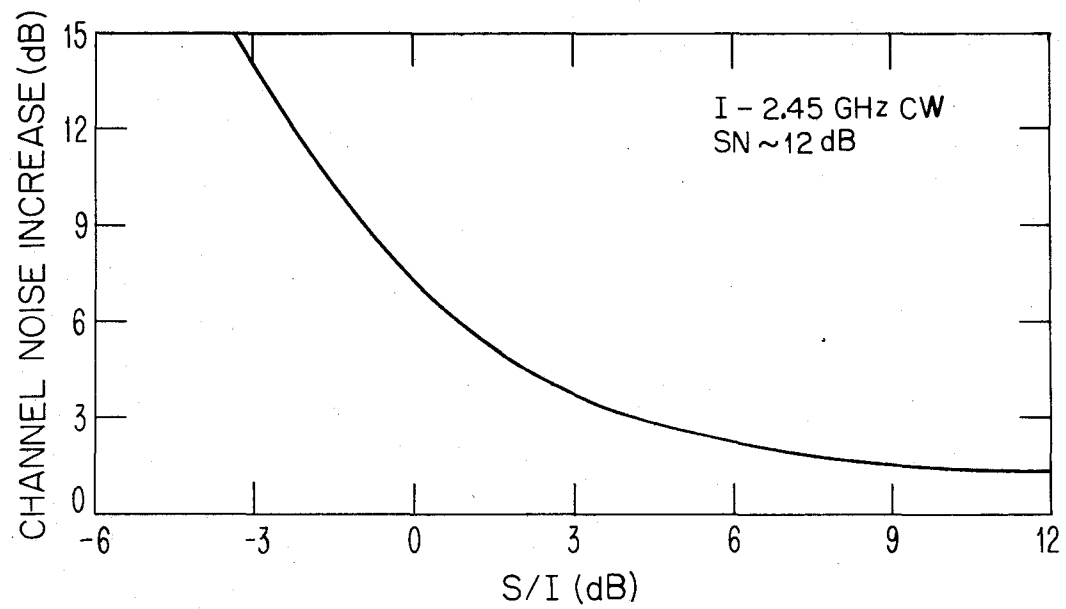


Figure 26. Matrix switched transponder response.

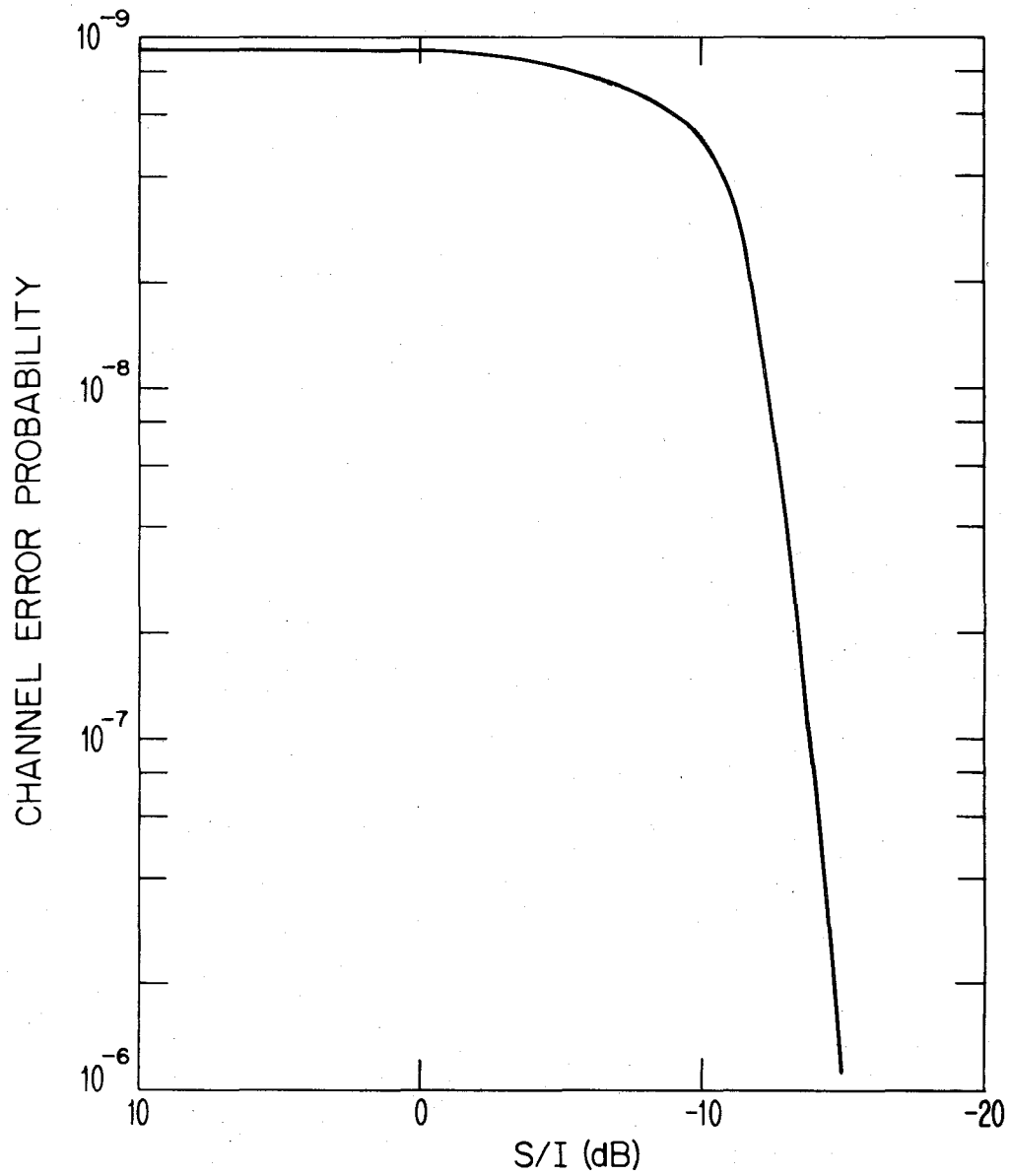


Figure 27. SS-TDMA repeater error characteristic - two cw interferer cases.

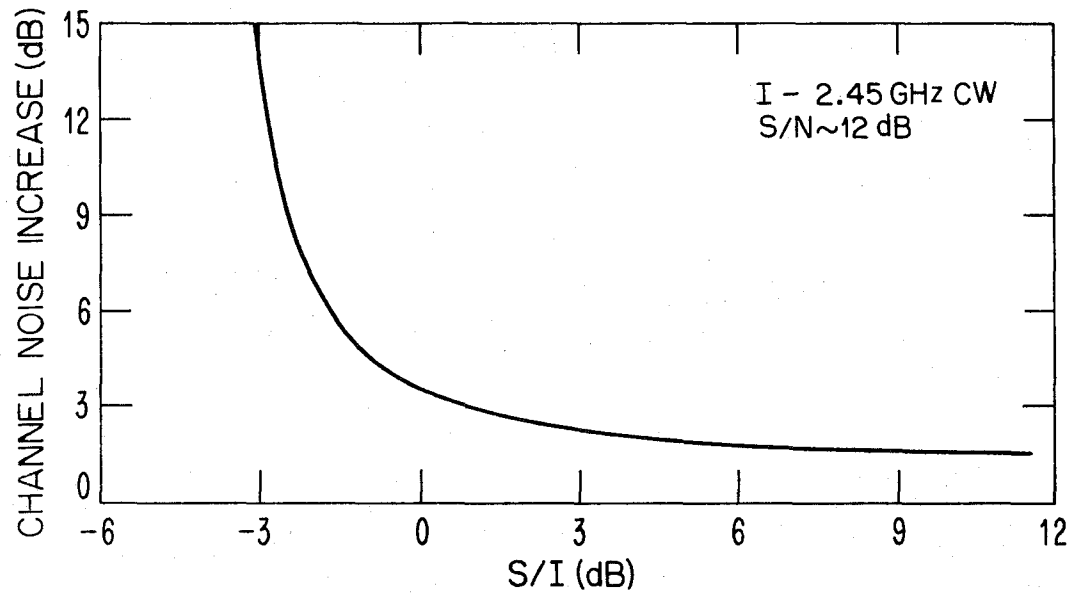


Figure 28. Single conversion transponder response.

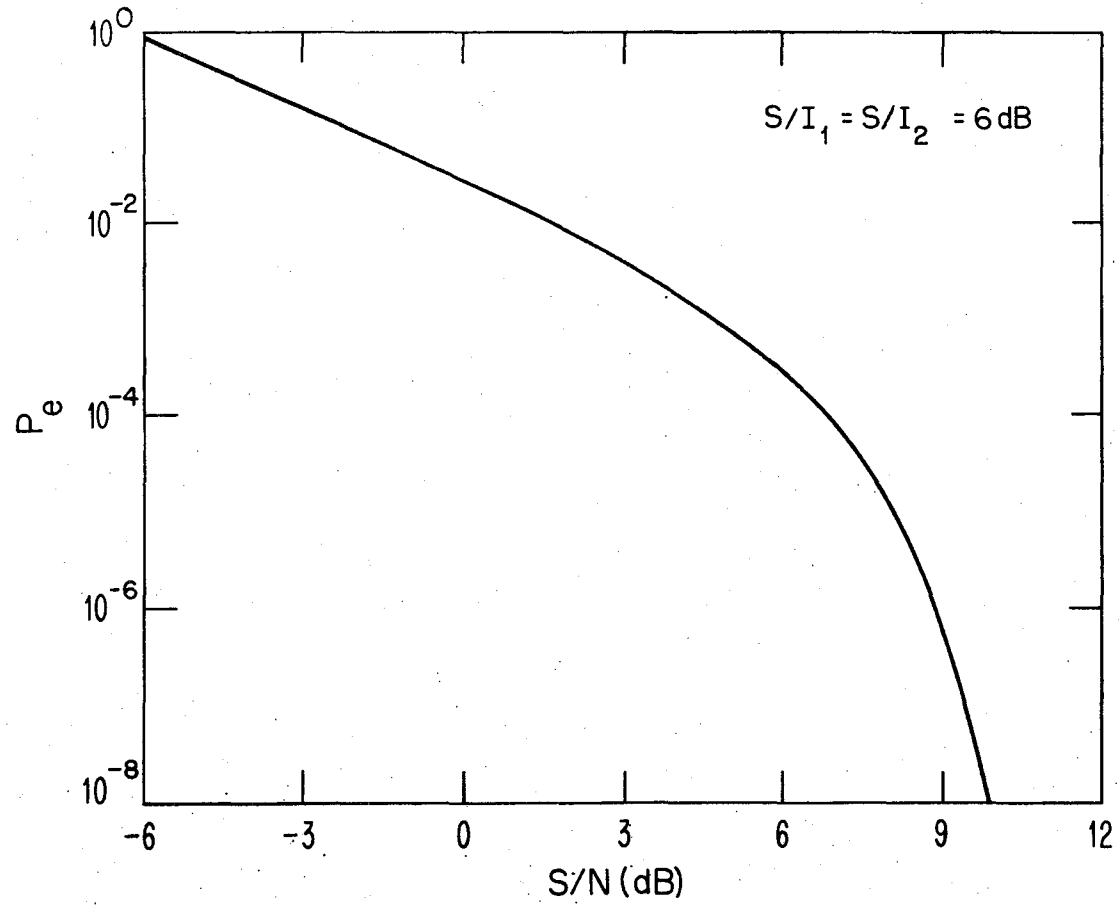


Figure 29. TDMA/PCM error characteristic - two signal interferer.

WESTAR	99° W & 91° W
SBS	106° W & 122° W
ANIK A-2, A-3	108.5° W & 114° W
LEASAT	100° W
Brazil Communications	65° W or 78° W
Columbia Communications	79° W
DSCS II & III	Atlantic & Pacific
Hughes Communications	75° W
RCA Alaska COM	(to be assigned)
Advanced WESTAR	103° W
INTELSAT	61.4° E.

Communication satellite uplink and downlink frequency trends are shown in Figure 30. This trend to higher frequencies will reduce SPS direct coupling at the primary frequency. Mitigation emphasis for commercial services will primarily relate to harmonic and spurious emissions.

## 2.5 Interference to Geostationary Satellites

Interference between SPS and GEO satellites includes adjacent orbit and cross orbit geometry of the latter relative to the SPS communication satellite coupling path through an interconnecting chord passing nearly tangent to the Earth. This mode will be addressed in subsequent discussions concerning SPS-INTELSAT interference coupling. The following discussion will show that substantial signal levels can be expected at other orbiting satellites, particularly when they are within 0.1 degrees of orbital separation from SPS.

The power flux density at a distance  $r$  from SPS is given by

$$f_d = \frac{P_t G_t}{4\pi r^2}, \quad (2)$$

where  $G_t$  is the SPS antenna gain in the direction  $r$ , and  $P_t$  is the input power to the transmit antenna. The distance  $r$  can also be expressed in terms of degrees of orbital arc  $\phi$ , where

$$\phi \doteq \frac{r}{d} 57.3, \quad (3)$$

$d$  is the distance from the center of the earth to the geostationary orbit. Substituting (3) into (2) results in

$$f_d = \frac{261.3 P_t G_t}{d^2 \phi^2}. \quad (4)$$

Figure 31 shows a plot of the power density that can be expected for

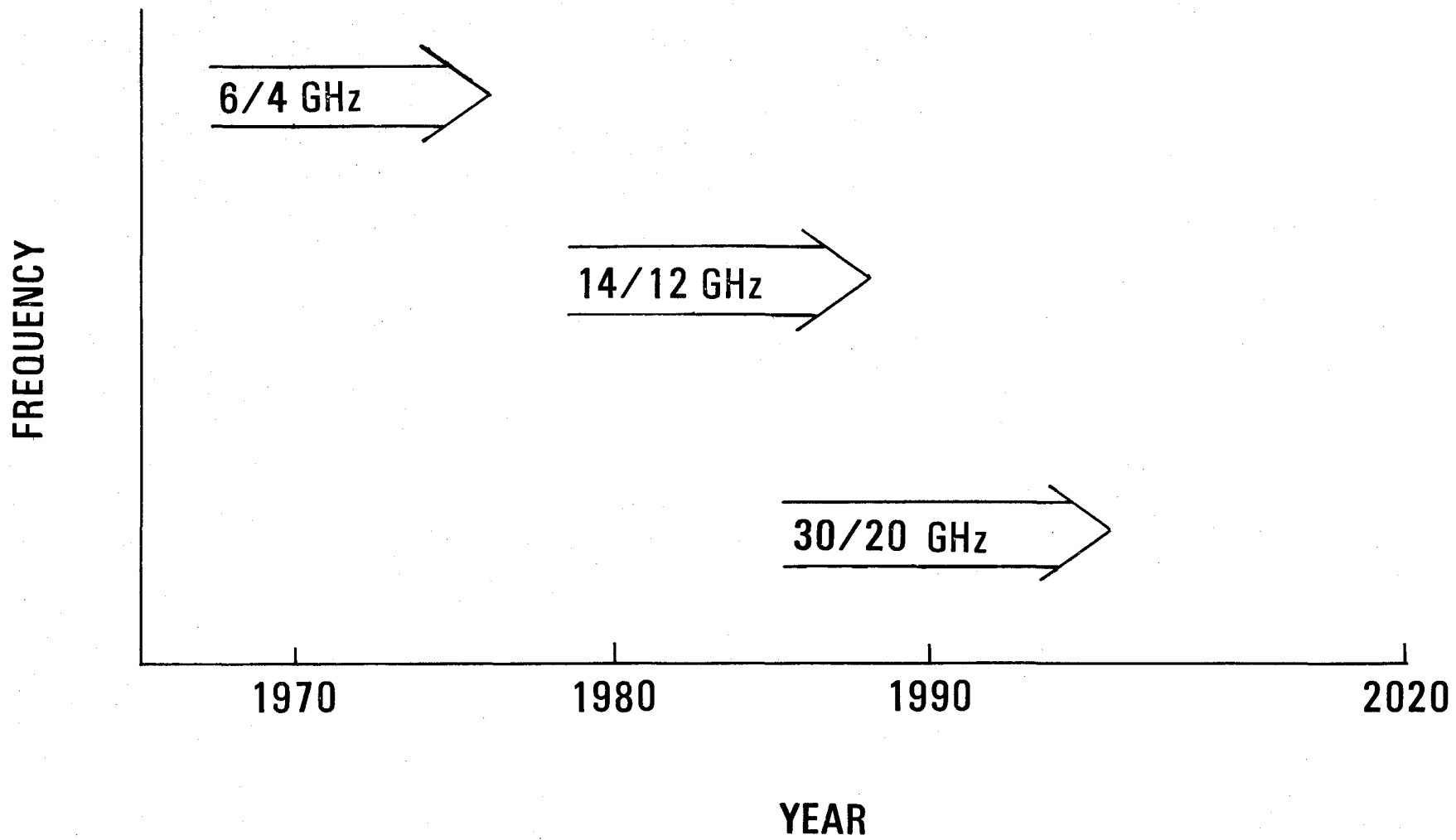


Figure 30. Communication satellite uplink/downlink frequency trends.

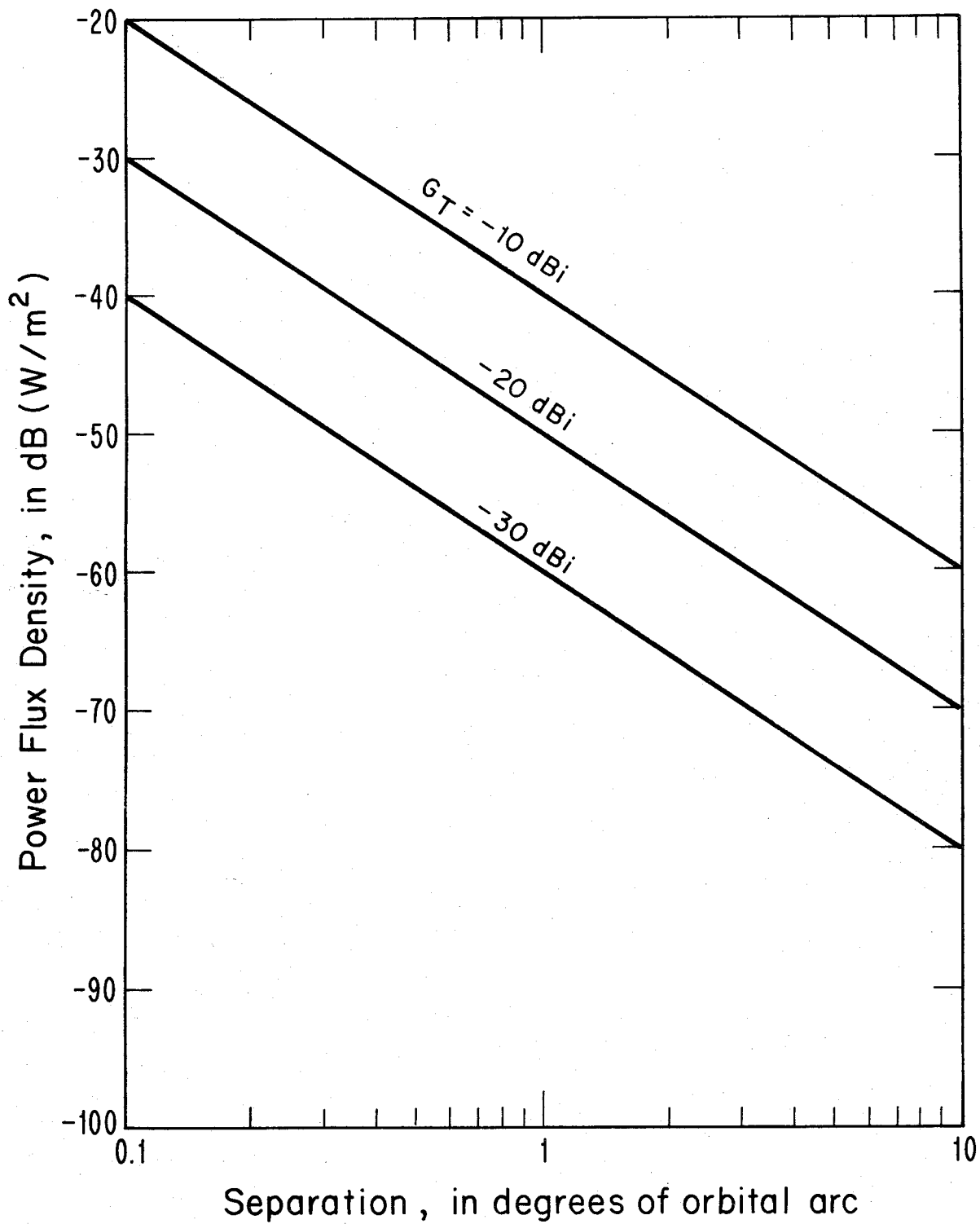


Figure 31. SPS power density at 2.45 GHz as a function of distance along the geostationary orbit.

$$\begin{aligned}
 P_t &= 6.85 \times 10^9 \text{ watts,} \\
 d &= 4.22 \times 10^7 \text{ m,} \\
 G_t &= 87 \text{ dB (boresight)}
 \end{aligned}$$

and three values of  $G_t$ , the spaceteenna gain at 90 degrees off boresight. Accurate data for  $G_t$  at 90 degrees off boresight (gain in the direction of adjacent geostationary orbit) are not available at the present time. However, it is acknowledged that these calculations are accurate only for signals at or near boresight and do not consider quantities such as aperture phase distortion and control system tolerances which significantly affect the radiation pattern 90 degrees off boresight. The current technology in satellite antennas results in  $G_t$  values as large as -10 dBi (dB relative to an isotropic radiator) given by the CCIR in Report 558-1 (CCIR, 1978c). This report will assume an SPS antenna gain in the direction of the geostationary orbit of  $G_t = -10$  dBi until more accurate estimates are available.

However the -10 dBi gain is applicable at the normal victim operating frequency, which for MARISAT is 1640 MHz. A -10 dBi antenna gain at 1640 MHz is equivalent to an effective antenna aperture of  $-35.7 \text{ dBW/m}^2$ . The following will assume that the effective victim antenna aperture 90 degrees off boresite is the same at 2450 MHz as it is at 1640 MHz.

Given the above assumptions, the power incident to a victim receiver aperture can be evaluated as shown in Table 1. This table is prepared for a separation between SPS and victim of 0.1 degrees, and satellite reference bandwidths of 4 kHz and 1 MHz. Note that the I/N ratio for the 4 kHz reference bandwidth system after filtering is 22.1 dB with  $0.1^\circ$  separation and 2.1 dB with  $1.0^\circ$  separation. Again, these figures should be less than zero to minimize the potential for interference. These calculations show that a potential for interference exist to satellites separated from 0.1 to 1.0 degrees from an SPS.

#### 2.5.1 INTELSAT

An example of possible interference from SPS to geostationary satellites is the cross orbital interference situation involving INTELSAT IV or IVA in geostationary orbit over the Indian Ocean at about  $61.4^\circ$  East longitude, (Bargellini, 1972; Dicks, 1978). Figure 32 shows the global beam footprint as viewed from INTELSAT IV or IVA. The global beam (NASA, 1975) for INTELSAT will have a 3 dB beamwidth equal to the optical horizon or "limb line," and the half-cone angle subtended at the satellite by the limb line is about  $8.65^\circ$  as shown in Figure 33.

TABLE 1. Estimates of the Power Coupled into a 1640-MHz Satellite Transponder Separated 0.1° and 1.0° from SPS

	4-kHz Reference Bandwidth	1-MHz Reference Bandwidth'
<u>Separation 0.1°</u>		
SPS power density at victim ( $g_t = -10$ dBi)	-20 dBW/m <sup>2</sup>	-20 dBW/m <sup>2</sup>
Victim antenna gain in direction of SPS at 1640 MHz	-10 dBi	-10 dBi
Effective victim antenna aperture at 1640 MHz	-35.7 dB·m <sup>2</sup>	-35.7 dB·m <sup>2</sup>
Effective victim antenna aperture at 2450 MHz	-35.7 dB·m <sup>2</sup>	-35.7 dB·m <sup>2</sup>
SPS power received on victim antenna	-55.7 dBW	-55.7 dBW
Victim noise power in reference bandwidth ( $t = 3000$ K)	-157.8 dBW	-133.8 dBW
I/N prior to transponder filtering	102.1 dB	78.1 dB
Estimate of transponder filtering 1640 MHz to 2450 MHz	80 dB	80 dB
I/N after filtering	22.1 dB	-1.9 dB
<u>Separation 1.0°</u>		
SPS power density at victim ( $g_t = -10$ dBi)	-40 dBW/m <sup>2</sup>	-40 dBW/m <sup>2</sup>
Victim antenna gain in direction of SPS at 1640 MHz	-10 dBi	-10 dBi
Effective victim antenna aperture at 1640 MHz	-35.7 dB·m <sup>2</sup>	-35.7 dB·m <sup>2</sup>
Effective victim antenna aperture at 2450 MHz	-35.7 dB·m <sup>2</sup>	-35.7 dB·m <sup>2</sup>
SPS power received on victim antenna	-75.7 dBW	-75.7 dBW
Victim noise power in reference bandwidth ( $t = 3000$ K)	-157.8 dBW	-133.8 dBW
I/N prior to transponder filtering	82.1 dB	58.1 dB
Estimate of transponder filtering 1640 MHz to 2450 MHz	80 dB	80 dB
I/N after filtering	2.1 dB	-21.9 dB

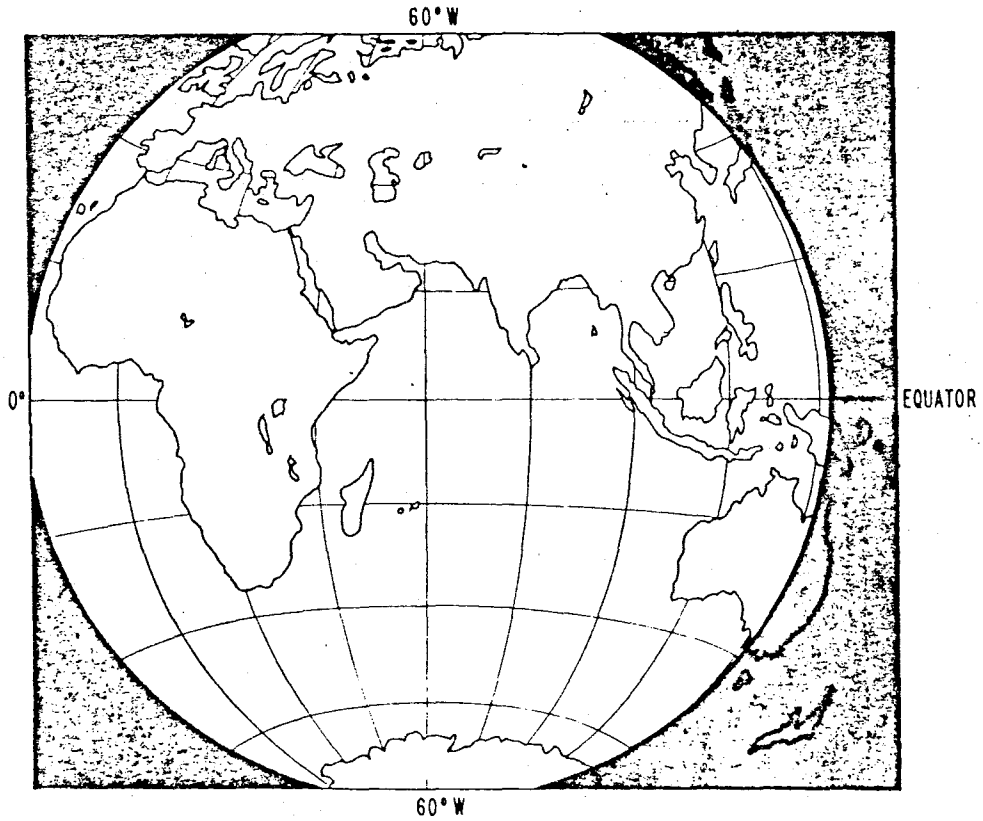


Figure 32. Global beam footprint from INTELSAT IV.

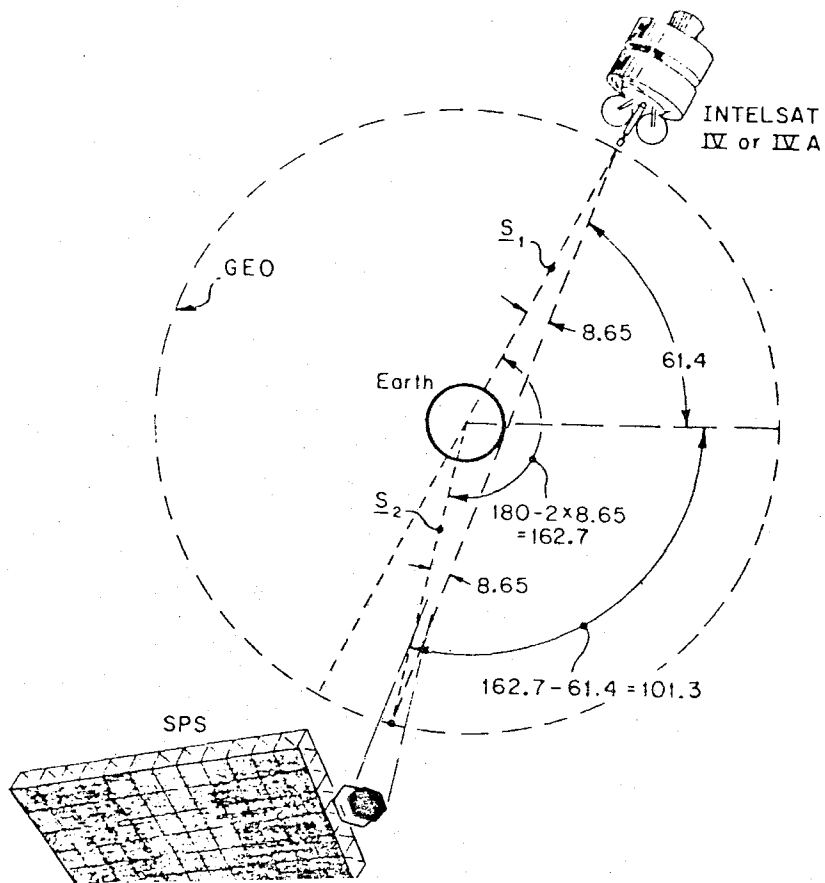


Figure 33. Geometry for calculating angle from SPS boresight to line joining INTELSAT IV.

The geometry for calculating the angle from boresight on the SPS spacetenna to a line from the SPS spacetenna joining INTELSAT IV or IVA is shown in Figure 33. Assume the SPS antenna is oriented with its boresight direction (x-axis in Figure 33) pointing toward an arbitrary aim point on the surface of the earth specified by latitude,  $\phi$ , and longitude  $\lambda$ . A unit vector from SPS to this arbitrary aim point on the earth; i.e.,

$$\frac{e_{\xi}}{s} = \frac{\frac{e_x}{s} (\cos\lambda\cos\phi - s\cos\lambda_{02}) + \frac{e_y}{s} (\sin\lambda\cos\phi - s\sin\lambda_{02}) + \frac{e_z}{s} \sin\phi}{[1 + s^2 - 2s\cos\phi\cos(\lambda - \lambda_{02})]^{1/2}} \quad (5)$$

where  $s = 6.619$  earth radii, is the distance to geostationary orbit from the earth's center, and  $\lambda_{01}$  and  $\lambda_{02}$  are the longitude of SPS and INTELSAT, respectively. From Figure 34, the angle  $\alpha$  between boresight of SPS to INTELSAT is

$$\cos\alpha = \frac{e_R}{s} \cdot \frac{e_{\xi}}{s} \quad (6)$$

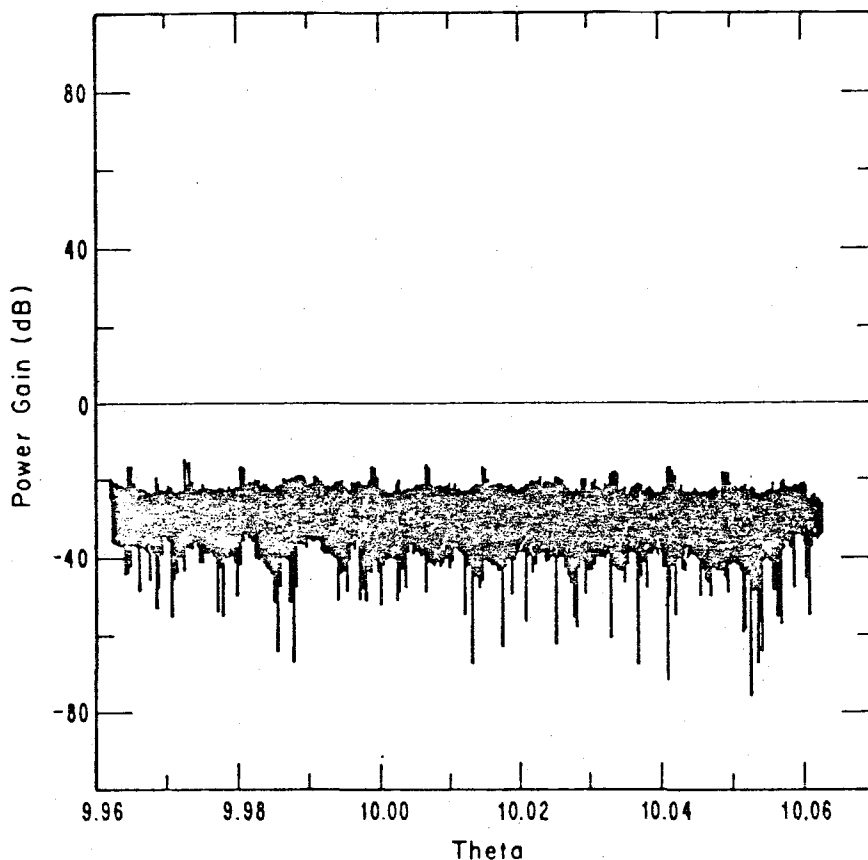


Figure 34. SPS rectenna gain versus range of angles where possible interference with INTELSAT IV may occur.

where a unit vector,  $\underline{e}_R$ , from SPS to INTELSAT is

$$\underline{e}_R = \frac{S_1 - S_2}{S_1 - S_2} = \frac{e_x (\cos\lambda_{02} - \cos\lambda_{01}) + e_y (\sin\lambda_{02} - \sin\lambda_{01})}{\sqrt{2} [1 - \cos(\lambda_{02} - \lambda_{01})]^{1/2}} \quad (7)$$

Assume the rotational orientation of the SPS antenna about its boresight axis is such that the INTELSAT lies in the E-plane (or H-plane) of the SPS pattern (this will correspond to a worst case interference). Then  $\phi = 0$  and  $\alpha = \pi/2 - \theta$ . If we substitute (5) and (7) into (6) using  $\lambda_{01} = 61.4^\circ$ ,  $\lambda_{02} = -101.3^\circ$ , (c.f. Figure 33)  $\phi = 34^\circ$ ,  $\lambda = -101.3^\circ$  (the latter latitude and longitude close to Lubbock, Texas), we find  $\alpha \approx 10.25^\circ$ . In Figure 34 we plot the SPS rectenna gain in region around  $\alpha = 10.25^\circ$ .

The power flux density at any point in space is found from

$$\begin{aligned} W(\text{watts/m}^2) &= e.i.r.p./4\pi r^2 \\ &= G_T(\theta, \phi) P_T / 4\pi^2 \end{aligned} \quad (8)$$

where  $G_T$  is the transmitting antenna gain,  $P_T$  the input power, and  $r$  the distance from the transmitter to the point in question. Although the gain of the receiving antenna does not enter into the calculation of power flux density, it needs to be accounted for when calculating basic transmission loss. For the INTELSAT example, we use in (8)

$$\begin{aligned} P_T &= 6.85 \times 10^9 \text{ watts} \\ r &= 2 \times 6.619 \times 6.37 \times 10^6 \text{ m} \\ G(10^\circ, 0^\circ) &= .01 \text{ (envelope of sidelobe packs)} \end{aligned}$$

yielding

$$W \approx -91.15 \text{ dBW/m}^2. \quad (\text{INTELSAT}) \quad (9)$$

The sharp drop of  $S$  from its value at the center of the rectenna of about  $3.8 \text{ dBW/m}^2$  to about  $-91.15 \text{ dBW}\cdot\text{m}^2$  is a result of the extremely sharp roll-off of the sidelobes reducing the gain from  $87.65 \text{ dBi}$  at boresight to about  $-10$  to  $-20 \text{ dBi}$  at  $10^\circ$  from boresight. The increase in path length from SPS to INTELSAT over the distance from SPS to the earth corresponds to a decrease in power flux density of only about  $7.44 \text{ dB}$ . At the limb, the difference would be about  $6 \text{ dB}$ . The added  $1.44 \text{ dB}$  is due to distance change from limb to satellite subpoint. From Figure 34, the radiated power toward the earth's limb is about  $80 \text{ dBW}$ . This increases to about  $186 \text{ dBW}$  at boresight.

The uplink frequency for INTELSAT is in the 5.930-6.420 GHz band (NASA Compendium, 1975). The third harmonic of the 2.45 GHz SPS signal at 7.35 GHz may cause intolerable interference with the uplink frequency band for INTELSAT if the edge of the modulation passband is within a distance or frequency separation from an SPS vehicle to cause an S/I at the input to the INTELSAT receiver of  $\geq 12-15$  dB. This constraint is based on the adjacent channel interference effects characteristics of FDMA transponder receivers' interference coupling occurring through the receiver signal channel. Receiver interference responses include AGC suppression and intermodulation products generated by the desired communication signal, the SPS fundamental, and the SPS third harmonic. The intermodulation sensitivity of the INTELSAT uplink is increased by about 9-12 dB because of the SPS third harmonic being in the uplink channel. These separation constraints and sensitivity increase are based on the test of an FDMA transponder receiver of the type used for commercial satellite multichannel relay service. The SPS characteristics assumed include the fundamental and harmonic emission and spatial radiation characteristics previously cited in Section 1 (ref. Figures 2 through 5). The SPS orbital intermodulation products will be of no consequence in this INTELSAT receiver since no significant emissions are anticipated in the uplink bands because of the electrical parameters of the structure equivalent circuits and solar panel components.

#### 2.5.2 Advanced WESTAR

As a second example of possible interference caused by the SPS with a communications satellite, consider the planned domestic communications satellite "Advanced WESTAR" with a tentative launch date scheduled for the early 1980's. This satellite is sponsored by Western Union Space Communications Corporation (Morgan, 1978). The Tracking and Data Relay Satellite System (TDRSS) is leased by NASA (US) from the Western Union Space Communications Corporation for 10 years. These satellites will carry both TDRSS and Advanced WESTAR equipment. The CONUS beam from WESTAR at 103° W longitude is shown in Figure 35 with 3 dB beamwidths of 3.5° x 6.8°. The footprint in Figure 35 is computed using an assumed aimpoint of 35° latitude and 103°W longitude (close to Amarillo, Texas). The slight change from the aim point in the previous example is used to show a relatively uniform CONUS coverage footprint. For this interference example, assume the SPS satellite in geostationary orbit displaced 5° from Advanced

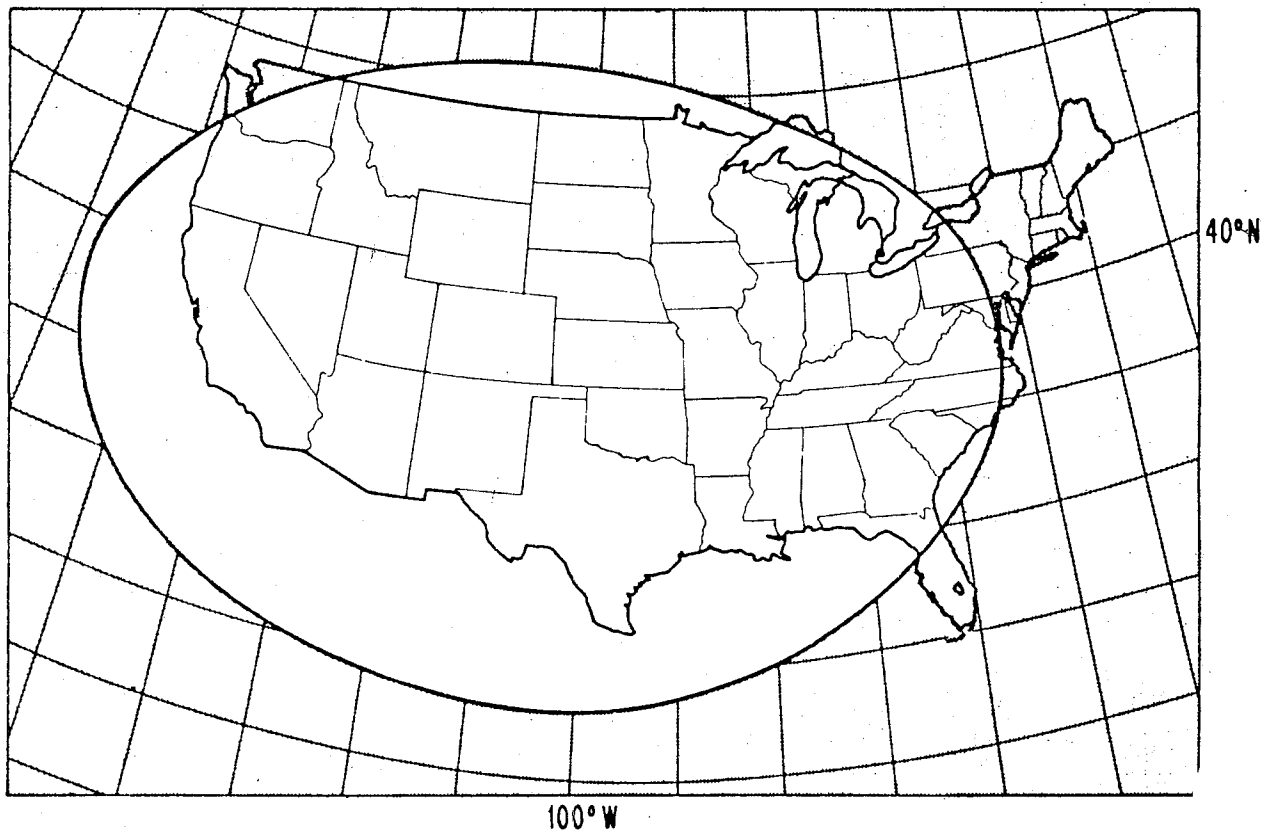


Figure 35. CONUS beam for the advanced WESTAR.

WESTAR, corresponding to a separation at geostationary orbit of  $3.68 \times 10^3$  km. The parameter values used in (9) for this example are

$$\begin{aligned}
 P_T &= 6.85 \times 10^9 \\
 r &= 3.68 \times 10^6 \text{ m} \\
 G_T &= 1.493 \times 10^{-6} \text{ (-58.26 db from Figure 18)}
 \end{aligned}$$

yielding

$$W \approx -92.21 \text{ dBW/m}^2 \text{ (WESTAR)}. \quad (10)$$

Although power flux density regulations exist for (ITU, 1977) satellite-earth station geometries, there are no specific corresponding regulations for satellite-to-satellite geometries.

Another example of interference along the geosynchronous orbit, is the potential for interference between SPS and the TDRSS, Tracking and Data Relay Satellite System (Poza, 1977). This system of relay satellites and earth terminals supplies communications support for various space research missions. The satellites can support both wideband and narrowband communications at S and K band frequencies. One of the functions of TDRSS, and the subject of the following analysis, is to supply communications relays for space shuttle missions (Batson et al., 1977).

The TDRSS communications frequencies closest to SPS are the S band link with uplink frequencies of 2287.5 and 2217.5 MHz. Downlink assignments from TDRSS are at 2042 and 2106 MHz. The downlink from TDRSS uses spread spectrum signaling techniques, with a 11.232 Mchip/s signaling rate, to prevent interference to ground based terminals. The uplink to TDRSS, however, does not require spread spectrum signaling. It is this narrowband mode that is the subject of discussion here.

One of the typical transmission rates in the low-data-rate mode is 96 kbps. This information stream is encoded with a 1/3 rate, constraint length 7, convolutional code. The resulting 288 kbps coded waveform is transmitted with phase shift keying of the carrier. Typical signal levels that are involved during a TDRSS/ space shuttle communication relay are given in Table 2. Also shown in the table are estimates of SPS interference levels that would exist with a 1° separation between SPS and TDRSS. The reference bandwidth for TDRSS has been assumed to be 228 kHz. From Table 2, one can see that the interference-to-system-noise ratio after filtering is estimated to be  $I/N = -12.1$  dB. Although an  $I/N$  ratio less than -10 dB normally would not degrade transmission efficiency, the 2 dB margin is inadequate considering SPS pattern variabilities and small gain fluctuations because of orbit wander.

As a final example of interference that may be emitted by the SPS spacetenna, we discuss briefly the possibility that over the passband of the Klystrons, say  $\pm 10$  MHz, the noise power may cause interference with neighboring communication satellites. The noise power can be calculated using

$$\text{Noise power} = 10 \log_{10} (kTB) \quad (11)$$

and, if we assume  $B = 2 \times 10^7$  Hz,  $k = 1.38 \times 10^{-23}$ , and  $T = 300^\circ\text{K}$  in (11), yields a noise power of -130.8 dBW. However, the noise generated in amplifiers and/or

TABLE 2. TDRSS Interference Estimates

<u>Victim</u>	
Space Shuttle EIRP	15.2 dBW
Path loss, shuttle to TDRSS (R=22786 nmi, f=2287.5 MHz)	-192.1 dB
Pointing and polarization losses	-1.0 dB
TDRSS receive antenna gain	36.0 dB
Receive signal level	-141.9 dBW
TDRSS noise temp	27.7 dBK
Boltzmanns constant	-228.6 dBW/°K·Hz
TDRSS noise density	-200.9 dBW/Hz
Information bandwidth, 96 kbps mode	49.8 dB·Hz
RF bandwidth, 228 kbps PSK mode	53.5 dB·Hz
TDRSS noise power in RF bandwidth	-147 dBW
<u>Interference</u>	
SPS transmit power, 6.5 GW	98 dBW
SPS antenna gain 90° off boresight	-10 dBi
Path loss, SPS to TDRSS, (700 km, 1° separation, 2450 MHz)	-157.1 dB
TDRSS antenna gain to SPS signal 90° off boresight	-10 dBi
SPS interference power at input to TDRSS receiver	-79.1 dBW
Receiver diplexer filtering attenuation to SPS signal	-80 dB
SPS interference power after filtering	-159.1 dBW
<u>Summary</u>	
Signal to interference ratio at input to receiver diplexer prior to filtering	-62.8 dB
Signal to interference ratio after filtering in TDRSS receiver	17.2
Interference to system noise ratio prior to filtering (-79.1 + 141.9)	67.9 dB
Interference to system noise ratio after filtering in TDRSS diplexer	-12.1

oscillators preceding the 50 to 70 kw klystrons are unknown, and thus the exact noise levels cannot be calculated. This could be an important problem in consideration of interference effects.

## 2.6 Station Keeping Problems

Satellites in GEO are not able to stay exactly in the position assigned to them. The wander involved depends very much on orbit insertion errors related to track instrumentation errors and the station-keeping power budgets. The SPS, for example, will probably have an altitude wander of approximately 80 km. INTELSAT IV has an apogee altitude of 36230.5 km and a perigee altitude of 35739.5 km. This gives an altitude wander of 491 km. Other GEO satellites vary in altitude from 300 km to 550 km. This poses the question of interaction between satellite systems in adjacent orbit slots as the satellites change altitude with respect to one another. Figure 36 depicts an INTELSAT 0.5 degree from an SPS with the INTELSAT apogee (maximum altitude) with respect to the adjacent SPS. The implications of altitude variation between an SPS and adjacent communications satellites are demonstrated by a single example: orbit separation 0.5°, 40 km altitude difference, and uplink receiver beamwidth of 2° circular. The SPS reflection cross section in the direction of the communications satellite would be about 2.82 km<sup>2</sup> (structure configuration of SPS reference design, graphite composite material  $\sigma \sim 0.5$  metal equivalent area). Uplink S/I ratios for the link with this multipath component would be in the range of 5 to 9 dB for this single geometry. This S/I ratio is unacceptable because of normal link signal variations caused by meteorological and ionosphere effects.

## 2.7 Mitigation Techniques

The study reported here concludes that one would not expect interference between SPS and other GEO satellites when separated by 0.5 to 1.0 degrees. However, looking at what has been placed in GEO to date, and what is planned between now and the year 2000, it would appear that a slot problem will exist if 60 SPS were actually planned. It would seem profitable at this time to start looking at the utility of multiple use space platforms. Instead of each satellite being designed for a narrow range of functions and each needing an assigned slot in the GEO orbit, a space platform could serve many functions (communications, data relays, navigation, etc.) all from one slot location. This would allow more systems for the given space with less likelihood for EMC problems.

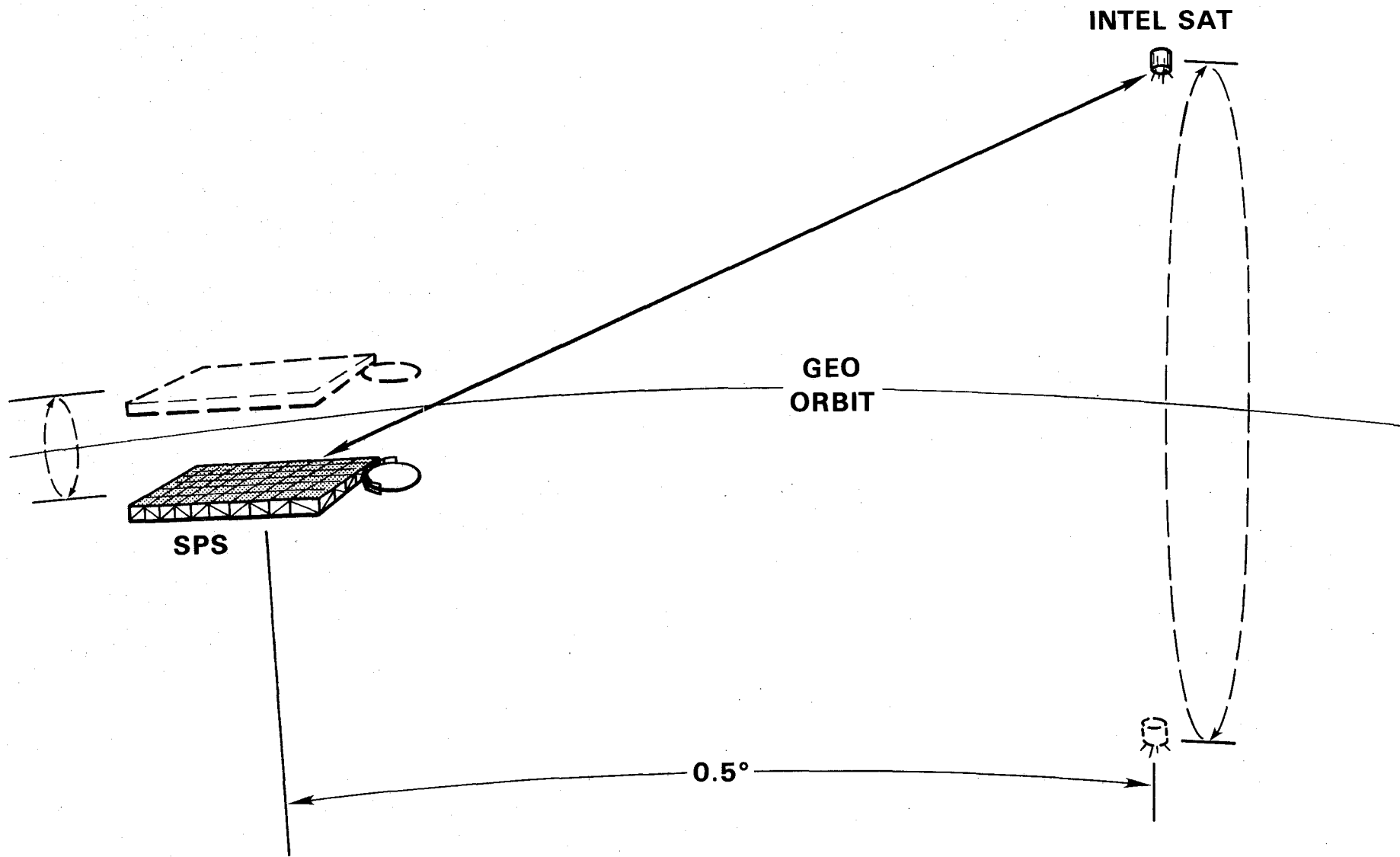


Figure 36. Satellite station-keeping problem potential interference.

Communications satellite receivers should be separated from an SPS by  $0.5^\circ$  at GEO radii. These receivers must have band stop filters for the SPS fundamental and primary harmonics (2nd through 5th) with a notch depth of at least 60 dB and a notch bandwidth of 5 MHz. Such filters are available with an out-of-band insertion loss of  $<2$  dB. For SPS harmonics that are within a communications band, the notch filter must be replaced by a tracking and nulling function to provide a 50 to 60 dB suppression of the SPS harmonic prior to the first conversion stage in the communications receiver. This nulling technique is tractable since the SPS emissions are unmodulated. With a separation of  $0.5^\circ$ , the SPS noise sidebands present no interference problem for communications with directional antennas oriented toward the earth. These filter and nulling suppression levels apply to earth or hemisphere coverage, spot, and wide/narrow beam antennas as with signal processing functions.

Since array antennas will predominate for higher frequency communications, the nulling operation can be accomplished as a secondary function of the primary array. A separate array allows less complex signal control circuitry, but represents increased weight and physical complexity with no advantages in reliability or cost.

An engineering analysis of the multiple use platform concept applies to the SPS as well as communications satellites. Arndt et al., (1980) has published a preliminary description of multiple SPS emitter configurations and applications for single platforms including multiple satellite transponders, satellite-satellite modes between platforms, and possible sensor utilities. The latter represent the only EMC negative area because of the interference sensitivities of optical and passive microwave sensor systems.

### 3. LEO SATELLITES

Another major concern of the EMC program was the effect on satellites in low earth orbit which might pass through an SPS power beam. The large powers involved represent illumination levels as high as 319 volts per meter for satellites such as the proposed space telescope at an orbit altitude of 10,900 miles. Operational effects for LEO satellites depend on orbits, equipment complement, equipment usage, and vehicle physical configuration. Existing and planned LEO systems include remote sensing, navigation and position fixing, and communications functions.

On-board sensors sensitive to SPS interference include electro-optical devices, active and passive microwave systems, and particle detectors.

The susceptibility of various operational and planned LEO satellites have been examined during the course of the SPS EMC evaluation program. Functional degradation for the electronic systems on LANDSAT, GPS, and the space telescope is described in relation to the amplitude of the SPS illumination components. Analysis and tests include the modes of coupling to on-board devices and sub-systems, and performance effects in relation to satellite missions.

The susceptibility evaluations for LANDSAT, GPS, and SPACE TELESCOPE indicate the character of functional degradation for data sensors, communications, attitude/stabilization, and processing or control systems for power beam encounter periods. Penetration through antenna and physical apertures and modes of coupling to internal devices and modules are examined to support sensor and circuit module tests for degradation measurement and mitigation technique specification.

Military satellites have been addressed separately. These considerations have concerned SPS illumination effects on scanning and staring sensors (visual and IR optics, passive RF receivers, radiation and particle detectors) oriented towards the earth.

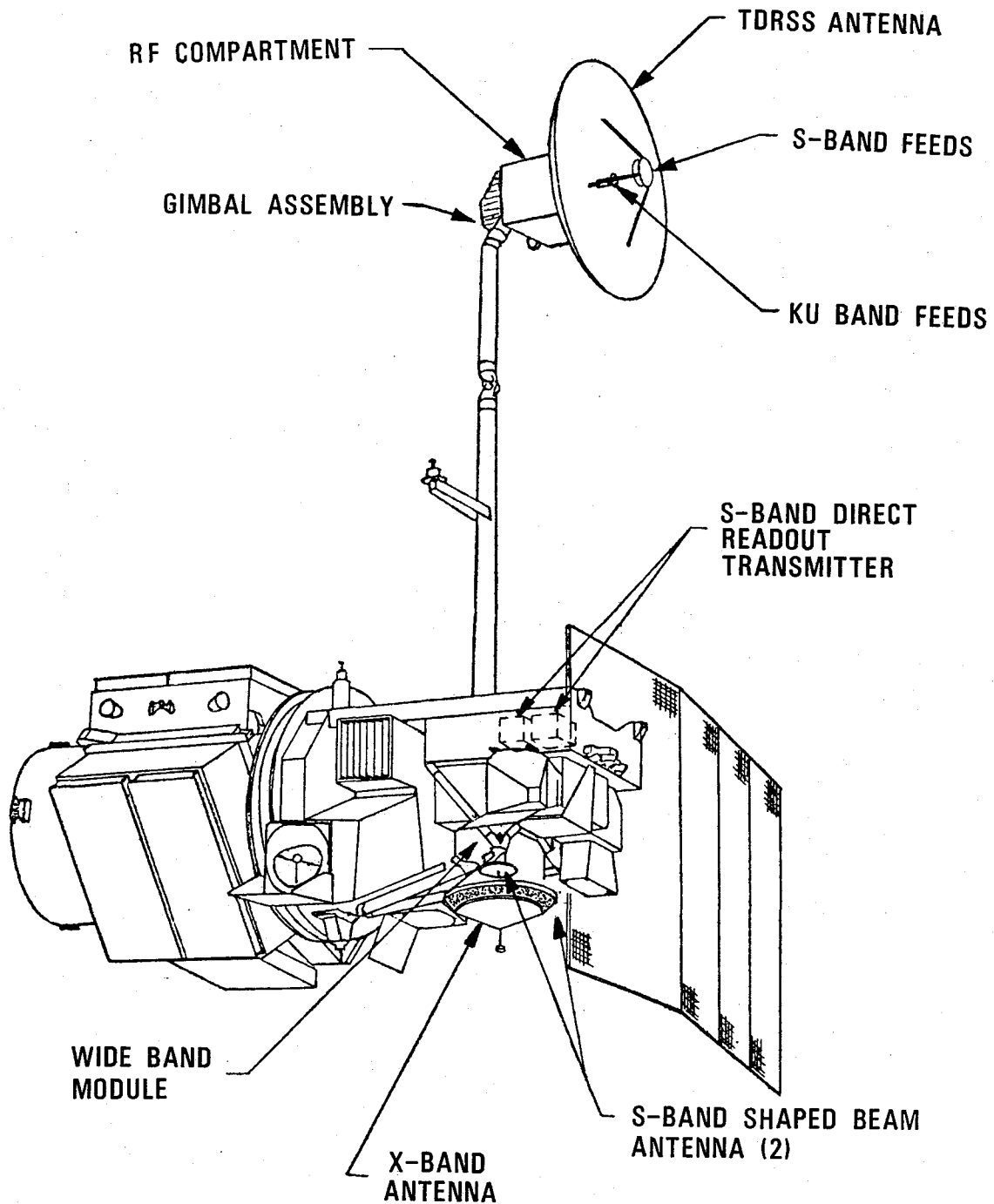
### 3.1 LANDSAT Satellite

The LANDSAT satellite program is intended to develop and demonstrate a capability for global monitoring support to Earth Resources Management. Launch of LANDSAT-D is scheduled in the third quarter of 1981. A subsequent launching is anticipated during 1982-83 by the Space Transportation System. An advanced system, LANDSAT-H, is also being planned for periods which would overlap initial SPS operations.

The LANDSAT-D, Figure 37, will provide imagery from a sun synchronous circular orbit altitude of 705.3 km with a 98.2° inclination. Imagery is derived from a Multispectral Scanner (MSS) and Thermal Mapper (TM) on the satellite. Scanner and mapper image data and system status are transmitted to CONUS and foreign control stations directly and through TDRSS. These communications links are diagrammed in Figure 38.

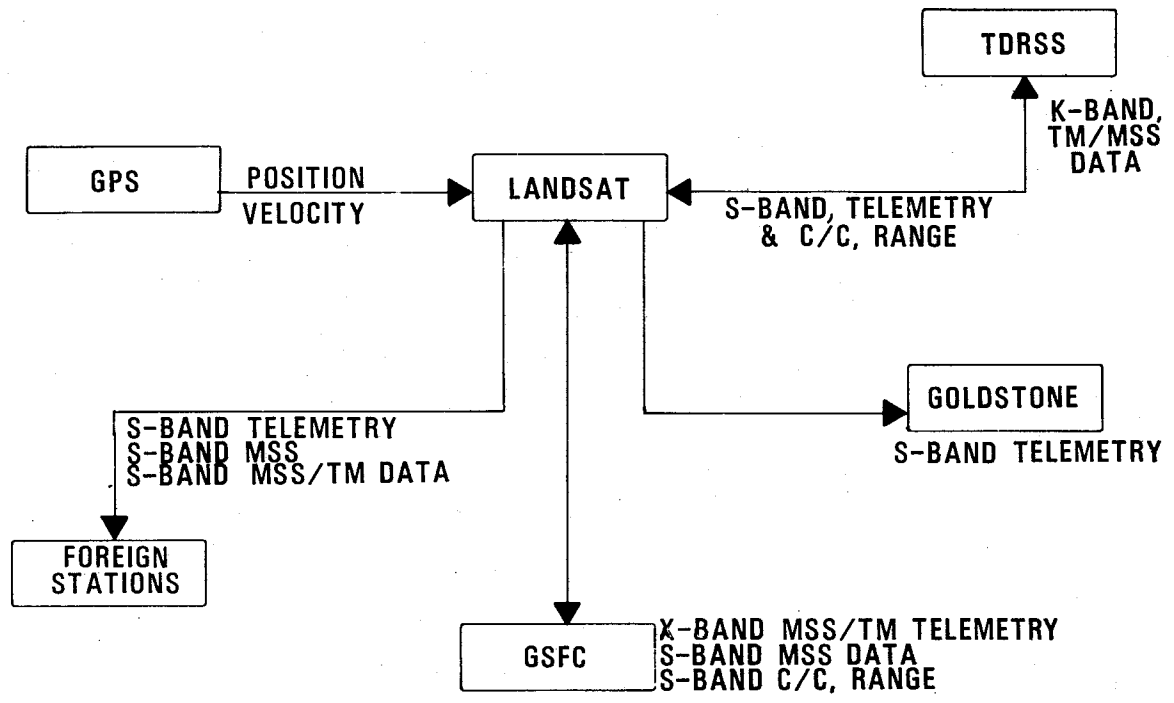
A power density-time plot for the case of orbit coincidence with the SPS main beam is presented in Figure 39. This situation may occur frequently because of the 6 to 8 orbit tracks over CONUS.

The SPS energy coupling into LANDSAT systems is indicated in Figure 40. As diagrammed, the communications, sensor, power bus, and attitude control functions



## WIDEBAND COMMUNICATIONS SUBSYSTEM MECHANICAL CONFIGURATION

Figure 37. LANDSAT wideband communications subsystems mechanical configuration.



**LANDSAT COMMUNICATIONS LINKS**

ITS/3-ACTAG

Figure 38. LANDSAT communication links.

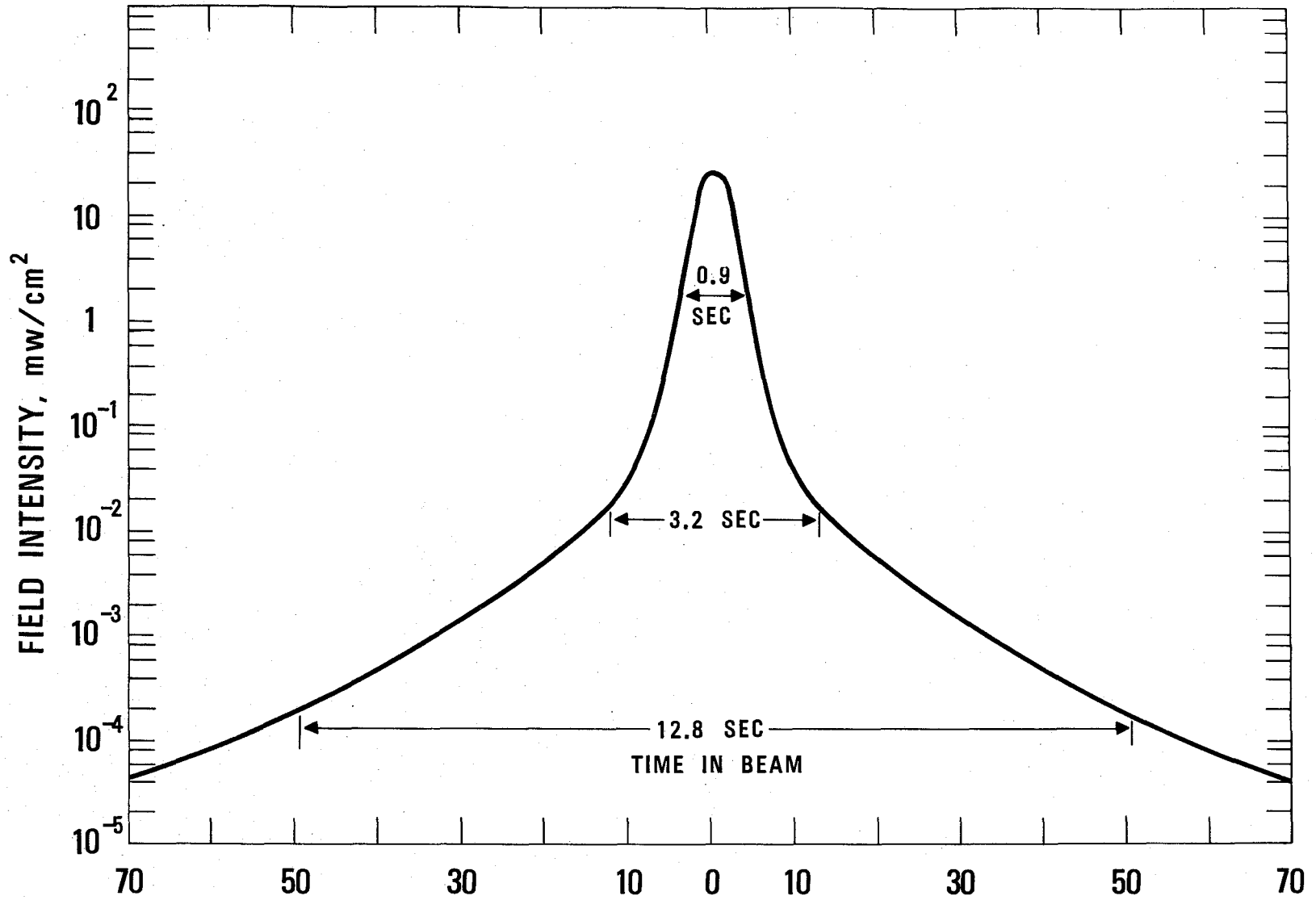


Figure 39. SPS microwave beam geometry at LANDSAT orbit altitude.

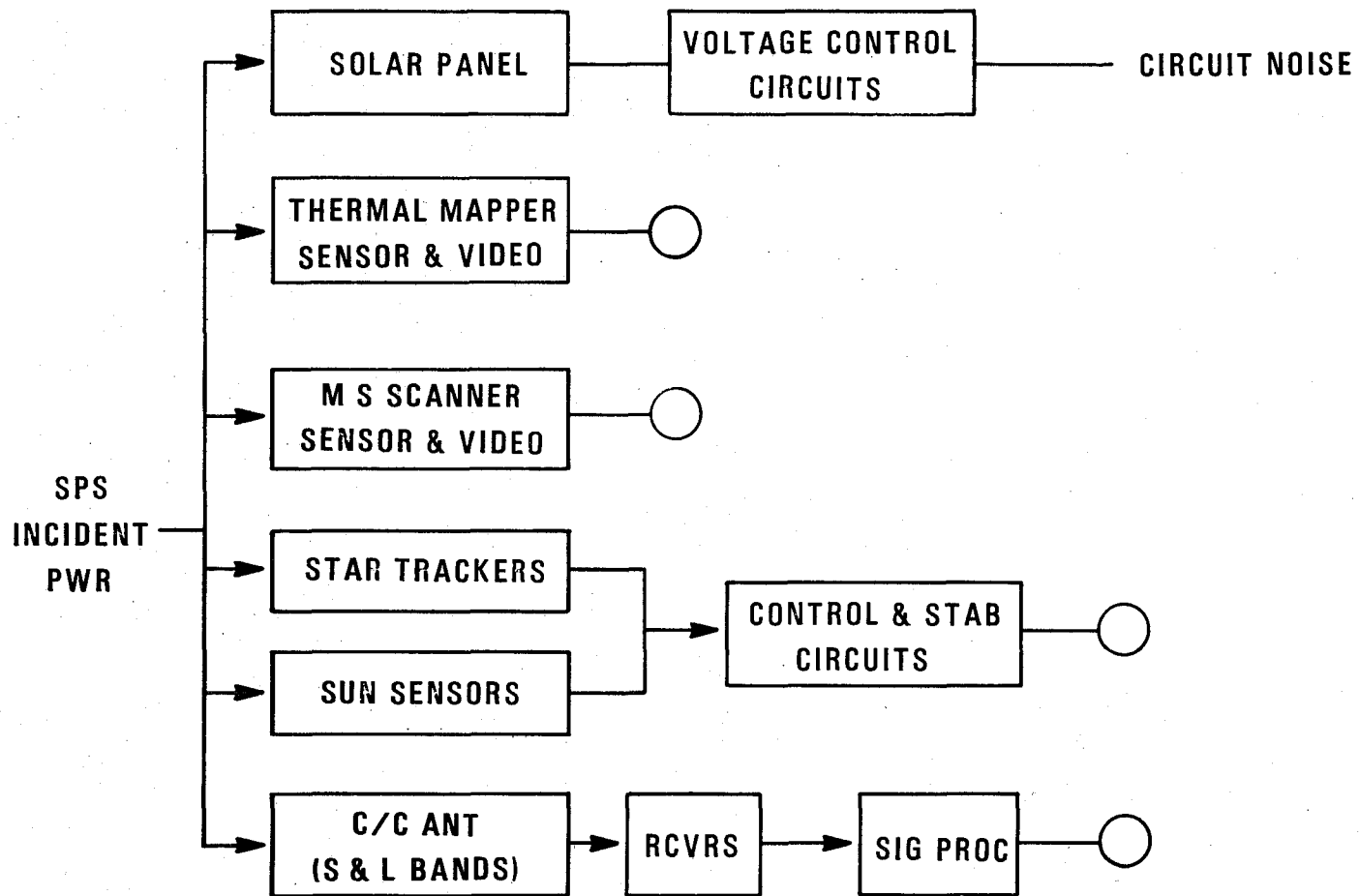


Figure 40. LANDSAT functional impact modes.

can be affected. Coupling would occur through the communications antennas, attitude sensor optical apertures, and the optical apertures and thermal louvers of the Multispectral Scanner and Thematic Mapper. Energy coupling through the solar panels to the power units, transmitting noise to the computers and instrumentation, is not affected because of the filtering and regulation circuitry. Unshielded area and scanner locations on the satellite indicate that the optical aperture is the principal coupling mode for these sensors.

Star tracker noise and angle error ranges in relation to microwave illumination levels are indicated in Figure 41. The LANDSAT star tracker provides error data to the attitude control software. Attitude error would accumulate over a period of about 4 to 5 seconds within the SPS beam. This attitude deviation (pointing deviation magnitude and rate, hemisphere orbit distance for the error increase, and restabilization phases) will be derived for SPS main beam and primary sidelobe illumination of LANDSAT orbit passes.

Because of the locations of the Thematic Mapper (TM) and Multispectral Scanner (MSS) on the satellite, the sensor responses will be sensitive to SPS orbit position. Sensor performance was evaluated for the peak and average SPS power density magnitudes indicated in Figure 39. As shown, the satellite will be subjected to microwave field intensities greater than 100 v/m for about 1 second, intensities greater than 10 v/m for 3.2 seconds, and intensities greater than 1 v/m for about 13 seconds at LANDSAT velocity. Coupling of this energy into the TM and MSS systems may occur through the thermal control louvers or directly through the optical aperture.

The performance degradation of the TM/MSS subsystems in an SPS environment takes the form of the following:

- General increased video noise resulting in overall degradation of image.
- Introduce control signal jitter through the multiplexer timing electronics and introduce image line stagger.
- Reduce spatial frequency which effect picture edge sharpness.
- Reduced dynamic range which affects range of contrast.

Figure 42 shows the thematic mapper test plan configuration. A test was conducted using normal test procedures with no simulated SPS illumination. Bar targets were scanned and recorded impulse response to a 0.2°C resolution were measured. This gave the normal imaging performance of the system.

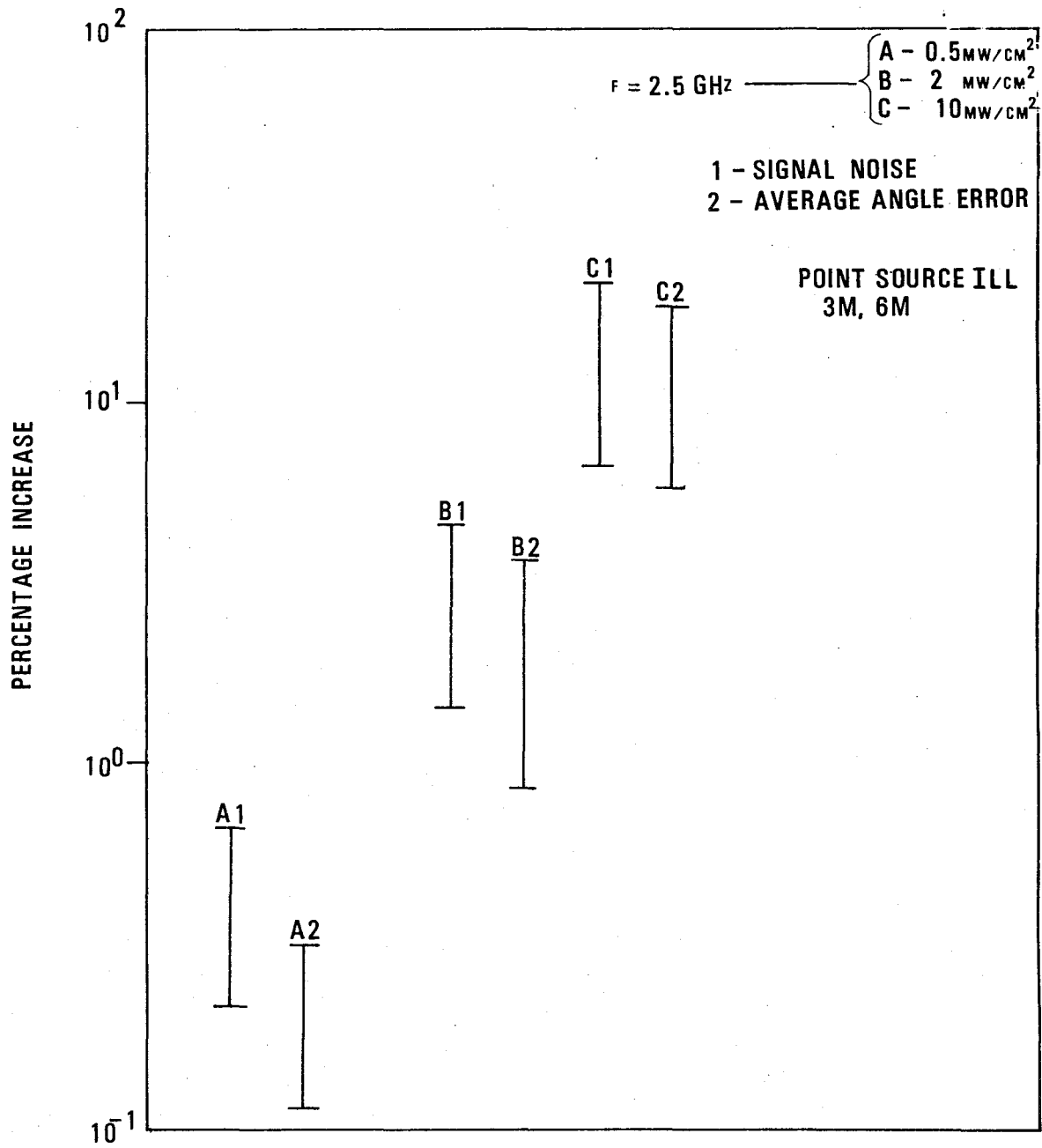


Figure 41. Image dissector star tracker error characteristics.

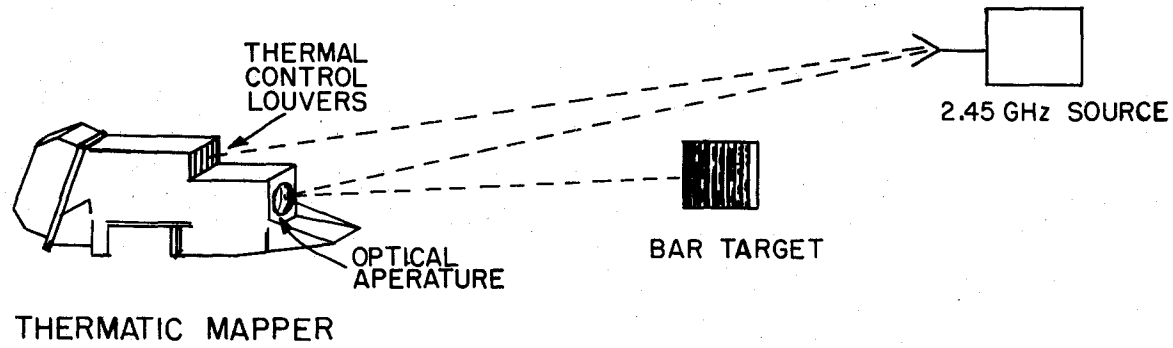


Figure 42. Thematic mapper test plan configuration.

Identical tests were then conducted using the bar targets, recording impulse response, with the addition of a microwave signal illuminating the optical aperture as illustrated in Figure 42. The microwave signal level was varied in steps from 1 mw/cm<sup>2</sup> until complete malfunction occurred at 16 mw/cm<sup>2</sup>. The microwave illumination was then aimed directly into the thermal control louvers with the louvers open to the position which gave maximum coupling. The bar target tests were conducted again at various levels of illumination. A preliminary data set indicates an increase in video channel noise of 8%, and a decrease in modulation transfer function of 18 to 20% which affects the spatial imaging capability by approximately 20%.

The satellite-earth station uplinks use an S-band channel at 2106.4 MHz with wideband modulation modes through the TDRSS. Other satellite receiver channels include a 1377.5 MHz track signal from TDRSS, and the 1227.6 MHz and 1575.4 MHz transmissions from GPS. For the direct earth-station to satellite S-band link (2 kbps - NRZ/PM), a bit-error-rate (BER) increase of 70-85% would occur for SPS main beam exposure period of approximately 16 seconds. For the wide band TDRSS channel, the BER increase would be 20 to 40%, the higher range caused by nonlinear responses in the first conversion and amplifier stages of the receiver decreasing exposure to SPS power densities of  $\geq 8$  mw/cm<sup>2</sup>.

For perhaps 1 to 3 SPS operations maximally separated over CONUS, the LANDSAT mission profile could be modified to eliminate S band command/control transmission during the specific orbit time slots corresponding to SPS illumination. This is obviously not a satisfactory mode, except for temporary operation of an operational satellite while functional modifications are incorporated into future vehicles. These modifications should eliminate the BER effects for the narrowband and wideband transmissions to the satellite, thus removing all mission dependencies between LANDSAT and SPS operations.

Mitigation techniques to be investigated include rejection filters and antenna modifications. The former are preferred because of the relative simplicity, and the elimination of antenna control command and steering software additions. This filter should have a bandwidth of about 10 MHz, and an out-of-band insertion loss of less than 2 dB.

For the multispectral scanner and thermatic mapper, mitigation techniques to be confirmed include circuit filters, noise extraction (spectral density-correlation models) in the data analysis process, and extended shielding for the detectors and colocated video amplifiers. Additional shielding for the video channel and scan

control circuitry is recommended to eliminate jitter in the line scans for situations where coupling occurs directly into these circuits and not through internal common connections. For the star tracker, circuit shielding and optical aperture wire mesh shielding is recommended. The latter is applicable here since focusing optical components are used in front of the image dissector tube. Attitude control is implemented by stored commands based on satellite ephemeris. The star tracker error data updates attitude commands by modification of the Kalman filter coefficients, minimizing image degradation because of attitude transients. Star tracker error distribution spread induced by SPS noise would propagate over approximately 30% of the orbit because of the indirect control action, reducing image registration and an effective reduction in spatial resolution of about 20%. These effects could be corrected by processing software at the CONUS or other receiving centers, but represent additional processing time for imagery collected over about 30% of an orbit track after SPS exposure. Effects of the sun sensors are insignificant, approximately 2% increase in noise, primarily because of SPS harmonics. This noise should cause less than 2° to 5° orientation error for the solar panels over a period of 1 to 1.3 seconds of maximum SPS beam exposure, and be corrected within 2 to 5 seconds after LANDSAT departs the SPS beam. The error magnitude is limited by the solar panel control bandwidth and the small aperture of the sun sensors. Where sun acquisition by the sun sensors is occurring during SPS main beam exposure, the solar panel transient time would be extended by approximately 3 to 5 seconds because of the signal channel noise and related angular uncertainties, the sun-SPS illuminating power ratios also being minimal during this event.

### 3.2 GPS Satellite

The GPS is a navigation and position-fixing system being implemented by the Department of Defense to support worldwide strategic and tactical combat system operations and non-defense users through the reduced precision, single frequency modes. The orbiting complement will include 18 satellites by 1984. The satellites have a 10900 mile circular orbit, with a 12-hr orbit time.

This system provides a passive operational mode for users (receive only). The satellites provide 2 frequency transmissions at 1227.6 GHz and 1575.4 GHz in a QPSK format. Signals include time, ephemeris, identification, data to compute propagation errors, and user location. Users include satellites, aircraft, surface vehicles, and individuals. A position measurement accuracy of  $\pm 30$  to 100 ft has been verified. The variance depends on local-user multipath severity and signal thresholds, and receiver velocity in the case of low-altitude, high-speed military aircraft.

Earth-to-satellite communications provide ephemeris update, orbiting clock corrections, and command/control data to the satellite computer directly and through TDRSS relay. The uplink communications use S-band. Satellite conical spiral receiver antennas are located on the space and earth-pointing planes.

The GPS power density variations for SPS beam interaction are plotted in Figure 43. Power coupling modes into the GPS satellite are diagrammed in Figure 44. This diagram indicates the coupling to sensors and communications in a manner similar to LANDSAT. The GPS vehicle has the additional mode of direct entry through the thermal control louvers that control the temperature of the principal electronic functions: clock, computer, and command/control receiver and decoder components. As indicated on the coupling diagram, this direct penetration energy would primarily couple to the various electronic functions through cables and interface circuits (impedances  $Z_1$  through  $Z_4$ ).

Maximum and average SPS power levels reflected into the satellite electronics are 25 W and 2.8 W, respectively, considering power densities about  $0.1 \text{ mw/cm}^2$  and louver openings of  $10^\circ$ ,  $30^\circ$ , and  $45^\circ$ . Induced jitter in the internal clock and message decoder logic is in the 10% to 65% range for SPS power in the 10 W to 25 W range. These initial measurements will be further verified in future tests of modular logic components configured to represent GPS systems/ physical arrangement.

The S-band communications receiver and associated processor would experience an increase in BER in the range of 50 to 1000 with the antennas exposed to SPS power densities of  $10 \text{ mw/cm}^2$  to  $100 \text{ mw/cm}^2$ . Loss of lock because of intermodulation noise and sensitivity suppression occurs during SPS main-beam and higher sidelobe exposure.

Mitigation technique tests to be completed for the GPS communications receivers are identical to those indicated for LANDSAT. Functional differences will result from the increased SPS maximum power density and the broad band GPS signal mode.

Sun sensor control of solar panel orientation will be affected only in the same manner as discussed for LANDSAT. The short exposure times and the low control bandwidth limit the possible roll of the solar panels because of signal noise. The statement regarding sun acquisition when exposed to SPS illumination is also applicable to GPS.

The earth sensors on GPS are effectively shielded from SPS exposure by the satellite structure for all possible SPS-GPS geometric relationships over the western hemisphere. For geometries where GPS is over European or Asian areas but

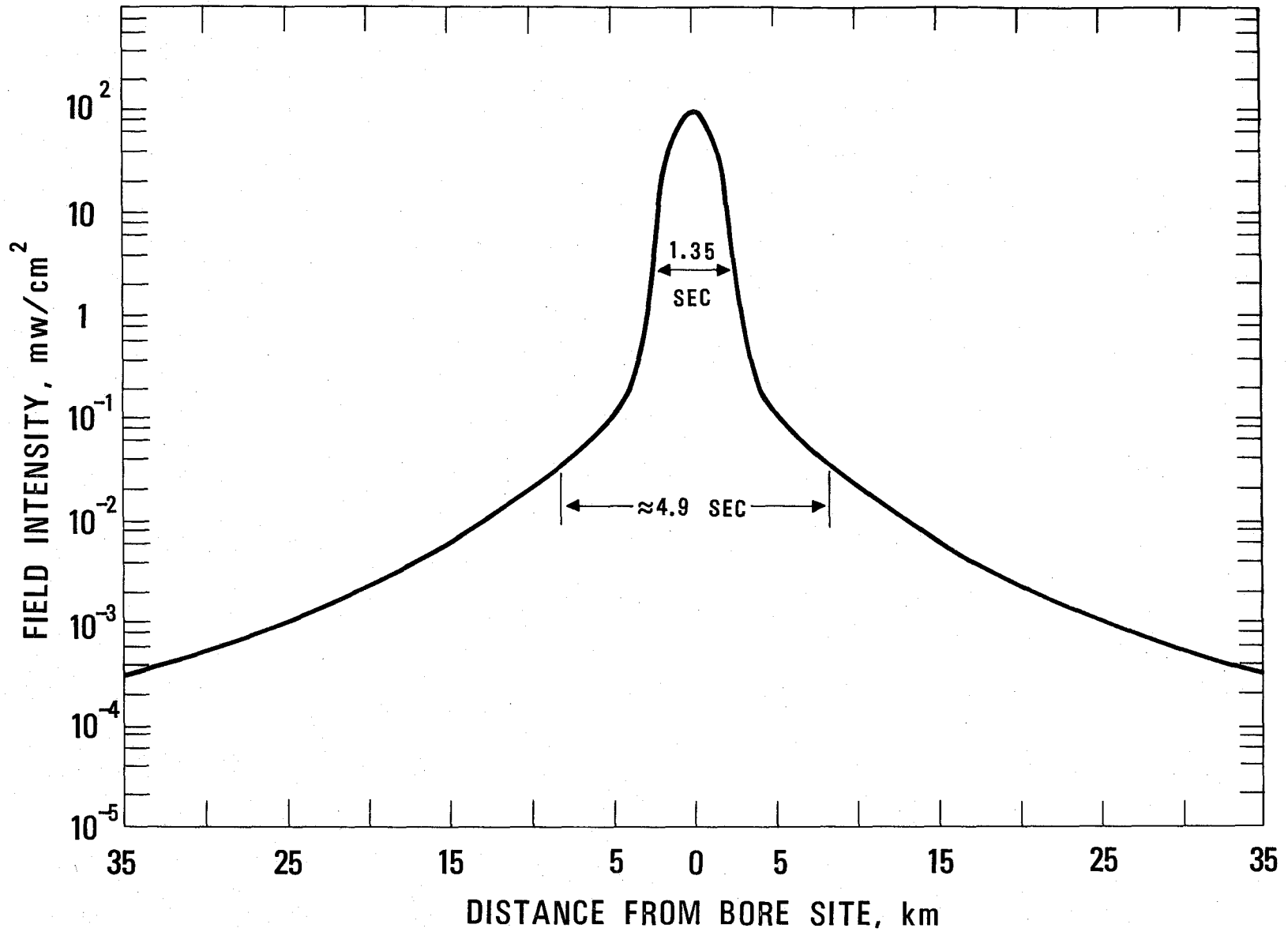


Figure 43. SPS microwave beam geometry at NAVSTAR orbit altitude.

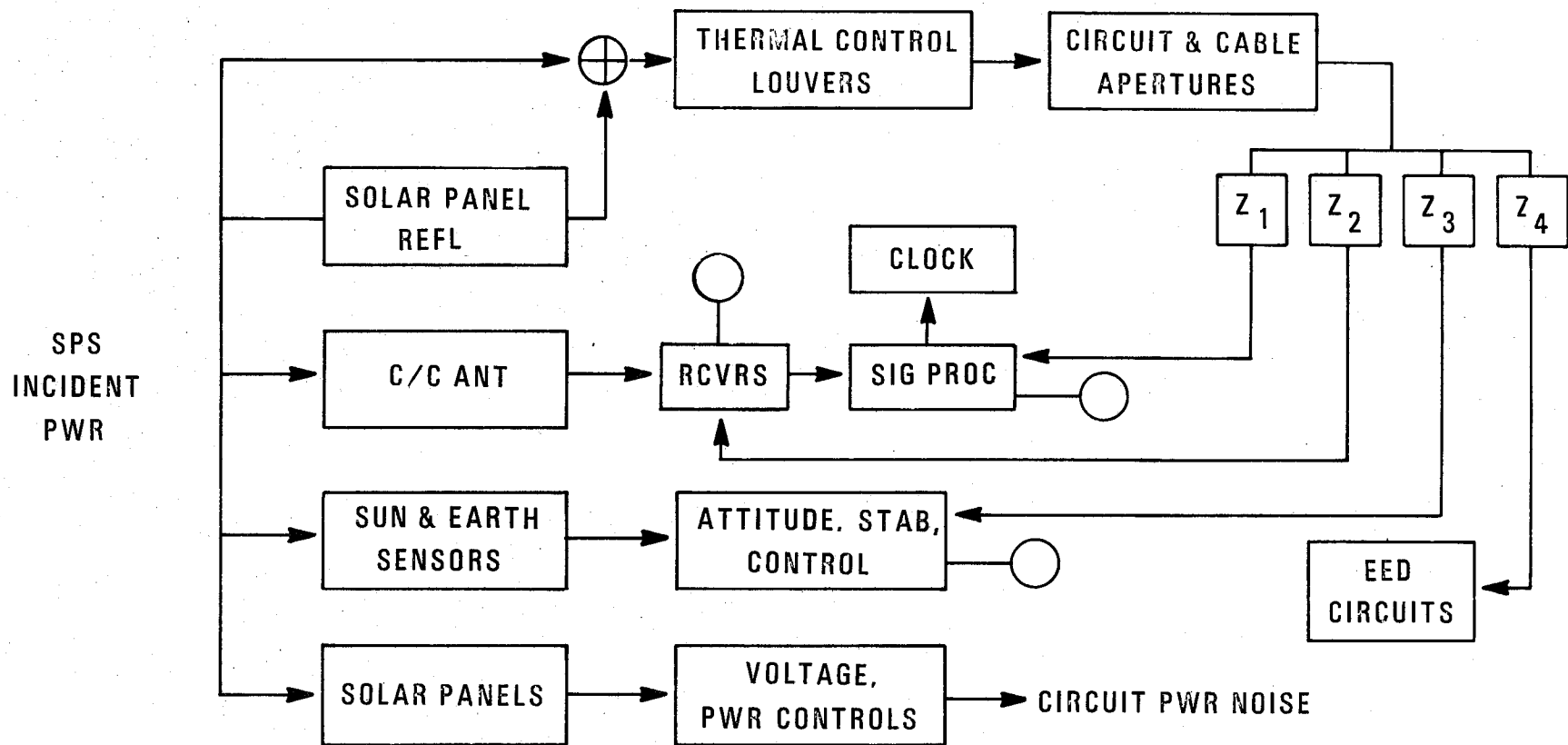


Figure 44. GPS functional impact modes.

has a line-of-sight with an SPS sidelobe, those power densities are at least  $10^3$  to  $10^4$  below any satellite pointing upset threshold.

The GPS transmitters will be unaffected by SPS penetration at the levels indicated. Power and driver amplifier circuitry and the physical configuration indicate no possibility of induced PM jitter on the transmitted signal attributable to coupling into transmitter circuitry. Transmitter antennas are shielded from direct SPS power exposure by the body of the GPS. The  $50 \Omega$  power amplifier impedance, the wideband output tuned filters, and the output-input coupling of the power and driver stages indicate a net coupling of -40 dB to -65 dB for the SPS fundamental frequency, and values of -70 dB to -80 dB for the SPS second harmonic.

The attitude stabilization responses of a direct tracking stabilized platform were measured with respect to illumination of the star tracker sensor system with microwave energy. This track loop configuration is applicable to direct control attitude stabilization for space systems and terrestrial astronomical telescope star tracking. Detectors include image dissectors and split image photomultipliers. Microwave effects include induced detector noise and video amplifier noise, which causes increased dynamic errors, and bias for larger illumination magnitudes. These effects are magnified when tracking higher magnitude number sources. Figure 45 shows attitude error in arc-seconds versus time in seconds. The lower data set shows normal settling time in a single axis with no illumination. Here it can be seen that in less than 10 seconds the platform will be in a stable condition from a disturbed condition. The upper data set shows what happens if the platform were caged with the star tracker illuminated with a  $15 \text{ mw/cm}^2$ , 2.6 GHz microwave signal. Instability is introduced, which increases with time, with ultimate loss of loop lock.

However, satellites will not be in the beam for more than a few seconds, as indicated in the case of LANDSAT and GPS. There may be between three to eight arc-seconds of error introduced during a passage through the SPS beam, but as the lower curve of Figure 45 shows, for systems having the tracker directly in the attitude control loop (e.g., GPS, Space Telescope), this will settle out in five to ten seconds after leaving the beam.

### 3.3 Space Telescope

In 1977, the space telescope project was approved by the United States Congress. The space telescope has major advantages over ground-based telescopes in three important areas: 1) the first and most significant is an order of magnitude improvement in angular resolution, 2) twenty-four hour per day observing

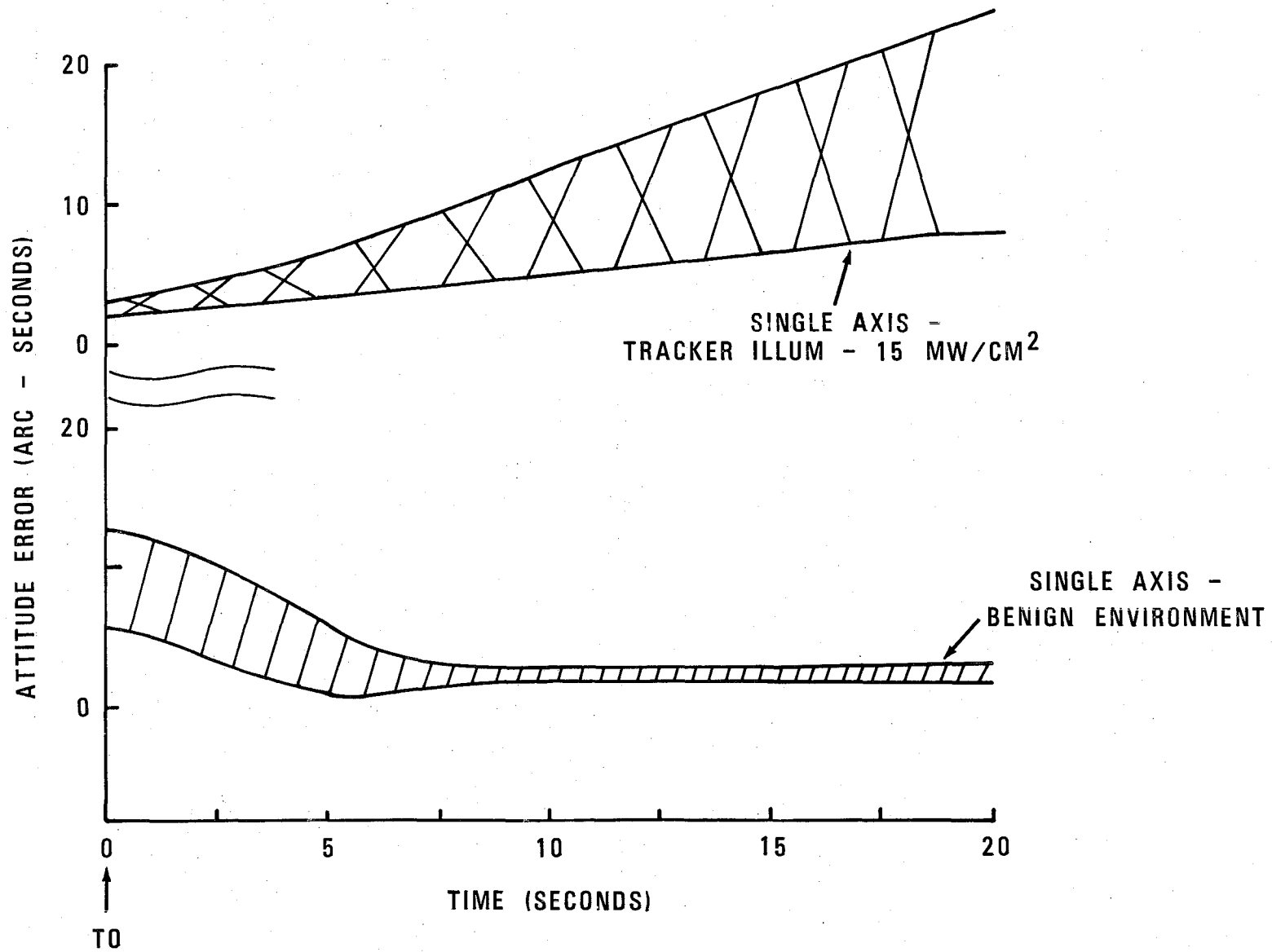


Figure 45. Star tracker - stabilized platform altitude responses.

time, 3) the telescope being beyond the Earth atmosphere allows photometric data collection over a much wider wavelength range - ultraviolet, infrared, and submillimeter wavebands as well as the visual spectrum.

The planned schedule shows the initial launch in the last quarter of 1983. The design lifetime is fifteen years in orbit. The orbit is circular at a 500 km altitude and 28.8° inclination. A cross-sectional view of the satellite observatory is shown in Figure 46. The telescope consists of the primary and secondary mirrors, the metering structure for maintaining the relative positions of the mirrors, the internal light baffling system, and the fine guidance sensors. Communications with the satellite will be via the TDRSS. The scientific instruments on-board are as follows:

Wide Field/Planetary Camera - the camera contains eight charge coupled device (CCD) detectors, each consisting of 800 x 800 elements.

Faint Object Spectrograph - uses digicon detectors, each of which consists of a linear array of 512 independent diode elements.

Faint Object Camera - the design uses a three-stage image intensifier with an intensified silicon target television camera tube.

High Resolution Spectrograph - the detector is a digicon device consisting of a linear array of 512 diode elements.

High Speed Photometer/Polarimeter - the device consists of a number of image dissectors, their associated electronics and a focal plane aperture mask and filter plate.

Fine Guidance System - Uses three independent sensors and detectors located in annular segments around the field of view in the focal plane. This system provides great astrometric potential. These three high resolution sensors provide data for star field maps to support future stellar experiment planning. These sensors must acquire stars at  $M = 13$  with an accuracy of  $7 \times 10^3$  arc sec.

The SPS microwave power beam geometry at space telescope orbit altitude is shown in Figure 47. Coupling of electromagnetic energy into the satellite instrumentation will occur mainly through the telescope's 2.4 meter optical aperture. The SPS peak field intensity would be approximately  $28 \text{ mw/cm}^2$ . This would be equivalent to 12.67 kw of microwave energy on top of the telescope. About 40% of the energy would be coupled through the baffled area to the primary mirror. Some 20% of this energy would then be reflected through the mirror system into the detector areas. There would be about a 60% penetration into the detector areas, which would be equivalent to 55 watts of 2.45 GHz energy directly into the instrumentation area.

The impact of SPS radiations on the scientific instruments would be to increase detector channel noise, reduce spatial resolution, and reduce dynamic range. For the satellite guidance system and astrometry missions, there would be increased

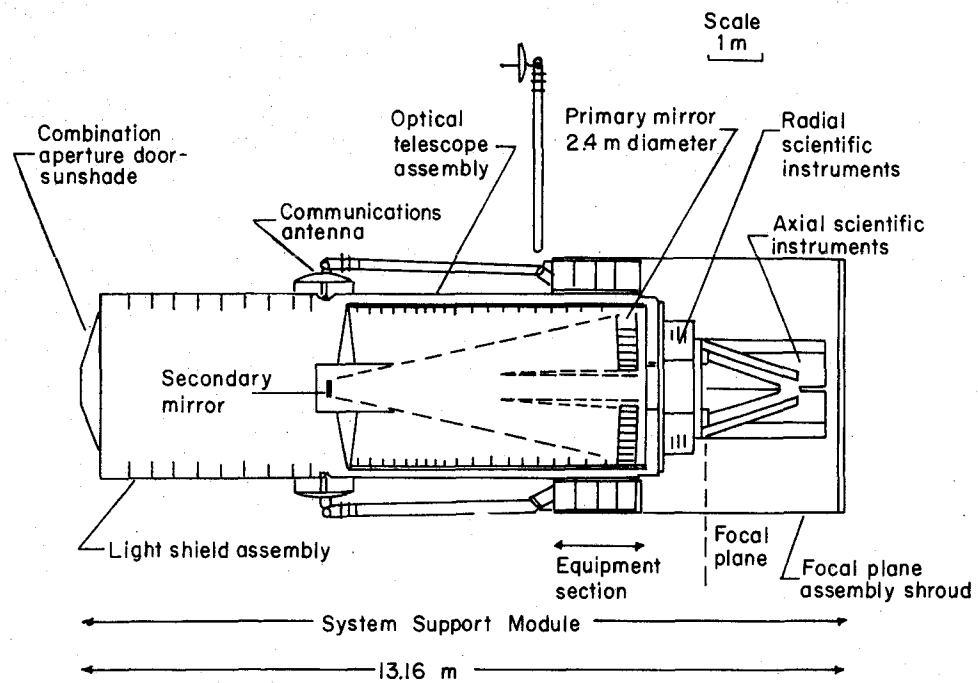


Figure 46. Cross-sectional view of the satellite observatory.

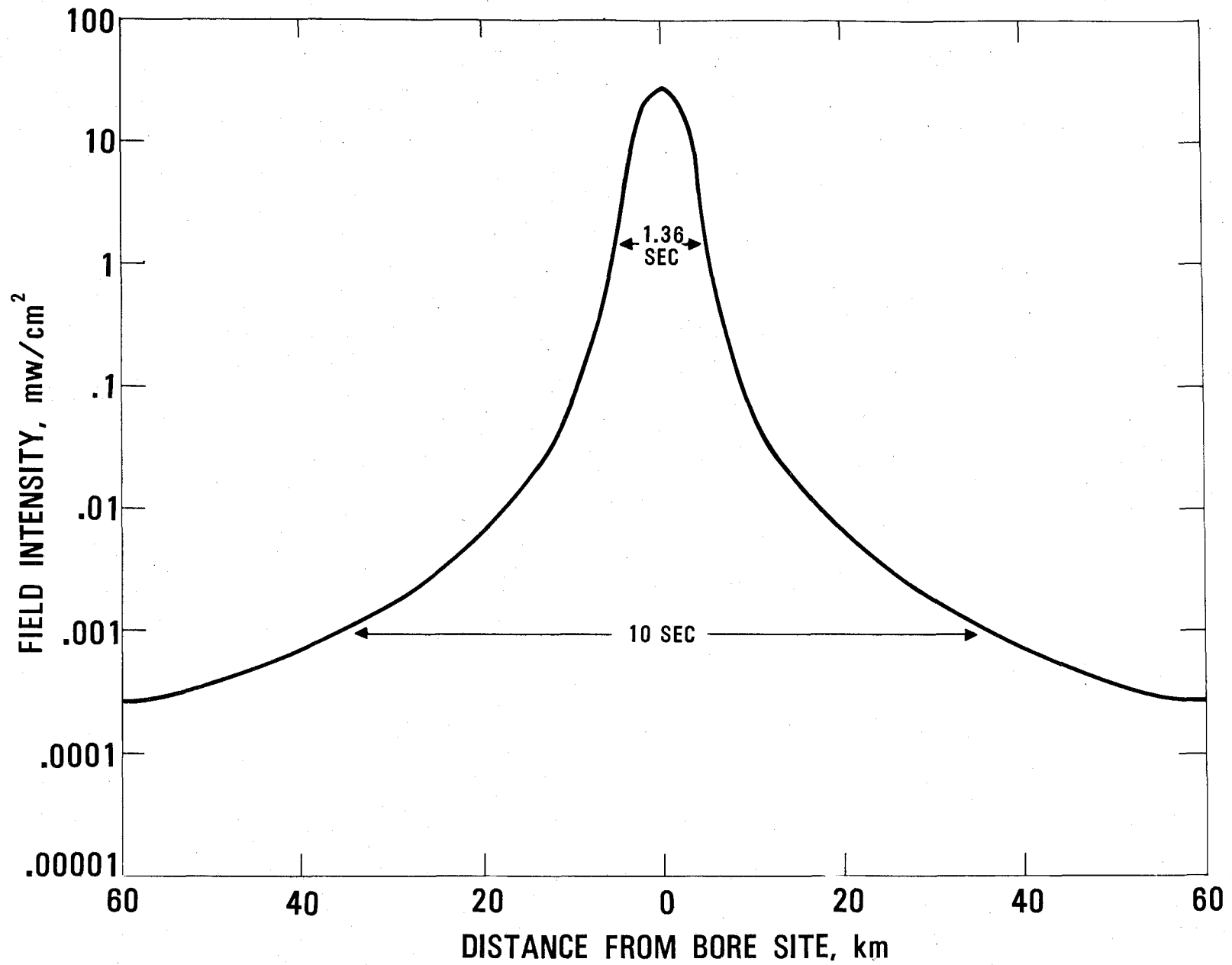


Figure 47. SPS power beam geometry for space telescope EMC analysis.

detector channel noise and reduced spatial resolution, which would increase attitude instabilities for the few seconds the space telescope is in the SPS beam.

Figure 48 shows voltage output vs. illuminating frequency for a 512 element CCD array at two widely separated temperatures given in degrees kelvin. These video noise spectra show the normal response curves for CCD arrays. Figure 49 shows the CCD array spectra in the presence of a 2.5 GHz  $2 \text{ mW/cm}^2$  field. Comparing Figures 48 and 49, it is seen that the frequency resolution has degraded considerably in the illuminated case, particularly above 100 hertz. This would adversely effect the imaging capability of such an array.

Figure 50 shows the same CCD array being illuminated with a normal source signal and the associated resolution given in lines per minute. The line A is the normal response of such an array. The line B shows the degradation in resolution in the presence of a 2.5 GHz,  $2 \text{ mW/cm}^2$  rf field. Here it can be seen that it takes a higher source illumination for a given resolution in the presence of the microwave field, particularly below  $10^{-5} \text{ mW/cm}^2$ .

The CCD matrices, digicon devices, image intensifiers, and image dissectors will experience degraded capabilities in the presence of SPS energy as the satellite observatory intersects the main power beam and major sidelobes. The apertures in front of the detectors afford very limited protection since the axial length will be much less than  $\lambda/2$  for the SPS fundamental or primary harmonics. Figure 41, (page 59) shows the percent increase in noise and average angle error for an image dissector subjected to microwave illumination in a star tracker configuration.

Mitigation techniques would include wire mesh shielding for image dissectors, digicon devices, and CCD arrays where focusing optics are employed. For sub-millimeter, infrared, or ultraviolet detectors, the wire mesh would cause unacceptable distortion and large data errors. Increasing the axial length of the apertures for the instrument detectors to 6 cm will provide 40-60 dB microwave attenuation. Uplink communications through TDRSS should not be accomplished during beam intersection. Crystal lenses in the optical link would attenuate microwave energy to keep unacceptable interference from the fine guidance system or other on-board systems used in stabilization and tracking for the telescope. Upset in attitude stabilization would be corrected over a considerable portion of an orbit to stabilize the total system after passage through an SPS beam. A provision for "coasting" through the power beam should also be acceptable because of the short transit time. To maintain specification accuracy, a rate memory mode will be required in the attitude stabilization system.

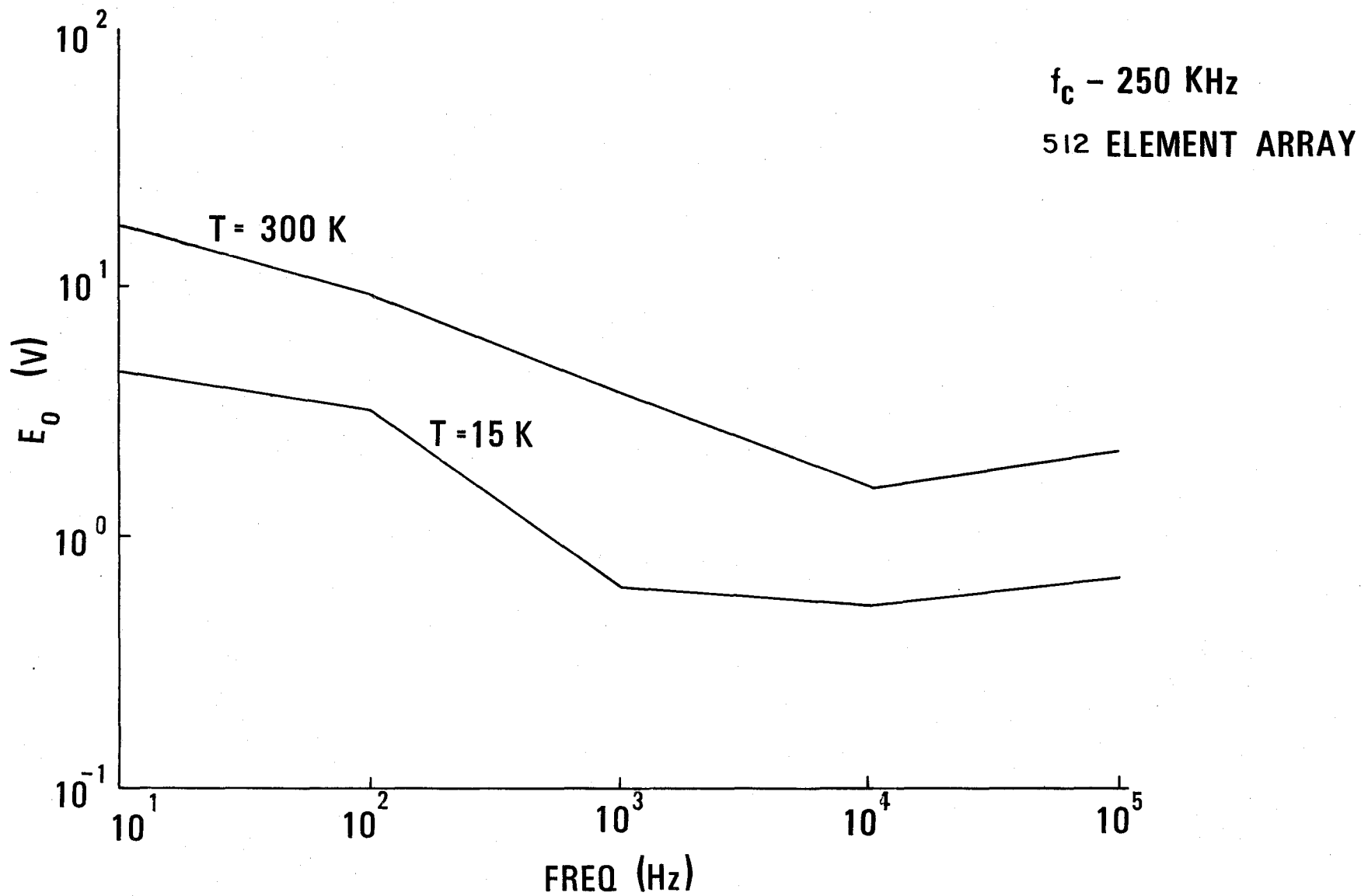


Figure 48. CCD video noise spectra.

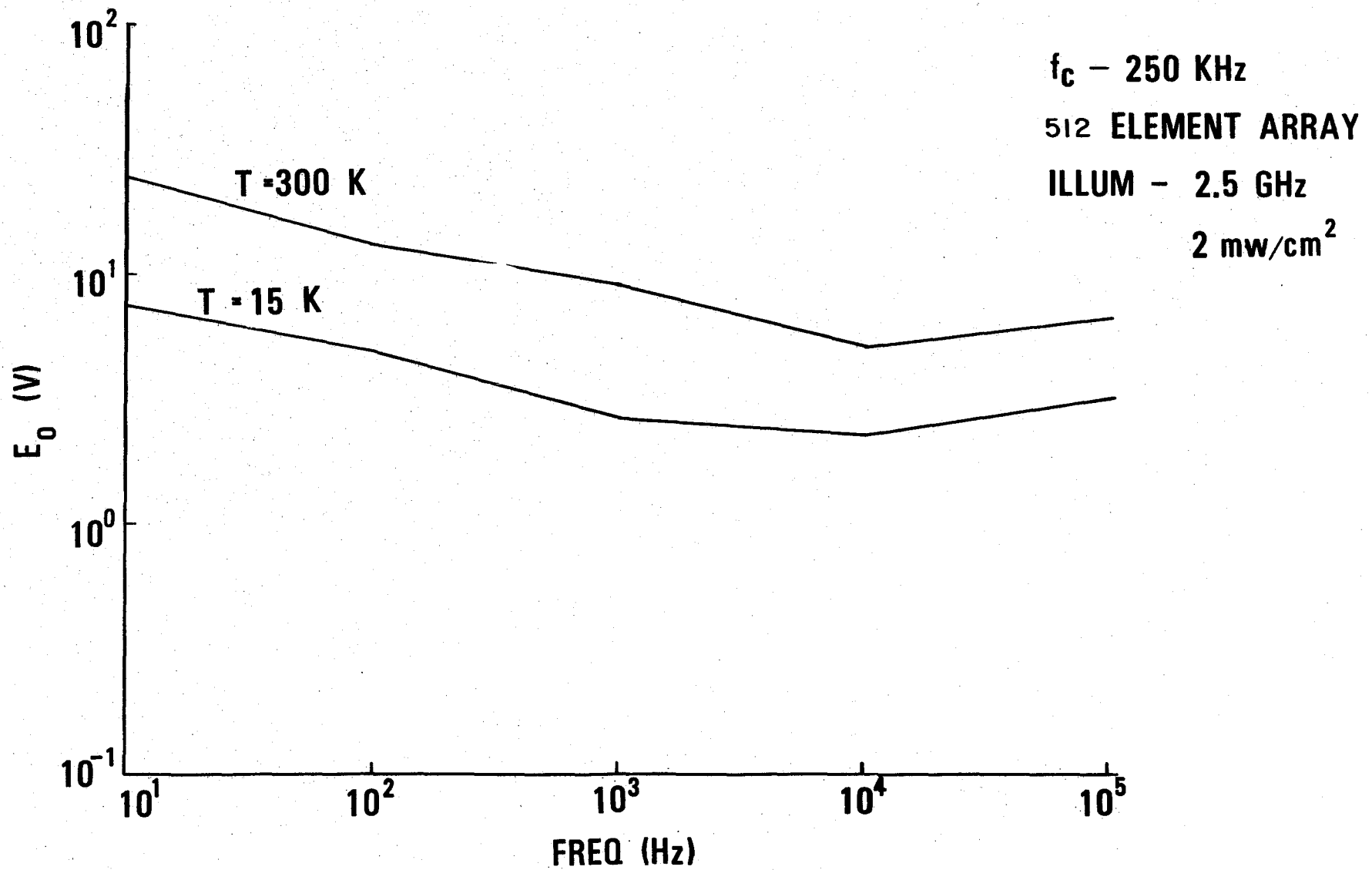


Figure 49. CCD video noise spectra - SPS illumination.

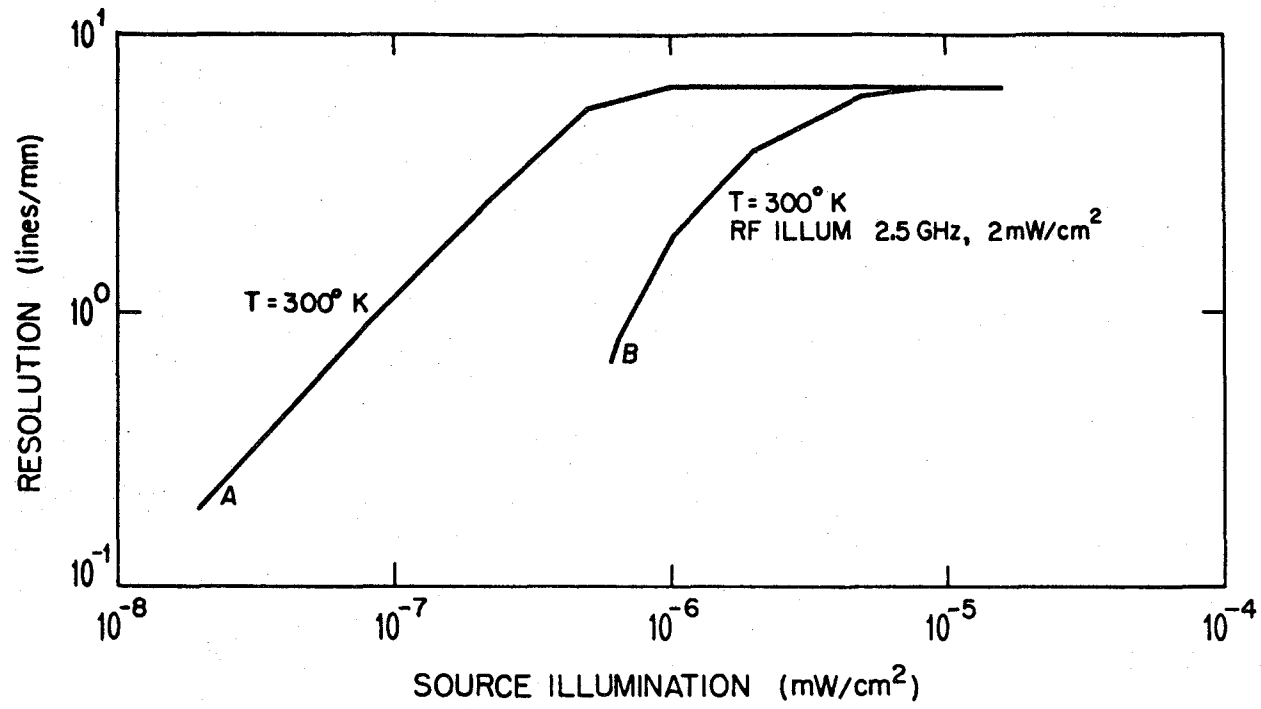


Figure 50. CCD array imaging characteristic.

The SPS interaction with LEO satellites involves primarily periods of orbit intercept with the SPS power beam. Performance effects concern uplink communications, sensors for data collection and attitude control, and internal modules that are directly exposed to penetration apertures (e.g., thermal control louvres). Mitigation methods for these LEO satellite functions are listed.

1. Silence uplink receivers when encountering SPS power densities  $>0.2 \text{ mw/cm}^2$ . This will involve an orbit period of from 0.5 to 3 sec, depending on orbit altitude.
2. Add mesh shields to all thermal control apertures; mesh  $<2$  cm diagonal dimension.
3. Single point grounding and complete metal shielding for all logic, computer, and clock components. All signal, control, and signal ground cabling must use coaxial cabling.
4. Attitude control sensors (star trackers) should be covered with a wire mesh ( $d <2$  cm) if focusing optics are employed. Mesh is placed at defocused axial positions, and AWG 26 to 32 copper wire grounded to the satellite structure should be used.
5. Attitude sensors not using focusing optics should use crystal mirrors or a metal cylindrical collimator having an axial length  $\geq 6.5$  cm. These methods will provide  $\sim 20$  to 30 db suppression.
6. Earth sensors (visual and IR optical staring or scanning devices) should use a metal collimator with axial length  $\geq 6.5$  cm, and complete shielding around video amplifiers and control circuits coupling from the sensor elements.
7. Where the recommended data sensor shielding must be compromised in axial dimension, image enhancement software will be required in data reduction to remove periodic noise components and restore higher spatial frequencies.

#### 4. SUMMARY OF POTENTIAL INTERFERENCE TO SATELLITE COMMUNICATIONS SYSTEMS

Interference would be likely in the 2500-MHz to 2690-MHz direct broadcast satellite frequency band adjacent to SPS. The adjacent channel noise from SPS in this frequency band was estimated at  $-124 \text{ dBc/4 kHz}$  and  $-100 \text{ dBc/1 MHz}$ . A second potential problem is the 7350-MHz 3d harmonic from SPS that falls within the 7300-MHz to 7450-MHz space-to-earth, government satellite band. Estimates of 3rd harmonic signal levels based on current klystron technology are from  $-57$  to  $-105 \text{ dBc/4 kHz}$ .

Co-channel interference levels below  $-185 \text{ dB(W/m}^2 \cdot 4 \text{ kHz)}$  will be needed to protect earth terminals with antenna apertures of equal or less than 1 square meter. These figures apply to narrowband systems such as single channel voice systems and FM-FDM voice systems with a 4-kHz reference bandwidth. Wideband satellite earth terminals with a 1-MHz reference bandwidth can withstand higher

interference levels of up to  $-161 \text{ dBW/m}^2 \cdot \text{MHz}$ . Earth terminals whose operating frequency is separated by 3-4 times the RF bandwidth from the SPS power transmission frequency can withstand interference levels substantially higher than those quoted above because of filtering in the receiver. Estimates of the maximum amount of filtering available in satellite receivers are 110-130 dB. Laboratory testing needs to be conducted to define more precisely the range of filtering available in satellite receivers.

Calculations of the potential interference between SPS and NAVSTAR GPS navigation receivers showed that SPS does not represent an interference threat to either navigation signal. The combined rf and IF filtering of the navigation receivers should be sufficient to prevent interference even in an SPS power flux density of  $-10 \text{ dBW/m}^2$  ( $0.01 \text{ mW/cm}^2$ ). A similar conclusion was also reached in a study of interference to MARISAT earth terminals in an SPS microwave field of  $-40 \text{ dBW/m}^2$  ( $1 \times 10^{-5} \text{ mW/cm}^2$ ). However, a potential interference problem does exist with MARISAT terminals in a field of  $-10 \text{ dBW/m}^2$ .

Interference problems are also possible between SPS and other satellites closely spaced in geosynchronous orbit. This study estimates that a power flux density as high as  $-20 \text{ dBW/m}^2$  can be expected at victim satellites within  $0.1^\circ$  of separation from SPS. This figure is based on an SPS antenna gain in the direction of the geosynchronous orbit of  $-10 \text{ dBi}$ . Signal levels of this magnitude can be sufficient to cause interference to satellite systems with reference bandwidths of 4 kHz. It is estimated that separations of  $0.5^\circ$  to  $1.0^\circ$  may be required to prevent interference to other satellites in geosynchronous orbit.

## 5. CONCLUSIONS AND RECOMMENDATIONS

The evaluation of the SPS operation effects on other GEO and LEO satellites indicates the character of EM functional interactions, including modes of penetration into satellite receivers, sensors, and circuits, and the resultant functional degradation in data collection and processing.

GEO communications satellites should be separated from an SPS by  $0.5^\circ$  at orbit altitude to assure acceptable uplink performance, where SPS interference effects include coupling of SPS fundamental and harmonics from spaceterminal sidelobes, and reflective multipath from the SPS structure. This separation will allow an  $S/I > 15 \text{ dB}$  for the adjacent communications links.

Future satellites using array antennas can employ nulling techniques for SPS harmonic components that are within communication bands. This method can provide

about 20-30 dB suppression from unmodulated interferers, which is sufficient for a 0.5° orbital separation.

Satellite-satellite communications modes with an SPS between communications satellites cannot be satisfactorily accomplished without a frequency translator-repeater operating on the SPS vehicle because of reflection multipath interference. Without the SPS repeater, the fade depths of 20-34 dB would severely restrict link utility for digital or medium bandwidth analog data transmission.

Multiple use communications platforms and multiple spaceteenna-SPS platform configurations represent a viable option for elimination of the orbit slot contention problems for a 60 SPS deployment. A detailed configuration plan must be developed for both platforms, and international allocation and procedure agreements negotiated for combined communications systems operations.

#### 6. REFERENCES

1. Arndt, G. D., and J. W. Seyl (1980), Letter Report, RF Interference Orbital Spacing for SPS, NASA Johnson Space Center, Organization Code NASA EH2-M/80-021, February.
2. Bargellini, P. L. (1972), The Intelsat IV Communication System, COMSAT Tech. Rv. No. 2.
3. Batson, B. H., S. W. Novosad, and T. W. Sheehan (1977), Space shuttle utilization of TDRSS services, IEEE NTC'77 Conference Record, Vol. I, pp. 09:4-1, 09:4-5.
4. CCIR, International Radio Consultative Committee (1978c), Report 558-1, Satellite Antenna Patterns in the Fixed Satellite Service, XIVth Plenary Assembly, Vol. IV, Kyoto, Japan, pp. 243-262.
5. Computer Sciences Corporation (1975), NASA Compendium of Satellite Communications Programs, Prepared for National Aeronautics & Space Admin., Goddard Space Flight Center, Greenbelt, Maryland 20771. Contracts Nos. NAS-5-204011 and NAS 5-24012, Dec.
6. Dicks, J., and M. Brown (1978), Intelsat V Satellite Transmission Design Design, IEEE/ICC, June.
7. Edelson, B., and R. Davis (1978), Satellite communications in the 1980's and after, Telecommunications in the 1980's and After, London, The Royal Society.
8. Fuenzalida, J., O. Shimbo, and W. Cook (1973), Time domain analysis of intermodulation effects caused by nonlinear amplifiers, COMSAT Tech. Rv., Spring.
9. Getsinger, W. (1977), Current developments at COMSAT Laboratories in the 20/30 GHz communications satellite bands, Symposium on Advanced Communications Satellite Systems, Genoa, Italy, December.

10. Gould, R. and Y. F. Yum (1975), Communications Satellite Systems; An Overview of Technology (IEEE Press, New York).
11. Hiebert, A. (1977), Advanced Composites: Electromagnetic Properties, Vulnerabilities and Protective Measures, Rand 1979/May.
12. Hiebert, A. (1978), Advanced Composites: Natural Space Environment Simulation, Testing, and Analysis, Rand 1979/IAF December.
13. International Telecommunication Union (1977), Final Acts of the World Administrative Radio Conference for the Planning of the Broadcasting-Satellite Service in Frequency Bands 11.7-12.2 GHz (in Regions 2 and 3) and 11.7-12.5 GHz (in Region 1), Geneva, 1SNB 92-61-00491-1.
14. Morgan, W. L. (1978), Geosynchronous satellite log, COMSAT Technical Review 8, No. 1, Spring, pp. 219-237.
15. Morgan, W. (1978), Satellite characteristics summary, Acta Astronautica, May-June.
16. Palluel, P., G. Fleury, and P. Gosset (1973), Investigation of multicarrier operation of high efficiency TWT, Proc. European Microwave Conf., September.
17. Poza, H. B. (1977) TDRSS telecommunications payload: An overview, IEEE NTC'77 Conference Record, Vol. I, pp. 19:1-1, 19:1-7.
18. Roe, J. E. (1965), Nonlinear Electron Wave Interaction Phenomena, (Academic Press, New York).
19. Scherba, M. K. and J. E. Rowe (1971), Characteristics of multisignal and noise modulated high-power microwave amplifiers, IEEE Trans. on Electron Devices ED-18, June.
20. Skolnik, M. I. (1962), Introduction to Radar Systems (McGraw-Hill Book Company, Inc., New York, N.Y.), pp. 274-275.
21. U.S. Department of Energy/NASA (1978), Satellite power system, concept development & evaluation program, Ref. System Rpt. DOE/ER-0023, October.
22. Wallenberg, R. (1980), Advanced composite aircraft EM design and synthesis, ITTRI Interim Report, Contract No. 0014-79-C-0172, April.
23. Welti, G. (1978), Intersatellite link for multi access telephony, IEEE-EASCON.
24. Zaghoul, A., and R. McPhie (1978), Multimode analysis of mutual coupling between rectangular apertures, Conf. on Antennas and Propagation, London.

**BIBLIOGRAPHIC DATA SHEET**

1. PUBLICATION NO. NTIA Report 81-75		2. Gov't Accession No.	3. Recipient's Accession No.
4. TITLE AND SUBTITLE Effects of the Satellite Power System on Low Earth Orbit and Geosynchronous Satellites		5. Publication Date June 1981	
		6. Performing Organization Code	
7. AUTHOR(S) W. B. Grant, E. L. Morrison and J. R. Juroshek		9. Project/Task/Work Unit No.	
8. PERFORMING ORGANIZATION NAME AND ADDRESS National Telecommunications & Information Admin. Institute for Telecommunication Sciences 1-3449 325 Broadway Boulder, CO 80303		10. Contract/Grant No. DE-A106-79RL10077 and DE-A101-80ER10160.00	
		12. Type of Report and Period Covered	
11. Sponsoring Organization Name and Address U.S. Department of Energy Satellite Power System Project Office Washington, DC 20445		13.	
		14. SUPPLEMENTARY NOTES	
15. ABSTRACT (A 200-word or less factual summary of most significant information. If document includes a significant bibliography or literature survey, mention it here.) The large amount of power contained in the main beam and principal sidelobes of the proposed Solar Power System (SPS), now under study by DOE and NASA, potentially presents an EMC problem for other satellite systems. This report examines selected geosynchronous orbit (GEO) satellites in adjacent slots to an SPS, GEO satellites on a chord passing an earth horizon, and low-earth-orbit (LEO) satellites which may pass through the SPS power beam. Potential functional and operational impacts to on-board systems are analyzed. Mitigation techniques for SPS effects are examined, and recommendations summarized to allow satellites to operate satisfactorily in an SPS environment.			
16. Key Words (Alphabetical order, separated by semicolons)			
17. AVAILABILITY STATEMENT  <input checked="" type="checkbox"/> UNLIMITED.  <input type="checkbox"/> FOR OFFICIAL DISTRIBUTION.		18. Security Class. (This report) UNCLASSIFIED	20. Number of pages 78
		19. Security Class. (This page) UNCLASSIFIED	21. Price:

